

การสังเคราะห์สาร avicequinone C และอนุพันธ์เพื่อศึกษาฤทธิ์ใน  
การยับยั้งเอนไซม์ 5 $\alpha$ -รีดักเทส

นางสาววิรัชพัชร การสมวรรณ์

จุฬาลงกรณ์มหาวิทยาลัย  
CHULALONGKORN UNIVERSITY

บทคัดย่อและแฟ้มข้อมูลฉบับเต็มของวิทยานิพนธ์ตั้งแต่ปีการศึกษา 2554 ที่ให้บริการในคลังปัญญาจุฬาฯ (CUIR)  
เป็นแฟ้มข้อมูลของนิสิตเจ้าของวิทยานิพนธ์ ที่ส่งผ่านทางบัณฑิตวิทยาลัย

The abstract and full text of theses from the academic year 2011 in Chulalongkorn University Intellectual Repository (CUIR)  
are the thesis authors' files submitted through the University Graduate School.

วิทยานิพนธ์นี้เป็นส่วนหนึ่งของการศึกษาตามหลักสูตรปริญญาเภสัชศาสตรมหาบัณฑิต

สาขาวิชาเภสัชเวช ภาควิชาเภสัชเวชและเภสัชพฤกษศาสตร์

คณะเภสัชศาสตร์ จุฬาลงกรณ์มหาวิทยาลัย

ปีการศึกษา 2558

ลิขสิทธิ์ของจุฬาลงกรณ์มหาวิทยาลัย

SYNTHESIS OF AVICEQUINONE C AND ANALOGS TOWARD THE STUDY OF  
5 $\alpha$ -REDUCTASE INHIBITORY ACTIVITY

Miss Wiranpat Karnsomwan



A Thesis Submitted in Partial Fulfillment of the Requirements  
for the Degree of Master of Science in Pharmacy Program in Pharmacognosy  
Department of Pharmacognosy and Pharmaceutical Botany  
Faculty of Pharmaceutical Sciences  
Chulalongkorn University  
Academic Year 2015  
Copyright of Chulalongkorn University



วิรัชพัชร การสมวรรณ์ : การสังเคราะห์สาร avicequinone C และอนุพันธ์เพื่อศึกษาฤทธิ์ในการยับยั้งเอนไซม์ 5 $\alpha$ -รีดักเทส (SYNTHESIS OF AVICEQUINONE C AND ANALOGS TOWARD THE STUDY OF 5 $\alpha$ -REDUCTASE INHIBITORY ACTIVITY) อ.ที่ปรีชาวิทยานิพนธ์หลัก: รศ. ดร.วันชัย ดีเอกนามกุล, อ.ที่ปรีชาวิทยานิพนธ์ร่วม: อ. ดร.ศุภกานูจน์ ชานี, อ. ดร.ธัญญา รุ่งโรจน์มงคล, 150 หน้า.

สเตียรอยด์ 5 $\alpha$ -รีดักเทส หรือ 3-ออกโซ-5 $\alpha$ -สเตียรอยด์  $\Delta^4$ -รีดักเทส เป็นเอนไซม์ที่มี 3 ไอโซไซม์ ซึ่งเกี่ยวข้องกับกระบวนการสร้างสารสเตียรอยด์ เอนไซม์ชนิดนี้ทำหน้าที่เปลี่ยนเทสโทสเตอโรนเป็นไดไฮโดรเทสโทสเตอโรนโดยมี NADPH เป็นโคแฟกเตอร์ เอนไซม์ 5 $\alpha$ -รีดักเทสเป็นเอนไซม์ที่มีความสำคัญต่อกระบวนการเกิดโรคในมนุษย์ ได้แก่ โรคมะเร็งต่อมลูกหมาก โรคต่อมลูกหมากโต โรคหัวใจ และโรคผมร่วงที่เกิดจากพันธุกรรม ในปัจจุบันยังไม่มีกรายงานโครงสร้าง 3 มิติของเอนไซม์ 5 $\alpha$ -รีดักเทสเนื่องจากความไม่คงตัวของเอนไซม์ในระหว่างการสร้างผลึก ในการศึกษานี้ได้ทำการออกแบบโครงสร้าง 3 มิติโดยใช้เทคนิคทางเคมีคอมพิวเตอร์เพื่อทำนายโครงสร้าง 3 มิติของเอนไซม์ 5 $\alpha$ -รีดักเทส ชนิดที่ 1 และ 2 โดยใช้โปรแกรม SWISS-MODEL ในการคำนวณ และใช้เอนไซม์ไอโซพรีนิลซิสเทอีนคาร์บอกซิลทรานซ์เฟอเรส (ICMT, PDB code 4A2N) เป็นต้นแบบ บริเวณเร่งปฏิกิริยาของเอนไซม์ 5 $\alpha$ -รีดักเทสถูกตรวจสอบด้วยเทคนิคโมเลกุลาร์ดีค็อกกิง โดยทำการศึกษากับยา เช่น ฟินาสเทอไรด์ และดูเทสเทอไรด์ และสารที่ถูกรายงานว่ามีความสามารถในการยับยั้งเอนไซม์ 5 $\alpha$ -รีดักเทส จากการศึกษาก่อนหน้านี้พบว่า avicequinone C ซึ่งเป็นสารในกลุ่มฟุราโนแนพโทควิโนนสามารถยับยั้งเอนไซม์ 5 $\alpha$ -รีดักเทส ชนิดที่ 1 โดยมีค่า  $IC_{50} = 9.94 \mu\text{g/ml}$  งานวิจัยนี้จึงมีสมมุติฐานว่าโครงสร้างฟุราโนแนพโทควิโนนมีความสำคัญต่อฤทธิ์ยับยั้งเอนไซม์ 5 $\alpha$ -รีดักเทส สารกลุ่มฟุราโนแนพโทควิโนนและแนพโทควิโนนจากธรรมชาติจึงถูกนำมาศึกษาเพื่อทำนายแนวโน้มการยับยั้งเอนไซม์ 5 $\alpha$ -รีดักเทส ชนิดที่ 1 ด้วยเทคนิคโมเลกุลาร์ดีค็อกกิงโดยใช้โปรแกรม Autodock Vina กับโครงสร้าง 3 มิติของเอนไซม์ 5 $\alpha$ -รีดักเทส ชนิดที่ 1 และ 2 ที่คำนวณขึ้น ผลการศึกษาพบว่า avicequinone C มีค่าอันตรกิริยาในการเข้าจับกับบริเวณเร่งปฏิกิริยาของเอนไซม์ 5 $\alpha$ -รีดักเทสดีที่สุดในนั้น avicequinone C และอนุพันธ์ได้ถูกสังเคราะห์ขึ้นด้วยกระบวนการทางเคมีเพื่อศึกษาฤทธิ์ในการยับยั้งเอนไซม์ 5 $\alpha$ -รีดักเทส ในเซลล์ที่มีชีวิต โดยทำการศึกษาร่วมกับสารแนพโทควิโนนจากธรรมชาติ เซลล์ HaCaT ได้ถูกนำมาใช้ในการศึกษาฤทธิ์ยับยั้งเอนไซม์ 5 $\alpha$ -รีดักเทส จากผลการศึกษาพบว่าสาร 2-hydroxy-1,4-naphthoquinone มีฤทธิ์ในการยับยั้งเอนไซม์ 5 $\alpha$ -รีดักเทสดีที่สุดในนั้น โดยมีการยับยั้ง  $82.73 \pm 14.42 \%$  ที่  $40 \mu\text{M}$  และมีค่า  $IC_{50} = 23.93 \mu\text{M}$  โดย 2-hydroxy-1,4-naphthoquinone แสดงผลการยับยั้งเอนไซม์ 5 $\alpha$ -รีดักเทสได้ดีกว่าจากนั้น avicequinone C จากผลการศึกษาโมเลกุลาร์ดีค็อกกิงและการศึกษาฤทธิ์ยับยั้งเอนไซม์ 5 $\alpha$ -รีดักเทสในเซลล์ HaCaT สามารถสรุปได้ว่าโครงสร้างแนพโทควิโนนมีความสำคัญต่อฤทธิ์การยับยั้งเอนไซม์ 5 $\alpha$ -รีดักเทส และโครงสร้าง 3 มิติของเอนไซม์ 5 $\alpha$ -รีดักเทส ชนิดที่ 1 ที่สร้างขึ้นในการศึกษานี้สามารถนำไปใช้เพื่อการค้นหาและพัฒนาสารยับยั้งเอนไซม์ 5 $\alpha$ -รีดักเทสได้ในอนาคต

ภาควิชา เกษศาสตร์และเภสัชพฤกษศาสตร์

ลายมือชื่อนิสิต .....

สาขาวิชา เกษศาสตร์

ลายมือชื่อ อ.ที่ปรึกษาหลัก .....

ปีการศึกษา 2558

ลายมือชื่อ อ.ที่ปรึกษาร่วม .....

ลายมือชื่อ อ.ที่ปรึกษาร่วม .....



# # 5676233433 : MAJOR PHARMACOGNOSY

KEYWORDS: ANDROGENIC DISORDERS / HOMOLOGY MODELING / AVICEQUINONE C / LAWSONE / HACAT / FURANONAPHTHOQUINONE / NAPHTHOQUINONE / 5-ALPHA REDUCTASE

WIRANPAT KARNSOMWAN: SYNTHESIS OF AVICEQUINONE C AND ANALOGS TOWARD THE STUDY OF 5 $\alpha$ -REDUCTASE INHIBITORY ACTIVITY. ADVISOR: ASSOC. PROF. WANCHAI DE-EKNAMKUL, Ph.D., CO-ADVISOR: SUPAKARN CHAMNI, Ph.D., THANYADA RUNGROTMONGKOL, Ph.D., 150 pp.

Steroid 5 $\alpha$ -reductase (5 $\alpha$ -R) or 3-oxo-5 $\alpha$ -steroid  $\Delta^4$ -reductase, is an enzyme having 3 isozymes, which involves in steroid metabolism. It converts testosterone (T) to dihydrotestosterone (DHT) with the aid of NADPH as a cofactor. 5 $\alpha$ -R plays an important role in several human diseases such as prostate cancer, benign prostatic hyperplasia, acne, hirsutism and androgenic alopecia. To date, the three-dimensional structure of 5 $\alpha$ -R has not been available due to structural instability during the protein crystallization. In this study, we performed the *in silico* three-dimensional 5 $\alpha$ -R1 and 5 $\alpha$ -R2 homology modeling using SWISS-MODEL and the isoprenylcysteine carboxyl methyltransferase (ICMT, PDB code: 4A2N) was selected as a homologous protein template. The catalytic site of 5 $\alpha$ -R was verified by molecular docking simulation with 5 $\alpha$ -R inhibitors including the known drugs such as finasteride and dutasteride and a series of reported 5 $\alpha$ -R inhibitors. According to the previous study, avicequinone C, which is a furanonaphthoquinone, showed 5 $\alpha$ -R1 inhibitory activity with  $IC_{50} = 9.94 \mu\text{g/ml}$ . Therefore, we hypothesized that furanonaphthoquinone moiety potentially an essential pharmacophore controlling 5 $\alpha$ -R inhibitory activity. A series of avicequinone C and analogs and natural naphthoquinones were studied to evaluate for 5 $\alpha$ -R1 inhibiting potency by molecular docking simulations using Autodock Vina in conjugation with the resulting *in silico* three-dimensional 5 $\alpha$ -R1 and 5 $\alpha$ -R2. The results showed that avicequinone C displayed the best protein-ligand binding interactions at 5 $\alpha$ -R catalytic region. Next, avicequinone C and analogs were synthesized by chemical process for *in vitro* 5 $\alpha$ -R inhibitory assay along with natural naphthoquinones. HaCaT cell line was used for 5 $\alpha$ -R inhibitory activity investigation. The results showed that 2-hydroxy-1,4-naphthoquinone was the most potent 5 $\alpha$ -R inhibitor. It exhibited  $82.73 \pm 14.42$  %inhibition at  $40 \mu\text{M}$  with  $IC_{50} = 23.93 \mu\text{M}$ . Importantly, 2-hydroxy-1,4-naphthoquinone showed stronger 5 $\alpha$ -R inhibition than avicequinone C. Considering molecular docking together with the *in vitro* 5 $\alpha$ -R inhibitory assay toward HaCaT cell line, we found that the naphthoquinone motif is crucial for 5 $\alpha$ -R inhibitory activity. Moreover, the resulting *in silico* three-dimensional 5 $\alpha$ -R1 would be used for virtual screening and development of 5 $\alpha$ -reductase (5 $\alpha$ -R) in the future.

Department:	Pharmacognosy and Pharmaceutical	Student's Signature .....
	Botany	Advisor's Signature .....
Field of Study:	Pharmacognosy	Co-Advisor's Signature .....
Academic Year:	2015	Co-Advisor's Signature .....

## ACKNOWLEDGEMENTS

I would like to express my thankfulness to my advisor, Assoc. Prof. Dr.Wanchai De-eknamkul and my co-advisor, Dr.Supakarn Chamni of the Department of Pharmacognosy and Pharmaceutical Botany, Faculty of Pharmaceutical Sciences, for their counseling, encouragements, guidance and support throughout this thesis. Without their kindness and understanding this work could not be accomplished.

I also would like to express my appreciation to my co-advisor Dr. Thanyada Rungrotmongkol, of the Department of Biochemistry, Faculty of Science, Chulalongkorn University, for her support, guidance and help in the completion of this work.

I would like to thank all of my thesis committee for their constructive suggestion and useful discussion.

I would like to thank all staff members and graduate students of the Department of Pharmacognosy and Pharmaceutical Botany, Faculty of Pharmaceutical Sciences, Chulalongkorn University for their helpful advice, nice friendship, and kind cooperation.

Finally, I wish to express my gratitude to my beloved family for their love, care, support and encouragement which has enabled me to successfully complete my thesis.

## CONTENTS

	Page
THAI ABSTRACT .....	iv
ENGLISH ABSTRACT .....	v
ACKNOWLEDGEMENTS .....	vi
CONTENTS .....	vii
List of Tables .....	xi
List of Figures.....	xiii
List of Abbreviations.....	xvii
Chapter I Introduction .....	1
1.1 Background.....	2
1.2 Objectives.....	5
1.3 Scope of study .....	5
1.4 Research design and methods.....	6
Chapter II Literature Review .....	7
2.1 Biology of 5 $\alpha$ -reductase.....	8
2.1.1 Sequences and isozymes.....	8
2.1.2 Biochemical properties.....	8
2.2 Mechanisms of 5 $\alpha$ -reductase.....	10
2.3 Clinical roles of 5 $\alpha$ -reductase.....	11
2.4 5 $\alpha$ -Reductase Inhibitors .....	13
2.4.1 Steroidal 5 $\alpha$ -R Inhibitors.....	13
2.4.2 Non-steroidal 5 $\alpha$ -R Inhibitors.....	17
2.4.3 Natural products and plant extracts .....	20

	Page
Chapter III Homology modeling of 5 $\alpha$ -Reductase Type I & II .....	23
3.1 Introduction.....	24
3.2 Materials and methods.....	27
3.2.1 Homology modeling .....	27
3.2.2 Structure evaluation .....	28
3.2.3 Active site identification.....	29
3.2.4 Transmembrane site prediction .....	29
3.2.5 Docking study of known 5 $\alpha$ -R inhibitors .....	30
3.3 Results and discussion.....	32
3.3.1 Predicted three-dimensional structure of 5 $\alpha$ -R1 and 5 $\alpha$ -R2.....	32
3.3.2 Ramachandran Plot.....	40
3.3.3 Catalytic pocket and transmembrane site.....	41
3.3.4 Docking studies of 5 $\alpha$ -R1 with known 5 $\alpha$ -R inhibitors .....	47
3.3.5 Docking studies of 5 $\alpha$ -R2 with known 5 $\alpha$ -R inhibitors .....	52
3.4 Conclusions.....	58
Chapter IV Molecular Docking of Avicquinone C and Analogs.....	60
4.1 Introduction.....	61
4.1.1 Ligand-based drug design .....	61
4.1.2 Structure-based drug design .....	62
4.1.3 Molecular docking.....	62
4.1.4 Example of computational aided drug design researches.....	62
4.2 Materials and methods.....	63
4.3 Results and discussion.....	64

	Page
4.3.1 Docking studies of 5 $\alpha$ -R1.....	64
4.3.2 Docking studies of 5 $\alpha$ -R2.....	70
4.4 Conclusions.....	76
Chapter V Synthesis of Avicequinone C and Analogs .....	77
5.1 Introduction.....	78
5.2 Material and methods .....	80
5.3 Synthesis of avicequinone C and analogs .....	81
5.3.1 Synthesis of 2-propionylnaphtho[2,3-b]furan-4,9-dione (5.8, WNK-1) .81	
5.3.2 Synthesis of 2-acetyl-2,3-dihydronaphtho[2,3-b]furan-4,9-dione (5.10, WNK-3)82	
5.3.3 Synthesis of 2-acetylnaphtho[2,3-b]furan-4,9-dione (5.11, WNK-4).....83	
5.3.4 Synthesis of avicequinone C (5.2, WNK-5).....85	
5.3.5 Synthesis of 2-(2-hydroxypropan-2-yl)-2,3-dihydronaphtho[2,3-b]furan-4,9-dione (5.12, WNK-6).....85	
5.3.6 Synthesis of naphtho[2,3-b]furan-4,9-dione (5.14, WNK-7) .....86	
5.4 Spectroscopic data of synthetic avicequinone C and analogs.....88	
5.4.1 2-Propionylnaphtho[2,3-b]furan-4,9-dione (5.8, WNK-1).....88	
5.4.2 2-Acetyl-2,3-dihydronaphtho[2,3-b]furan-4,9-dione (5.10, WNK-3).....89	
5.4.3 2-Acetylnaphtho[2,3-b]furan-4,9-dione (5.11, WNK-4) .....90	
5.4.4 2-(2-Hydroxypropan-2-yl)naphtho[2,3-b]furan-4,9-dione (Avicequinone C, 5.2, WNK-5).....91	
5.4.5 2-(2-Hydroxypropan-2-yl)-2,3-dihydronaphtho[2,3-b]furan-4,9-dione (5.12, WNK-6) .....92	
5.4.6 Naphtho[2,3-b]furan-4,9-dione (5.14, WNK-7) .....93	

	Page
5.5 Results and discussion.....	93
5.6 Conclusions.....	97
Chapter VI Evaluation of <b>5<math>\alpha</math></b> -Reductase Inhibitory Activity <i>via</i> HaCaT Cell-line Assay.....	98
6.1 Introduction.....	99
6.2 Material and methods .....	100
6.2.1 Culturing of HaCaT cells.....	100
6.2.2 Cytotoxicity of avicequinone C and analogs and natural naphthoquinones against HaCaT cell line.....	100
6.2.3 <b>5<math>\alpha</math></b> -reductase inhibitory activity of avicequinone C and analogs and natural naphthoquinones by HaCaT cell-based assay .....	102
6.3 Results and discussion.....	103
6.3.1 Cytotoxic activity evaluation of avicequinone C and analogs and natural naphthoquinones against HaCaT cell line .....	103
6.3.2 The standard curve of <b>5<math>\alpha</math></b> -DHT .....	106
6.3.3 Analysis of <b>5<math>\alpha</math></b> -reductase inhibitory activity of avicequinone C and analogs and natural naphthoquinones using HaCaT cell-based assay .....	107
6.3.4 IC <sub>50</sub> values of 2-hydroxy-1,4-naphthoquinone (6.9).....	111
6.4 Conclusions.....	113
Chapter VII Conclusions.....	114
REFERENCES .....	116
APPENDIX.....	125
VITA.....	150

## List of Tables

<b>Table 1</b> Amino acid sequence similarity of 5 $\alpha$ -R isozymes .....	9
<b>Table 2</b> Amino acid sequence identity of 5 $\alpha$ -R isozymes.....	9
<b>Table 3</b> Summary of steroidal 5 $\alpha$ -R inhibitors.....	16
<b>Table 4</b> Summarize of non-steroidal 5 $\alpha$ -R inhibitors .....	18
<b>Table 5</b> Summary of natural products and plant extracts isolated from medicinal plants .....	20
<b>Table 6</b> List of popular online protein structure prediction program.....	26
<b>Table 7</b> Free online web servers used for generated the in silico structures of the.....	28
<b>Table 8</b> Resulting in silico 5 $\alpha$ -R1 structures from web based servers .....	32
<b>Table 9</b> Resulting in silico 5 $\alpha$ -R2 structures from web based servers .....	34
<b>Table 10</b> Comparison of sequence identities and similarities between 5 $\alpha$ -R1 sequences and the template sequences.....	37
<b>Table 11</b> Comparison of sequence identities and similarities between 5 $\alpha$ -R2 sequences and the template sequences.....	38
<b>Table 12</b> Sequence alignment of 5 $\alpha$ -R1 and 5 $\alpha$ -R2 with isoprenylcysteine carboxyl methyltransferase (ICMT) and 5 $\beta$ -reductase .....	40
<b>Table 13</b> Docking studies of the in silico 5 $\alpha$ -R1 with NADPH and ligands.....	42
<b>Table 14</b> Docking studies of the in silico 5 $\alpha$ -R2 with NADPH and ligands.....	42
<b>Table 15</b> Docking studies of the in silico 5 $\alpha$ -R1 with known 5 $\alpha$ -R inhibitors .....	48
<b>Table 16</b> Docking studies of the in silico 5 $\alpha$ -R2 with known 5 $\alpha$ -R inhibitors .....	53
<b>Table 17</b> Docking studies of 5 $\alpha$ -R1 with avicequinone C and analogs.....	66
<b>Table 18</b> Docking studies of 5 $\alpha$ -R2 with avicequinone C and analogs.....	72

<b>Table 19</b> Reported biological activities of avicequinone C .....	78
<b>Table 20</b> NMR spectral data of WNK-5 (in CDCl <sub>3</sub> ) and avicequinone C (in CDCl <sub>3</sub> ) .	95
<b>Table 21</b> NMR spectral data of WNK-7 (in CDCl <sub>3</sub> ) and avicequinone B (in CDCl <sub>3</sub> )..	96
<b>Table 22</b> 5 $\alpha$ -Reductase inhibitory activity of selected naphthoquinones toward HaCaT cell-based assay .....	110





## List of Figures

<b>Figure 1</b> Conversion of testosterone to 5 $\alpha$ -dihydrotestosterone by steroidal 5 $\alpha$ -reductase.....	2
<b>Figure 2</b> (a) Non-radioactive HPTLC: dose-dependent response of avicequinone C at 1.25, 2.5, 5 and 10 $\mu$ g/mL (25.5%, 33.2%, 36.3% and 52% inhibition, respectively). Cell+T is the internal control and Cell-T is the negative control. (b) Structure of avicequinone C.....	4
<b>Figure 3</b> Mechanism of androgen action within cells [12].....	10
<b>Figure 4</b> Formation of dihydrotestosterone by steroid 5 $\alpha$ -reductase.....	11
<b>Figure 5</b> Structure of compounds isolated from medicinal plants .....	22
<b>Figure 6</b> A-ring metabolism: 5 $\alpha$ - and 5 $\beta$ - reduction of 3-keto-4-ene steroids.....	24
<b>Figure 7</b> Structures of NADPH (3.4), finasteride (3.5), and dutasteride (3.6).....	29
<b>Figure 8</b> Chemical structures of known 5 $\alpha$ -reductase inhibitors used for docking studies.....	30
<b>Figure 9</b> a) Sequence alignment between 5 $\alpha$ -R1 and isoprenylcysteine carboxyl methyltransferase b) Sequence alignment between 5 $\alpha$ -R2 and isoprenylcysteine carboxyl methyltransferase .....	39
<b>Figure 10</b> a) Ramachandran plot of in silico 5 $\alpha$ -R1 structure b) Ramachandran plot of in silico 5 $\alpha$ -R2 structure.....	41
<b>Figure 11</b> Ternary complex of the in silico 5 $\alpha$ -R1 with NADPH and dutasteride; a) 3D complex structure of 5 $\alpha$ -R1, NADPH and dutasteride b) 3D-diagram displaying a catalytic site; c) 2D-diagram displaying the binding interactions [46].....	44
<b>Figure 12</b> Ternary complex of the in silico 5 $\alpha$ -R2 with NADPH and dutasteride; a) 3D complex structure of 5 $\alpha$ -R2, NADPH and dutasteride b) 3D-diagram displaying a catalytic site; c) 2D-diagram displaying the binding interactions [45].....	45

<b>Figure 13</b> Transmembrane prediction; a) in silico 5 $\alpha$ -R1 b) in silico 5 $\alpha$ -R2.....	46
<b>Figure 14</b> Superimposition of steroidal compounds to verify the active sites of 5 $\alpha$ -R1 .....	52
<b>Figure 15</b> 2D-diagram displayed the binding interactions of 5 $\alpha$ -R2 with ligands;..	57
<b>Figure 16</b> Superimposition of steroidal compounds to verify the active sites of 5 $\alpha$ -R2 .....	58
<b>Figure 17</b> Structures of HIV inhibitors: VEC5 and RN8 .....	63
<b>Figure 18</b> Ternary complex of the in silico 5 $\alpha$ -R1 with NADPH and avicequinone C a) 3D-diagram displayed a catalytic site; c) 2D-diagram displayed the binding interactions.....	69
<b>Figure 19</b> Superimposition of dutasteride, avicequinone C and analogs and natural naphthoquinones with 5 $\alpha$ -R1.....	70
<b>Figure 20</b> Ternary complex of the in silico 5 $\alpha$ -R2 with NADPH and avicequinone C a) 3D-diagram displayed a catalytic site; c) 2D-diagram displayed the binding interactions.....	75
<b>Figure 21</b> Superimposition of dutasteride, avicequinone C and analogs and natural naphthoquinones with 5 $\alpha$ -R2.....	76
<b>Figure 22</b> Synthesis of avicequinone C from lapachol .....	79
<b>Figure 23</b> Synthesis of avicequinone C and analogs .....	80
<b>Figure 24</b> Synthesis of 2-propionyl-naphtho[2,3-b]furan-4,9-dione (5.8, WNK-1) ....	82
<b>Figure 25</b> Synthesis of 2-acetyl-2,3-dihydronaphtho[2,3-b]furan-4,9-dione.....	83
<b>Figure 26</b> Synthesis of 2-acetylnaphtho[2,3-b]furan-4,9-dione (5.11, WNK-4).....	84
<b>Figure 27</b> Synthesis of avicequinone C (5.2, WNK-5).....	85
<b>Figure 28</b> Synthesis of 2-(2-hydroxypropan-2-yl)-2,3-dihydronaphtho[2,3-b]furan-4,9-dione (5.12, WNK-6).....	86
<b>Figure 29</b> Synthesis of naphtho[2,3-b]furan-4,9-dione (5.14, WNK-7).....	87

<b>Figure 30</b> Structures of avicequinone C and analogs (6.1-6.6), natural naphthoquinones (6.7-6.9), non-naphthoquinones (6.10 and 6.11) and dutasteride (6.12).....	101
<b>Figure 31</b> 6-well plate diagram of HaCaT cell-based assay.....	102
<b>Figure 32</b> Cytotoxic activity evaluation against HaCaT cell line: a) Avicequinone C and analogs, b) Natural naphthoquinones, c) Non-naphthoquinones, and d) Dutasteride.....	104
<b>Figure 33</b> Standard Curve of 5 $\alpha$ -DHT.....	107
<b>Figure 34</b> Preliminary screening of 5 $\alpha$ -reductase inhibitory activity of test compounds by HPTLC a) Avicequinone C and analogs, b) Natural naphthoquinones and non-naphthoquinones.....	108
<b>Figure 35</b> Analysis of %inhibition at maximum concentrations without cytotoxicity of selected compounds by HPTLC.....	109
<b>Figure 36</b> Analysis of 5 $\alpha$ -R inhibitory activity (IC <sub>50</sub> ) of 2-hydroxy-1,4-naphthoquinone by HPTLC.....	112
<b>Figure 37</b> 5 $\alpha$ -R inhibitory activity (IC <sub>50</sub> ) curve of 2-hydroxy-1,4-naphthoquinone (6.9).....	112
<b>Figure 38</b> Mass spectrum of WNK-1.....	126
<b>Figure 39</b> IR spectrum of WNK-1.....	127
<b>Figure 40</b> <sup>1</sup> H NMR (300 MHz) spectrum of WNK-1.....	128
<b>Figure 41</b> <sup>13</sup> C NMR (300 MHz) spectrum of WNK-1.....	128
<b>Figure 42</b> COSY spectrum of WNK-1.....	129
<b>Figure 43</b> Mass spectrum of WNK-3.....	130
<b>Figure 44</b> IR spectrum of WNK-3.....	131
<b>Figure 45</b> <sup>1</sup> H NMR (300 MHz) spectrum of WNK-3.....	132
<b>Figure 46</b> <sup>13</sup> C NMR (300 MHz) spectrum of WNK-3.....	132

<b>Figure 47</b> COSY spectrum of WNK-3 .....	133
<b>Figure 48</b> Mass spectrum of WNK-4 .....	134
<b>Figure 49</b> IR spectrum of WNK-4.....	135
<b>Figure 50</b> $^1\text{H}$ NMR (300 MHz) spectrum of WNK-4.....	136
<b>Figure 51</b> $^{13}\text{C}$ NMR (300 MHz) spectrum of WNK-4 .....	136
<b>Figure 52</b> COSY spectrum of WNK-4 .....	137
<b>Figure 53</b> Mass spectrum of WNK-5 .....	138
<b>Figure 54</b> IR spectrum of WNK-5.....	139
<b>Figure 55</b> $^1\text{H}$ NMR (300 MHz) spectrum of WNK-5.....	140
<b>Figure 56</b> $^{13}\text{C}$ NMR (300 MHz) spectrum of WNK-5 .....	140
<b>Figure 57</b> COSY spectrum of WNK-5 .....	141
<b>Figure 58</b> Mass spectrum of WNK-6 .....	142
<b>Figure 59</b> IR spectrum of WNK-4.....	143
<b>Figure 60</b> $^1\text{H}$ NMR (300 MHz) spectrum of WNK-6.....	144
<b>Figure 61</b> $^{13}\text{C}$ NMR (300 MHz) spectrum of WNK-6 .....	144
<b>Figure 62</b> COSY spectrum of WNK-6 .....	145
<b>Figure 63</b> Mass spectrum of WNK-7 .....	146
<b>Figure 64</b> IR spectrum of WNK-7 .....	147
<b>Figure 65</b> $^1\text{H}$ NMR (300 MHz) spectrum of WNK-7.....	148
<b>Figure 66</b> $^{13}\text{C}$ NMR (300 MHz) spectrum of WNK-7.....	148
<b>Figure 67</b> COSY spectrum of WNK-7 .....	149

## List of Abbreviations

5 $\alpha$ -R	5 $\alpha$ -Reductase
5 $\alpha$ -R1	5 $\alpha$ -Reductase type 1
5 $\alpha$ -R2	5 $\alpha$ -Reductase type 2
5 $\alpha$ -R3	5 $\alpha$ -Reductase type 3
T	Testosterone
5 $\alpha$ -DHT	5 $\alpha$ -Dihydrotestosterone
HHDPCs	Human hair dermal papilla cells
HaCaT	Cultured human keratinocyte cell line
HREs	Specific hormone response elements
BPH	Benign prostatic hyperplasia
5 $\beta$ -R	5 $\beta$ -Reductase
ICMT	Isoprenylcysteine carboxyl methyltransferase
THF	Tetrahydrofuran
DBU	1,8-Diazabicycloundec-7-ene
TLC	Thin Layer Chromatography
HPTLC	High Performance Thin Layer Chromatography
DMEM	Dulbecco's Modified Medium
FBS	Fetal Bovine Serum
Abs	Absorbance
Ac	Area of 5 $\alpha$ -DHT obtained from internal control
At	Area of 5 $\alpha$ -DHT obtained from test compound
DU	Dutasteride
COU	4-Hydroxycoumarin
NAP	2-Hydroxy-1,4-naphthoquinone
BEN	2,5-Dihydroxy-1,4-benzoquinone
ANT	1,4-Dihydroxyanthraquinone
LAPA	Lapachol

## Chapter I

### Introduction

#### Contents

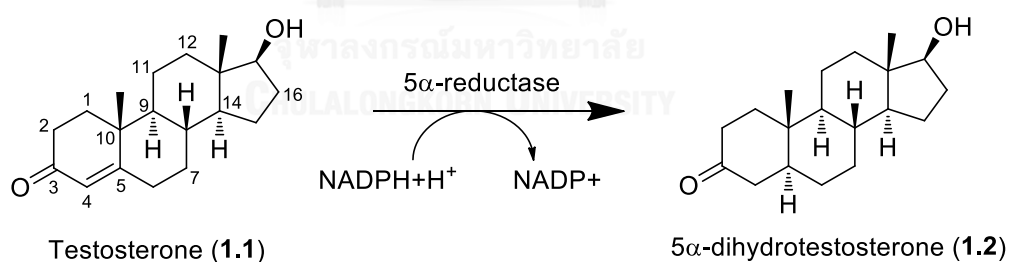
- 1.1 Background
- 1.2 Objectives
- 1.3 Scope of the study
- 1.4 Research design and methods



## 1.1 Background

Steroid  $5\alpha$ -reductase ( $5\alpha$ -R) or 3-oxo- $5\alpha$ -steroid is an enzyme in the oxidoreductase family. To date, three isozymes of  $5\alpha$ -R have been reported including  $5\alpha$ -reductase type 1 ( $5\alpha$ -R1),  $5\alpha$ -reductase type 2 ( $5\alpha$ -R2), and  $5\alpha$ -reductase type 3 ( $5\alpha$ -R3).  $5\alpha$ -R1 and  $5\alpha$ -R2 are the NADPH-dependent membrane-microsomal enzymes, which consist of 259 and 254 amino acids, respectively.  $5\alpha$ -R1 specifically locates in scalp, non-genital skin, sebaceous gland and liver, while  $5\alpha$ -R2 is mainly found in prostate gland, testis, epididymis and scrotum [1]. Recently,  $5\alpha$ -R3, which consists of 319 amino acids, has been initially found in benign and malignant tissues [2].

In the steroidogenesis pathway, mode of  $5\alpha$ -R action is to convert testosterone (T, **1.1**) into  $5\alpha$ -dihydrotestosterone ( $5\alpha$ -DHT, **1.2**) with the aid of NADPH as a cofactor (**Figure 1**). Under this condition, hydride anion ( $H^-$ ) is stereospecifically added to carbon 5 of T (**1.1**), which results in the  $\alpha$ -face attack of hydride at carbon 5 leading to form  $5\alpha$ -DHT (**1.2**) as the desired product, which is a more potent androgen than T (**1.1**) with 2-5 fold stronger activity [1].



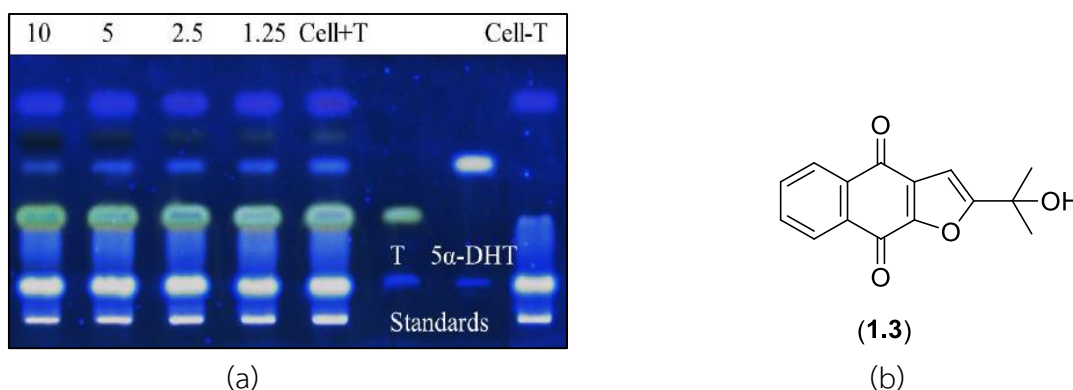
**Figure 1** Conversion of testosterone to  $5\alpha$ -dihydrotestosterone by steroidal  $5\alpha$ -reductase

Equilibrium between T and  $5\alpha$ -DHT has played an important role in the pathogenesis of various diseases. Overproduction of  $5\alpha$ -DHT has been found to involve in androgenic disorders such as prostate cancer, benign prostatic hyperplasia, acne, hirsutism, and androgenic alopecia [1]. Therefore, one of the most efficient

treatments for these androgenic disorders is to block 5 $\alpha$ -R action with suitable inhibitors [1]. Presently, finasteride and dutasteride are the two FDA-approved synthetic drugs used as 5 $\alpha$ -R inhibitors for treating androgenic disorders. Finasteride is a 5 $\alpha$ -R2 inhibitor, which enables to perform 71% suppression of serum 5 $\alpha$ -DHT [3]. However, finasteride has unpleasant side effects such as impotence and abnormal ejaculation, which physically and mentally impact the quality of patient's life [4]. In addition, dutasteride is an inhibitor for both 5 $\alpha$ -R1 and 5 $\alpha$ -R2, which can reduce serum 5 $\alpha$ -DHT concentration by 94.7% [3]. Although dutasteride showed stronger serum 5 $\alpha$ -DHT suppression than finasteride. Gynecomastia was observed as a major side effect [4]. Thus, the development of novel therapeutic candidates that possess more efficacy and less adverse effect is currently an essential need for the treatments.

Recently, Jain and co-workers have isolated avicequinone C (**1.3**), a furanonaphthoquinone from *Avicennia marina* and reported 5 $\alpha$ -R1 inhibitory activities in micromolar scale toward human hair dermal papilla cells (HHDPCs) (**Figure 2**) [5]. Even though the 5 $\alpha$ -R1 inhibitory activity of avicequinone C is not as potent as dutasteride, the discovery of a new chemical scaffold has provided a new future for the development of potential 5 $\alpha$ -R inhibitors.





**Figure 2** (a) Non-radioactive HPTLC: dose-dependent response of avicequinone C at 1.25, 2.5, 5 and 10  $\mu\text{g/mL}$  (25.5%, 33.2%, 36.3% and 52% inhibition, respectively). Cell+T is the internal control and Cell-T is the negative control. (b) Structure of avicequinone C

Regarding the importance of  $5\alpha\text{-R}$  toward human morbidity such as androgenic alopecia and cancer, searching for specific  $5\alpha\text{-R}$  inhibitors is still essential. However, the single crystal structure of  $5\alpha\text{-R}$  has remained unknown, which has caused the delay of discovery and development of  $5\alpha\text{-R}$  inhibitors. Moreover, the accurate computational guided drug design has not been conducted. Attempts to produce high quality  $5\alpha\text{-R}$  single crystal structure have failed, perhaps due to uncertain stability of the enzyme with the surfactant that was used for crystallization [6]. Therefore, our study has been started by constructing the homology models of  $5\alpha\text{-R1}$  and  $5\alpha\text{-R2}$ . The resulting *in silico* three-dimensional structures of  $5\alpha\text{-R1}$  and  $5\alpha\text{-R2}$  are used as the molecular templates for docking studies of avicequinone C and its analogs. Then, avicequinone C and interesting analogs will be synthesized along with the study of  $5\alpha\text{-R}$  inhibitory activities against cultured human keratinocytes cell line (HaCaT).

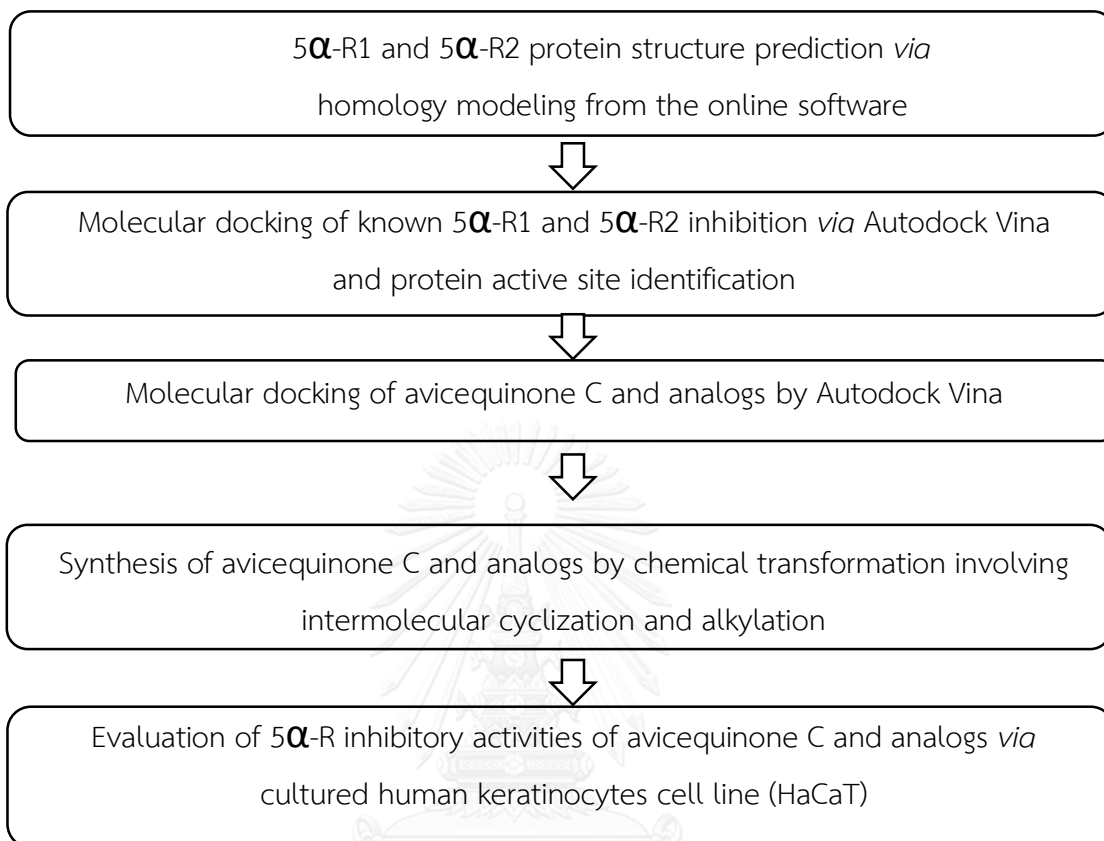
## 1.2 Objectives

- 1.2.1 Construction of the *in silico* models of 5 $\alpha$ -reductase type 1 (5 $\alpha$ -R1) and 5 $\alpha$ -reductase type 2 (5 $\alpha$ -R2) and prediction of their catalytic region
- 1.2.2 Design and synthesis of avicequinone C and analogs
- 1.2.3 Evaluation of 5 $\alpha$ -reductase inhibitory activity toward cultured human keratinocytes cell line (HaCaT) of avicequinone C and analogs and selected natural naphthoquinones,

## 1.3 Scope of study

In this study, we aim to demonstrate the homology models of 5 $\alpha$ -R1 and 5 $\alpha$ -R2 from the known single crystal structure of a homologous protein (template). The resulting *in silico* three-dimensional structure of 5 $\alpha$ -R1 and 5 $\alpha$ -R2 are validated *via* Ramachandran plot. In addition, the catalytic region and protein-ligand interactions are identified by docking simulation of known 5 $\alpha$ -R inhibitors. Molecular Docking of avicequinone C and analogs is conducted *via* Autodock Vina to identify the interaction between the ligands and the *in silico* three-dimensional structure of 5 $\alpha$ -R. Then, avicequinone C and analogs are synthesized by chemical transformations. The resulted compounds and some interesting natural naphthoquinones are evaluated for their 5 $\alpha$ -R inhibitory activities against cultured human keratinocytes cell line (HaCaT). Herein, an essential pharmacophore and inhibitory activity of new 5 $\alpha$ -R inhibitor and elaborated.

#### 1.4 Research design and methods

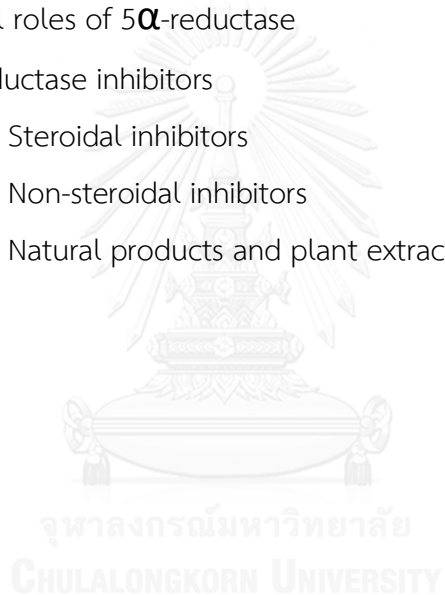


## Chapter II

### Literature Review

#### Contents

- 2.1 Biology of 5 $\alpha$ -reductase
  - 2.1.1 Sequences and isozymes
  - 2.1.2 Biochemical properties
- 2.2 Mechanisms of 5 $\alpha$ -reductase
- 2.3 Clinical roles of 5 $\alpha$ -reductase
- 2.4 5 $\alpha$ -reductase inhibitors
  - 2.4.1 Steroidal inhibitors
  - 2.4.2 Non-steroidal inhibitors
  - 2.4.3 Natural products and plant extracts



## 2.1 Biology of 5 $\alpha$ -reductase

Steroid 5 $\alpha$ -reductase or 3-oxo-5 $\alpha$ -steroid  $\Delta^4$ -reductase (EC 1.3.99.5) is an enzyme in the oxidoreductase family, which involves in the late steroidogenesis. It is an enzyme that converts T into 5 $\alpha$ -DHT by the aid of NADPH as a cofactor.

### 2.1.1 Sequences and isozymes

To date, three isozymes of 5 $\alpha$ -R have been identified as 5 $\alpha$ -R type 1, 2 and 3 (5 $\alpha$ -R1, 5 $\alpha$ -R2 and 5 $\alpha$ -R3). 5 $\alpha$ -R1 was expressed in scalp, non-genital skin, sebaceous gland, chest, adrenal glands, kidney tissues and liver, while 5 $\alpha$ -R2 was mostly found in male sexual organs, which are prostate gland, testis, epididymis and scrotum [7, 8]. Furthermore, 5 $\alpha$ -R3 has been recently documented. It was found in benign and malignant tissues in protein level and potentially relates to the formation of benign prostatic enlargement [2, 9].

### 2.1.2 Biochemical properties

The amino acid sequences of 5 $\alpha$ -R1, 5 $\alpha$ -R2, and 5 $\alpha$ -R3 are composed of 259, 254, and 318 amino acids, corresponding to molecular weight of 29.46, 28.39, and 36.52 kDa, respectively [8]. The difference of percent similarity and identity of their amino acid sequence are presented in **Table 1** and **2**, respectively.

**Table 1** Amino acid sequence similarity of 5 $\alpha$ -R isozymes

5 $\alpha$ -R isozymes	Amino acid sequence similarity (%)*		
	5 $\alpha$ -R1	5 $\alpha$ -R2	5 $\alpha$ -R3
5 $\alpha$ -R1	100	64.4	42.0
5 $\alpha$ -R2	64.4	100	45.2
5 $\alpha$ -R3	42.0	45.2	100

\*Calculated using Discovery Studio 2.5

**Table 2** Amino acid sequence identity of 5 $\alpha$ -R isozymes

5 $\alpha$ -R isozymes	Amino acid sequence identities (%)*		
	5 $\alpha$ -R1	5 $\alpha$ -R2	5 $\alpha$ -R3
5 $\alpha$ -R1	100	48.7	23.4
5 $\alpha$ -R2	48.7	100	25.0
5 $\alpha$ -R3	23.4%	25.0	100

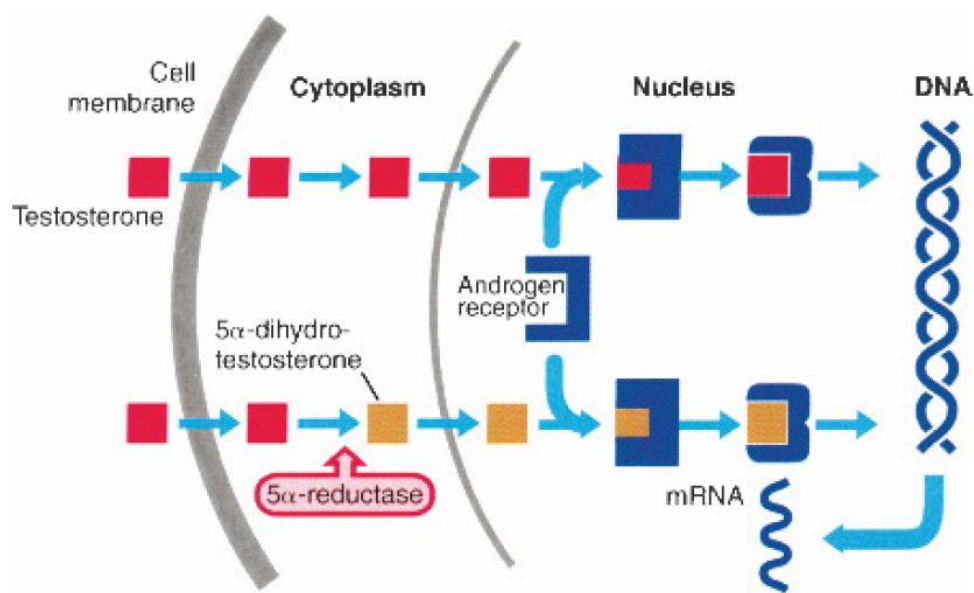
\*Calculated using Discovery Studio 2.5

5 $\alpha$ -R1 has been shown a broad pH optimum, ranging from 6.0-8.5 and has a lower substrate affinity for T,  $K_m = 1-5 \mu\text{M}$ , whereas 5 $\alpha$ -R2 exhibit a narrow acidic, ranging from pH 5.0-5.5 and is a higher substrate affinity for T,  $K_m = 0.004-1 \mu\text{M}$ . 5 $\alpha$ -R3 seems to be capable at pH 6.5-6.9 [10].

Furthermore, 5 $\alpha$ -R1 and 5 $\alpha$ -R2 are the NADPH-dependent membrane-bound enzymes. They consist of hydrophobic amino acids, which control the protein-substrate binding through the intrinsic membrane proteins deeply inside the lipid bilayer [11].

## 2.2 Mechanisms of 5 $\alpha$ -reductase

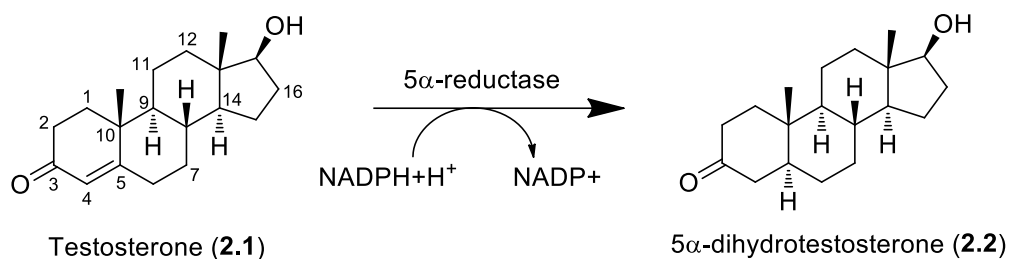
The mechanism of androgen action is shown in **Figure 3**. T generally diffuses from blood through plasma membrane and binds with androgen receptor that appears in many tissues such as skeletal muscle and axillary and pubic hair follicles. Importantly, T is converted into the more potent androgen 5 $\alpha$ -DHT by 5 $\alpha$ -R, which is located especially in the secondary sexual organs such as prostate, beard and balding hair follicles. When the 5 $\alpha$ -DHT is bound, the androgen receptor complex immediately responds by changing the conformation involving DNA binding sites, hormone-receptor complex and other connected co-activating proteins. The androgen receptor complex binds with specific hormone response elements (HREs) in the DNA, which change the expression of specific androgen-dependent genes [12].



**Figure 3** Mechanism of androgen action within cells [12].

T can be metabolized to the more potent androgen 5 $\alpha$ -DHT by 5 $\alpha$ -R. The key role of this enzyme involves the irreversible transformation of 4-en-3-oxosteroid to the corresponding 5 $\alpha$ -H-3-oxosteroid in the presence of NADPH as a hydride source

cofactor [13]. This condition leads to the stereospecific  $\alpha$ -face attack of hydride anion ( $H^-$ ) to the double bond of T (**2.1**) at C5 yielding  $5\alpha$ -DHT (**2.2**). The mechanism is shown in **Figure 4**.



**Figure 4** Formation of dihydrotestosterone by steroid  $5\alpha$ -reductase

### 2.3 Clinical roles of $5\alpha$ -reductase

$5\alpha$ -DHT is an androgen hormone that exhibits 2-5 folds higher binding affinity against androgen receptor and 10 folds higher potency toward induction signaling of androgen receptor than that of T [1]. This steroid hormone is found in various parts of human body such as prostate gland, testes, adrenal gland and hair follicles. It associates with the growth and function of sexual and general organs including utero differentiation, prostate gland growth, male external genitalia development (penis and scrotum) and growth of hair. Importantly, overexpression of steroid  $5\alpha$ -R causes overproduction of  $5\alpha$ -DHT that affects several androgenic disorders in human, which particularly increase health risks in men such as prostate cancer, benign prostatic hyperplasia, acne, hirsutism and androgenic alopecia [11, 14].



### 2.3.1 Prostate Cancer

Prostate is a gland in male, which controls the reproductive system. Prostate cancer usually develops in the peripheral zone of the human prostate. In addition, prostate luminal epithelial cells consist of the androgen receptor for T and related hormones that promote the prostate proliferation [15]. T is converted to 5 $\alpha$ -DHT promptly and irreversibly by 5 $\alpha$ -R. Next, the resulting 5 $\alpha$ -DHT binds to the androgen receptor in the cytosol and transport to the nucleus that activate a transcription factor for prostatic gene expression and prostatic cellular function [16].

### 2.3.2 Benign Prostatic Hyperplasia

Benign prostatic hyperplasia (BPH) is the benign enlargement of the prostate. BPH is associated with the excess in the number of prostatic stromal and epithelial cells, resulting in the formation of large nodules in the transition zone of the prostate [17]. Androgen (T and related hormones) plays an important role in the progression of BPH. 5 $\alpha$ -DHT is synthesized in the prostate from T by the action of 5 $\alpha$ -R2. This enzyme is located in the stromal cells, which is the main sites of the production of 5 $\alpha$ -DHT. The crucial effect of 5 $\alpha$ -DHT involves the nodular hyperplasia [18]. The treatment of BPH with 5 $\alpha$ -R inhibitors such as finasteride has successfully reduced the formation of 5 $\alpha$ -DHT, prostate volume and BPH symptoms.

### 2.3.3 Acne

Acne vulgaris is a skin condition, which frequently occurs in teenagers, in conjugation with follicular hyperkeratinization and a chronic inflammatory disease of the pilosebaceous unit. Androgen has been indicated as one of the influential factors for the follicular hyperkeratinization and stimulation of sebum production. 5 $\alpha$ -R1 is reported as the key enzyme involving acne. It is found in the keratinocytes in infrainfundibulum and epidermis in acne patients [19].

#### 2.3.4 Hirsutism

Hirsutism is the excessive hair growth in woman body, where terminal hair rarely locates such as beard or chest hair. The *in vitro* studies in genital skin of hirsute woman showed the expression of 5 $\alpha$ -R activity and high level of T [20]. T is converted to 5 $\alpha$ -DHT by 5 $\alpha$ -R2 that appears in the outer root sheath of the hair follicles [21].

#### 2.3.5 Androgenic alopecia

Androgenic alopecia is described as a form of scalp-hair loss by decreasing the growth of hair, which may lead to balding. Androgenic alopecia can happen in both male and female. Although the severity and frequency are greater in men and specific racial. The causes of androgenic alopecia are genetics and the overproduction of 5 $\alpha$ -DHT [22]. The first commercial drug for the treatment of androgenic alopecia is finasteride, which is 5 $\alpha$ -R2 inhibitor. Another 5 $\alpha$ -R inhibitor is dutasteride, which inhibits both 5 $\alpha$ -R1 and 5 $\alpha$ -R2. It is more effective than finasteride [23].

### 2.4 5 $\alpha$ -Reductase Inhibitors

With present publications, there are 2 main types of 5 $\alpha$ -R inhibitors; steroidal and non-steroidal inhibitors.

#### 2.4.1 Steroidal 5 $\alpha$ -R Inhibitors

The characteristic structure of steroidal compounds is four-fused carbon ring, which consists of six-six-six-five ring system. To date, 2 steroidal compounds are approved by FDA for the treatment of androgenic disorders including finasteride and dutasteride (**Table 3**).

#### 2.4.1.1 Finasteride (2.3)

Finasteride is the first  $5\alpha$ -R inhibitor, which have been approved by FDA for the treatment of benign prostatic hyperplasia and androgenic alopecia. It is a synthetic derivative of 4-azasteroid as a competitive inhibitor of  $5\alpha$ -R2 ( $IC_{50} = 69$  nM). This drug controls the stereospecific addition of hydride anion ( $H^-$ ) to both carbons 1 and 2 with aid of NADPH as a cofactor [24]. Although finasteride is an effective  $5\alpha$ -R inhibitor, its main side effect is loss of sexual activity, which impact to the quality of patient's life [4].

#### 2.4.1.2 Dutasteride (2.4)

Dutasteride is a potent dual inhibitor of  $5\alpha$ -R1 ( $IC_{50} = 7$  nM) and  $5\alpha$ -R2 ( $IC_{50} = 6$  nM). Dutasteride reduces the serum  $5\alpha$ -DHT better than finasteride, with 94.7% and 70.8% suppression for  $5\alpha$ -R1 and  $5\alpha$ -R2, respectively [3]. The mechanism of inhibition by dutasteride is similar to finasteride, which involves the formation of enzyme-NADPH binary complex, followed by the conjugation of dutasteride and the addition of hydride anion ( $H^-$ ) to carbon 1 and 2. The complex slowly releases from the enzyme resulting in irreversible inhibition. The major side effect of this drug is gynecomastia [4].

#### 2.4.1.3 4-MA (2.5)

4-MA is a potent dual inhibitor of  $5\alpha$ -R1 ( $IC_{50} = 1.7$  nM) and  $5\alpha$ -R2 ( $IC_{50} = 1.9$  nM) with the undesirable side effects such as impotence, impaired muscle growth and gynecomastia, as well as  $3\beta$ -hydroxysteroid dehydrogenase inhibition, which causes hepatotoxicity. Thus, this compound has been withdrawn from clinical studies [13].

#### 2.4.1.4 Turosteride (2.6)

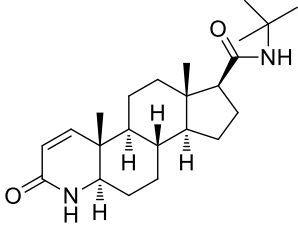
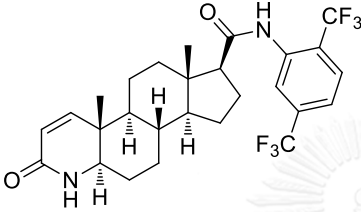
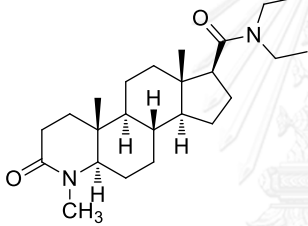
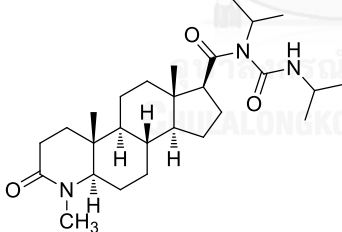
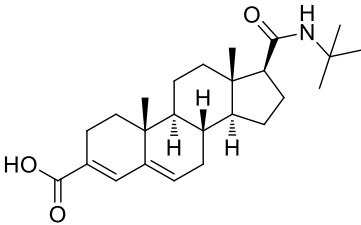
Turosteride mainly inhibits  $5\alpha$ -R2 ( $IC_{50} = 55$  nM). It is designed to reduce the side effects that occurs with the use of 4-MA. However, it shows less inhibition toward  $3\beta$ -hydroxysteroid dehydrogenase than 4-MA [13].

#### 2.4.1.5 Epristeride (2.7)

Epristeride is an androstanecarboxylic acid. It is a noncompetitive  $5\alpha$ -R2 inhibitor ( $K_i = 30$ - $36$  nM), which showed effective results in clinical study for the treatment of benign prostatic hyperplasia [13]



Table 3 Summary of steroidal 5 $\alpha$ -R inhibitors

Inhibitors	Type of inhibitors
 <p>Finasteride (2.3)</p>	5 $\alpha$ -R2 (IC <sub>50</sub> = 69 nM)
 <p>Dutasteride (2.4)</p>	5 $\alpha$ -R1 (IC <sub>50</sub> = 7 nM) 5 $\alpha$ -R2 (IC <sub>50</sub> = 6 nM)
 <p>4-MA (2.5)</p>	5 $\alpha$ -R1 (IC <sub>50</sub> = 1.7 nM) 5 $\alpha$ -R2 (IC <sub>50</sub> = 1.9 nM)
 <p>Turosteride (2.6)</p>	5 $\alpha$ -R2 (IC <sub>50</sub> = 55 nM)
 <p>Epristeride (2.7)</p>	5 $\alpha$ -R2 (K <sub>i</sub> = 30-36 nM)

## 2.4.2 Non-steroidal 5 $\alpha$ -R Inhibitors

Non-steroidal compounds have been currently developed to solve the side effects typically found when using steroidal 5 $\alpha$ -R Inhibitors. Steroid compounds generally participate in various drug interactions with several enzymes or receptors of the steroidal endocrine system. Therefore, the use of non-steroidal compounds is an alternative treatment to reduce drug interactions and serious adverse effects (**Table 4**).

### 2.4.2.1 Benzo[f]quinolones

Benzo[f]quinolones are derived from 4-azasteroid, however; the core carbon structure of these compounds consist of 3-fused six membered ring. The D ring of steroid structure is removed and the C ring is an aromatic. They are the first non-steroidal inhibitors that selectively inhibit 5 $\alpha$ -R1. LY191704 (**2.8**) is the most potent inhibitor in this group ( $IC_{50} = 8$  nM) [13].

### 2.4.2.2 Nonsteroidal aryl acids

Nonsteroidal aryl acids are androstanecarboxylic acid derivatives. They are selective non-competitive 5 $\alpha$ -R1 inhibitors interacting with positively charged enzyme-NADPH complex. KF20405 (**2.9**) is the most potent inhibitor in this series ( $IC_{50} = 0.48$  nM). The activity of nonsterodial aryl acids is 20 times more potent than finasteride [13].

### 2.4.2.3 Butanoic acid derivatives

Butanoic acid derivatives are composed of aromatic ring (benzene or indole) with butanoic acid chain. For instance, ONO-3805 (**2.10**) is a selective 5 $\alpha$ -R1 inhibitor

and FK 143 (**2.11**) is a potent dual inhibitor of  $5\alpha$ -R1 and  $5\alpha$ -R2. FK 143 is non-competitive inhibitor against human  $5\alpha$ -reductase with  $IC_{50} = 1.9$  nM [13].

#### 2.4.2.4 Polyunsaturated fatty acids

Long chain unsaturated free fatty acids (**2.12-2.15**) have been determined as potent  $5\alpha$ -R inhibitors. Due to the membrane-bound enzyme property of  $5\alpha$ -R, the inhibition of  $5\alpha$ -R by fatty acids may involve with lipid bilayer structure. However, the endogenous regulators of  $5\alpha$ -R have been remained unknown [1].

**Table 4** Summarize of non-steroidal  $5\alpha$ -R inhibitors

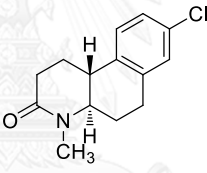
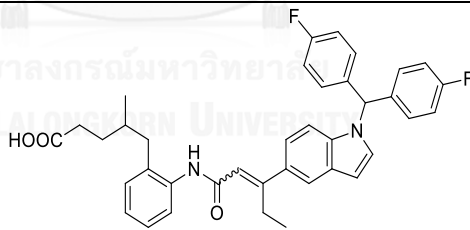
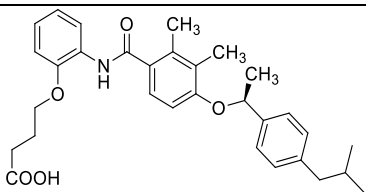
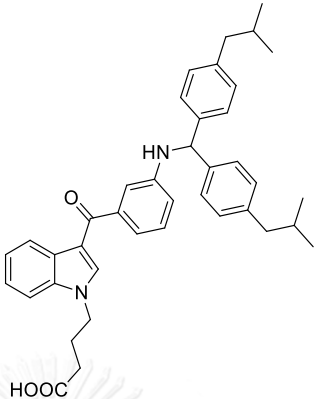
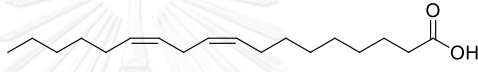
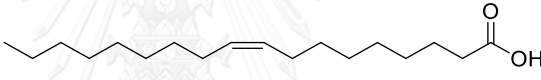

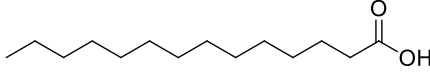
Non-steroidal compounds	Inhibitors	Type of inhibitor
Benzo[f]quinonolones	 LY191704 ( <b>2.8</b> )	$5\alpha$ -R1 ( $IC_{50} = 8$ nM) [13]
Nonsteroidal aryl acids	 KF20405 ( <b>2.9</b> )	$5\alpha$ -R1 ( $IC_{50} = 0.48$ nM) [13]
Butanoic acid derivatives	 ONO-3805 ( <b>2.10</b> )	$5\alpha$ -R1 [13]

Table 4 (Cont.) Summarize of non-steroidal 5 $\alpha$ -R inhibitors

Non-steroidal compounds	Inhibitors	Type of inhibitor
Butanoic acid derivatives	 <p style="text-align: center;">FK 143 (2.11)</p>	5 $\alpha$ -R1 and 5 $\alpha$ -R2 (human 5 $\alpha$ -R IC <sub>50</sub> = 1.9 nM) [13]
Polysaturated fatty acids	 <p style="text-align: center;">linoleic acid (2.12)</p>	5 $\alpha$ -R1 = 13 $\mu$ g/ml [1]
	 <p style="text-align: center;">Oleic acid (2.13)</p>	5 $\alpha$ -R1 = 4 $\mu$ g/ml [1]
	 <p style="text-align: center;">Lauric acid (2.14)</p>	5 $\alpha$ -R1 = 17 $\mu$ g/ml 5 $\alpha$ -R2 = 19 $\mu$ g/ml [1]
	 <p style="text-align: center;">Myristic acid (2.15)</p>	5 $\alpha$ -R2 = 4 $\mu$ g/ml [1]



### 2.4.3 Natural products and plant extracts

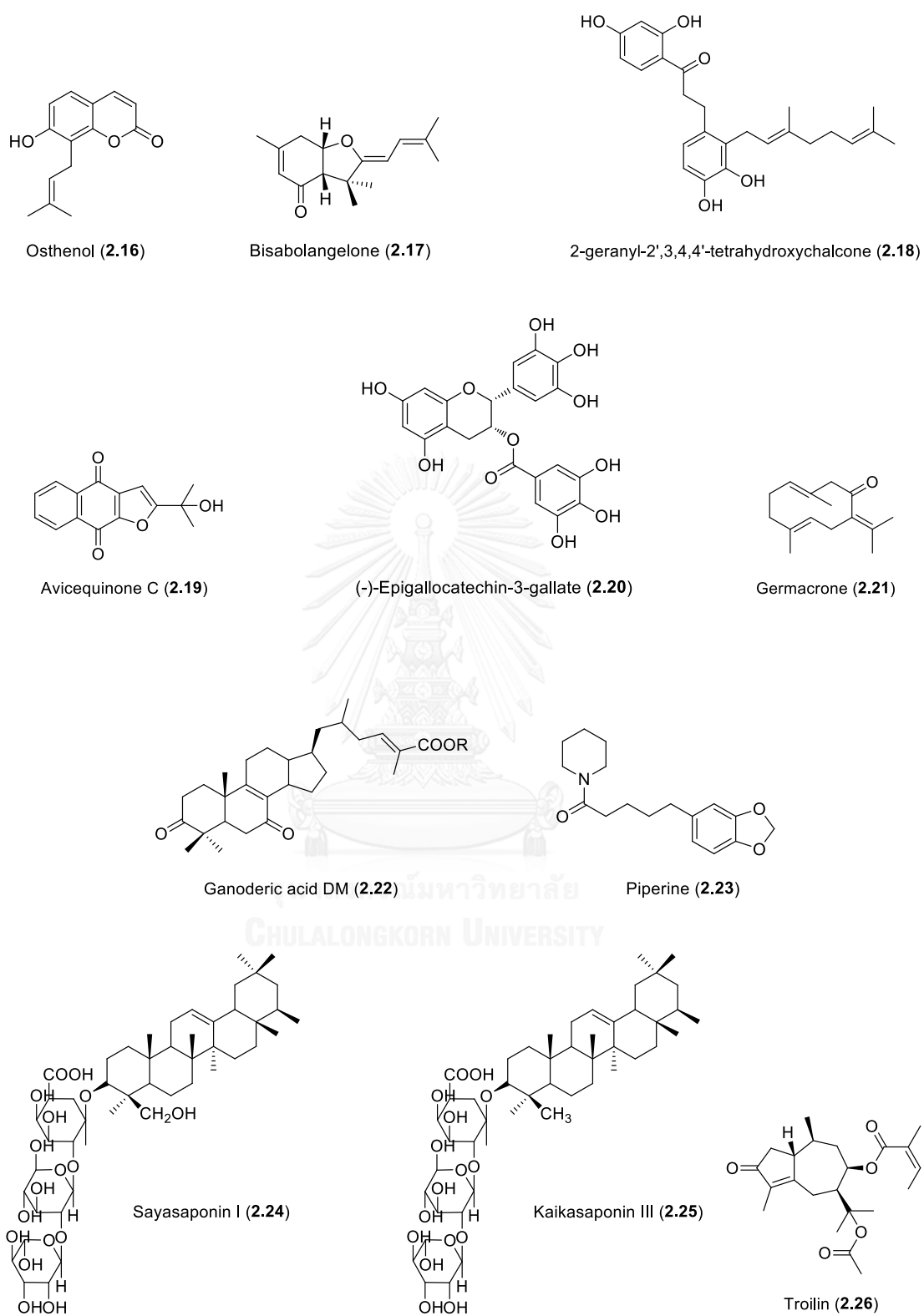
There have been many reports on some compounds and plant extracts from medicinal plants, which inhibit  $5\alpha$ -R with micro- to milli- molar range. Other compounds and plant extracts are summarized in **Table 5** and **Figure 5**.

**Table 5** Summary of natural products and plant extracts isolated from medicinal plants

Scientific Name	Compound/Extracts	Model	IC <sub>50</sub>	References
<i>Angelica Koreana</i>	Osthenol ( <b>2.16</b> ), Bisabolangelone ( <b>2.17</b> )	Prostate cancer cells	0.1 $\mu$ g/ml, 11.6 $\mu$ g/ml	Seo <i>et al.</i> , 2002 [25]
<i>Artocarpus altilis</i>	2-geranyl-2',3,4,4'- tetrahydrochalcone ( <b>2.18</b> )	Rat microsome	38 $\mu$ M	Shimizu <i>et al.</i> , 2000 [26]
<i>Avicennia marina</i>	Avicequinone C ( <b>2.19</b> )	Human hair dermal papilla cells	38.8 $\mu$ M	Jain <i>et al.</i> , 2004 [5]
<i>Camellia sinensis</i>	Epigallocate-3-gallate (EGCG, <b>2.20</b> )	Rat microsomes	$5\alpha$ -R1 = 12 $\mu$ M $5\alpha$ -R2 = 73 $\mu$ M	Hiipakka <i>et al.</i> , 2002 [27]
<i>Carthamus tinctorius</i>	Ethanollic extract	Rat microsome	FEA value = 24.30 mg	Kumar <i>et al.</i> , 2012 [28]
<i>Curcuma aeruginosa</i>	Germacrone ( <b>2.21</b> )	Prostate cancer cells	0.42 mg/ml	Suphrom <i>et al.</i> , 2012 [29]

**Table 5** (Cont.) Summary of natural products and plant extracts isolated from medicinal plants

Scientific Name	Compound/Extracts	Model	IC <sub>50</sub>	References
<i>Ganoderma lucidum</i>	Ganoderic acid DM (2.22)	Rat microsome	10.6 μM	Liu <i>et al.</i> , 2006 [30]
<i>Oryza sativa</i>	Supercritical Fluid extract	Prostate cancer cells	93.33 % inhibition	Ruksiriwanich <i>et al.</i> , 2011 [31]
<i>Piper nigrum</i>	Piperine (2.23)	Rat microsome	0.48 μM	Hirata <i>et al.</i> , 2007 [32]
<i>Pueraria flos</i>	Soyasaponin I (2.24), Kaikasaponin III (2.25)	Rat epididymis	112 μM, 61 μM	Murata <i>et al.</i> , 2012 [33]
<i>Thujae occidentalis</i>	Nonpolar fraction repeat extract with ethyl acetate	HEK293 5α-R2 cell line	IC <sub>50</sub> = 2.6 μg/ml	Park <i>et al.</i> , 2003 [34]
<i>Torilis japonica</i>	Triolin (2.26)	Rat prostate	31.7 μM	Park <i>et al.</i> , 2003 [35]



**Figure 5** Structure of compounds isolated from medicinal plants

## Chapter III

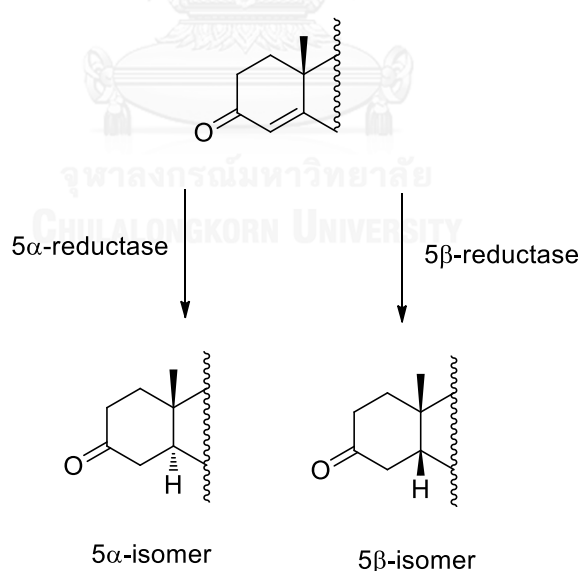
### Homology modeling of 5 $\alpha$ -Reductase Type I & II

#### Contents

- 3.1 Introduction
- 3.2 Materials and methods
  - 3.2.1 Homology modeling
  - 3.2.2 Structure evaluation
  - 3.2.3 Active site identification
  - 3.2.4 Transmembrane site prediction
  - 3.2.5 Docking studies of known 5 $\alpha$ -R inhibitors
- 3.3 Results and discussion
  - 3.3.1 Predicted three-dimensional structure of 5 $\alpha$ -R1 and 5 $\alpha$ -R2
  - 3.3.2 Ramachandran Plot
  - 3.3.3 Catalytic pocket and transmembrane site
  - 3.3.4 Docking studies of 5 $\alpha$ -R1 with known 5 $\alpha$ -R inhibitors
  - 3.3.5 Docking studies of 5 $\alpha$ -R2 with known 5 $\alpha$ -R inhibitors
- 3.4 Conclusions

### 3.1 Introduction

$5\alpha$ -R has been reported as a crucial biomolecule that associates with androgenic alopecia, through the overproduction of  $5\alpha$ -DHT (**3.2**) [1]. Today, there have been several reports on the discovery and development of new  $5\alpha$ -R inhibitors for baldness treatment, including steroid and non-steroid analogs [13]. However, most of the reported  $5\alpha$ -R inhibitors have not been designed specifically for the inhibition of  $5\alpha$ -R at the catalytic site, due to the lack of single x-ray crystal structure [36]. An up-to-date report regarding homology modeling of  $5\alpha$ -R was published by Min-Rui and co-workers by employing  $5\beta$ -reductase ( $5\beta$ -R, PDB: 3G1R) as a template protein for conducting the *in silico* three-dimensional structure of  $5\alpha$ -R [37]. However, the disadvantage of using  $5\beta$ -R as a template is the uncorrected mechanism of stereoselective hydride attack to an  $\alpha, \beta$ -unsaturated ketone of T (**3.1**) that happens on the  $\beta$ -phase, which is opposite to the result of  $5\alpha$ -reductase (**Figure 6**) [38].



**Figure 6** A-ring metabolism:  $5\alpha$ - and  $5\beta$ - reduction of 3-keto-4-ene steroids

Homology modeling is a computational technique that enable to predict the three-dimensional structure of the biological target from its original amino acid sequence and the homologous protein (template). In this method, each amino acid residue of the query sequence is aligned into the template sequence leading to the analysis of known protein structures, which potentially has a structure similar to the query sequence. The similarity of target protein and homologous protein is translated to the sequence identity. The minimum of 30% sequence identity can be accepted as a reasonable predicted protein structure, which is similar to a low-resolution X-ray structure [39]. There are 2 types of homology modeling. First, fold recognition (FR) or threading is a prediction of a protein structure, which is based on its amino acid sequence, the theory of a limited number of distinct protein folds, and a unique library of the template. Second, *ab initio* method (*ab initio*) is a prediction of the protein structure directly from the amino acid sequence. *Ab initio* method is employed to determine a suitable protein representation by using the efficient and reliable algorithms that can perform the conformation space calculation and minimize the energy function [40]. Homology modeling can be conducted by several software and web-servers. The list of online homology modeling programs web is shown in **Table 6**

**Table 6** List of popular online protein structure prediction program

Server Name	Web Address	Model building/ Confidence measure	FR/ ab initio
SWISS-MODEL	<a href="http://swissmodel.expasy.org">http://swissmodel.expasy.org</a>	Model + Confidence	FR + ab initio
Phyre	<a href="http://www.imperial.ac.uk/phyre">http://www.imperial.ac.uk/phyre</a>	Model + Confidence	FR
I-TASSER	<a href="http://zhang.bioinformatics.ku.edu/I-TASSER">http://zhang.bioinformatics.ku.edu/I-TASSER</a>	Model + Confidence	FR + ab initio
SP4	<a href="http://sparks.informatics.iupui.edu/SP4">http://sparks.informatics.iupui.edu/SP4</a>	Model + Z- score	FR
CPHModels	<a href="http://www.cbs.dtu.dk/services/CPHmodels">http://www.cbs.dtu.dk/services/CPHmodels</a>	Model + Confidence	FR + ab initio
FFAS	<a href="http://ffas.ljcrf.edu">http://ffas.ljcrf.edu</a>	FFAS score	FR
Robetta	<a href="http://robetta.bakerlab.org">http://robetta.bakerlab.org</a>	Confidence	FR
mGen Threader	<a href="http://bioinf.cs.uvl.ac.uk/psipred">http://bioinf.cs.uvl.ac.uk/psipred</a>	P-value	FR
SAM-T06	<a href="http://www.soe.ucsc.edu/compbio/SAM_T06/T06-query.html">http://www.soe.ucsc.edu/compbio/SAM_T06/T06-query.html</a>	Model + Confidence	FR
HHpred	<a href="http://toolkit.tuebinge.mpg.de/hhpred">http://toolkit.tuebinge.mpg.de/hhpred</a>	Confidence	FR
PCONS	<a href="http://pcons.net">http://pcons.net</a>	Model + $P_{cons}$ score	FR
Bioinfo	<a href="http://meta.bioinfo.pl">http://meta.bioinfo.pl</a>	Model + E- value	FR

In this chapter, we aim to build the *in silico* three dimensional structure of 5 $\alpha$ -R1 and 5 $\alpha$ -R2 by means of homology modeling with suitable template protein and to predict physico-chemical protein properties, including catalytic region and transmembrane site. The resulting data will be employed in the next step for the discovery and development of a new series of 5 $\alpha$ -R inhibitors toward androgenic alopecia.

## 3.2 Materials and methods

### 3.2.1 Homology modeling

The target protein sequences of 5 $\alpha$ -R1 and 5 $\alpha$ -R2 were obtained from National Center for Biotechnology Information (NCBI). The sequence code of 5 $\alpha$ -R1 and 5 $\alpha$ -R2 was NP\_001038 and P31213.1, respectively. Homology modeling of the 5 $\alpha$ -R1 and 5 $\alpha$ -R2 were operated by using the free online web servers as shown in **Table 7**. The sequence identity and similarity were analyzed and aligned by Discovery Studio 2.5. Sequence identity is the amount of characters, which match exactly between two different sequences. In this case, the gaps are not counted and the measurement is related to the shorter of the two sequences. Importantly, 100% identity does not mean two sequences are the same. Sequence similarity is an optimal matching algorithm to find the amount of characters, which is obtained from alignment one sequence into an exact copy of the other sequence. The resulting models were analyzed based on their sequence identity and similarity between target protein and selected templates. The model, which showed the highest sequence identity and similarity were selected for further experiments.



**Table 7** Free online web servers used for generated the *in silico* structures of the 5 $\alpha$ -R1 and 5 $\alpha$ -R2 in this study.

Server name	Web address	Model building/ Confidence measure <sup>a</sup>	FR/ ab initio
SWISS-MODEL	<a href="http://swissmodel.expasy.org/">http://swissmodel.expasy.org/</a>	Model + Confidence	FR + ab initio
Phyre	<a href="http://www.imperial.ac.uk/phyre">http://www.imperial.ac.uk/phyre</a>	Model + Confidence	FR
I-TASSER	<a href="http://zhang.bioinformatics.ku.edu/I-TASSER">http://zhang.bioinformatics.ku.edu/I-TASSER</a>	Model + Confidence	FR + ab initio
SP4	<a href="http://sparks.informatics.iupui.edu/SP4">http://sparks.informatics.iupui.edu/SP4</a>	Model + Z-score	FR
CPHModels	<a href="http://www.cbs.dtu.dk/services/CPHmodels">http://www.cbs.dtu.dk/services/CPHmodels</a>	Model + Confidence	FR + ab initio
FFAS	<a href="http://ffas.ljcrf.edu">http://ffas.ljcrf.edu</a>	FFAS score	FR
Robetta	<a href="http://rosetta.bakerlab.org">http://rosetta.bakerlab.org</a>	Confidence	FR
mGen Threader	<a href="http://bioinf.cs.uvl.ac.uk/psipred">http://bioinf.cs.uvl.ac.uk/psipred</a>	P-value	FR

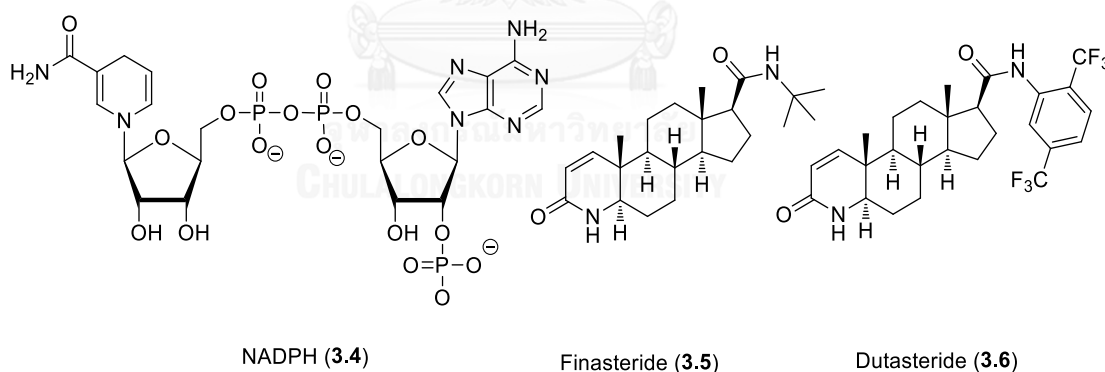
<sup>a</sup> See [41] for more explanation on each modeling definition and algorithm

### 3.2.2 Structure evaluation

The protein health report of the resulting three-dimensional structures was evaluated by Ramachandran Plot in Discovery Studio 2.5.

### 3.2.3 Active site identification

The docking studies of NADPH (cofactor, **3.4**) and a bound ligands; T (**3.1**), 5 $\alpha$ -DHT (**3.2**), finasteride (**3.5**), and dutasteride (**3.6**) (**Figure 7**) were conducted using Autodock Vina, which was based on genetic and lamakian algorithm [42]. First, NADPH was randomly docked into the derived *in silico* 5 $\alpha$ -R1 and 5 $\alpha$ -R2 structure with 100 numbers of docking mode to verify the NADPH pocket. Then, each ligand (**3.1**, **3.2**, **3.5**, and **3.6**) was docked into the resulting NADPH and 5 $\alpha$ -R1 binary complex with the grid box near the position of NADPH (center x=0.487, center y=36.43, and center z=96.802) and the grid box sizes are size x=38, size y=18, and size z=16. In the case of 5 $\alpha$ -R2, the resulting NADPH and 5 $\alpha$ -R2 binary complex with the grid box near the position of NADPH (center x=4.403, center y=51.086, and center z=113.368) and the grid box sizes are size x=18, size y=32, and size z=22. Both 5 $\alpha$ -R1 and 5 $\alpha$ -R2 were performed 100 docking number. Finally, the catalytic sites of both 5 $\alpha$ -R1 and 5 $\alpha$ -R2, which involved both the cofactor and the ligand were identified.



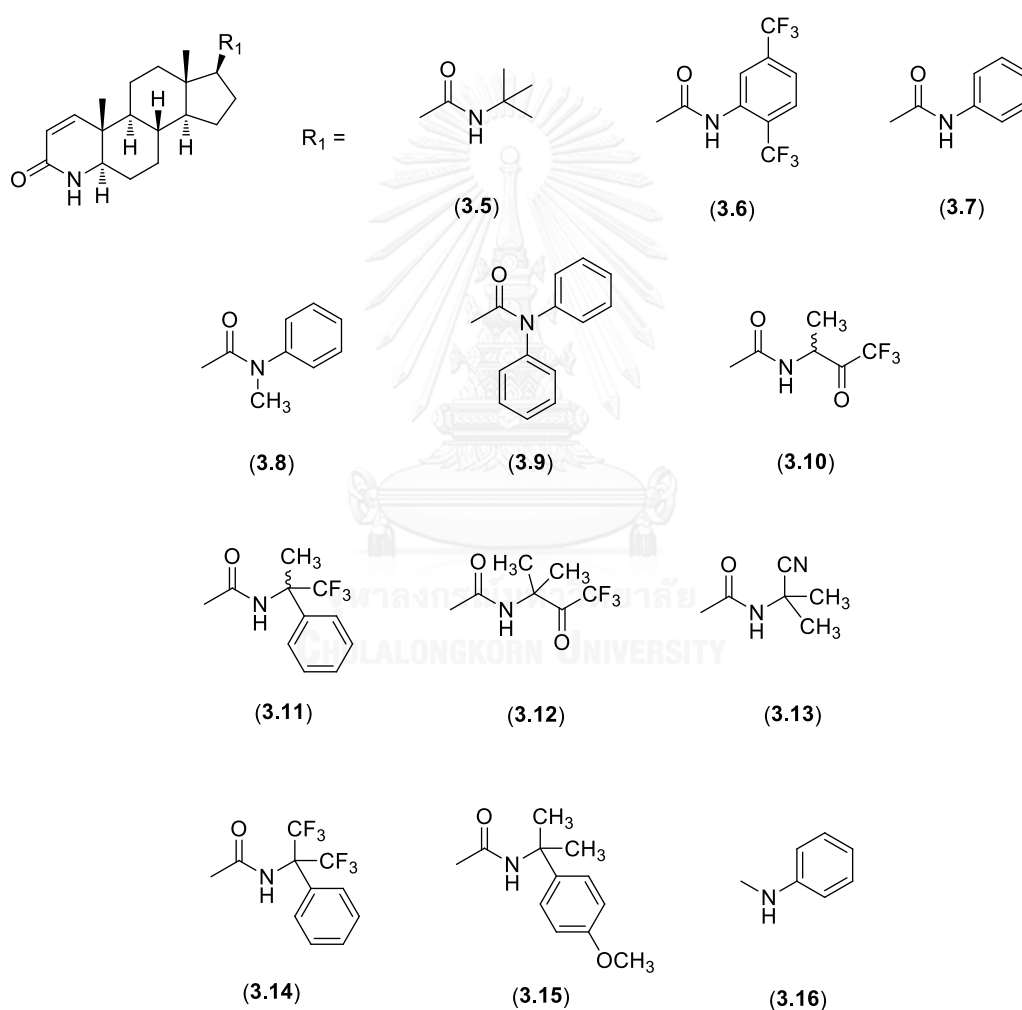
**Figure 7** Structures of NADPH (**3.4**), finasteride (**3.5**), and dutasteride (**3.6**)

### 3.2.4 Transmembrane site prediction

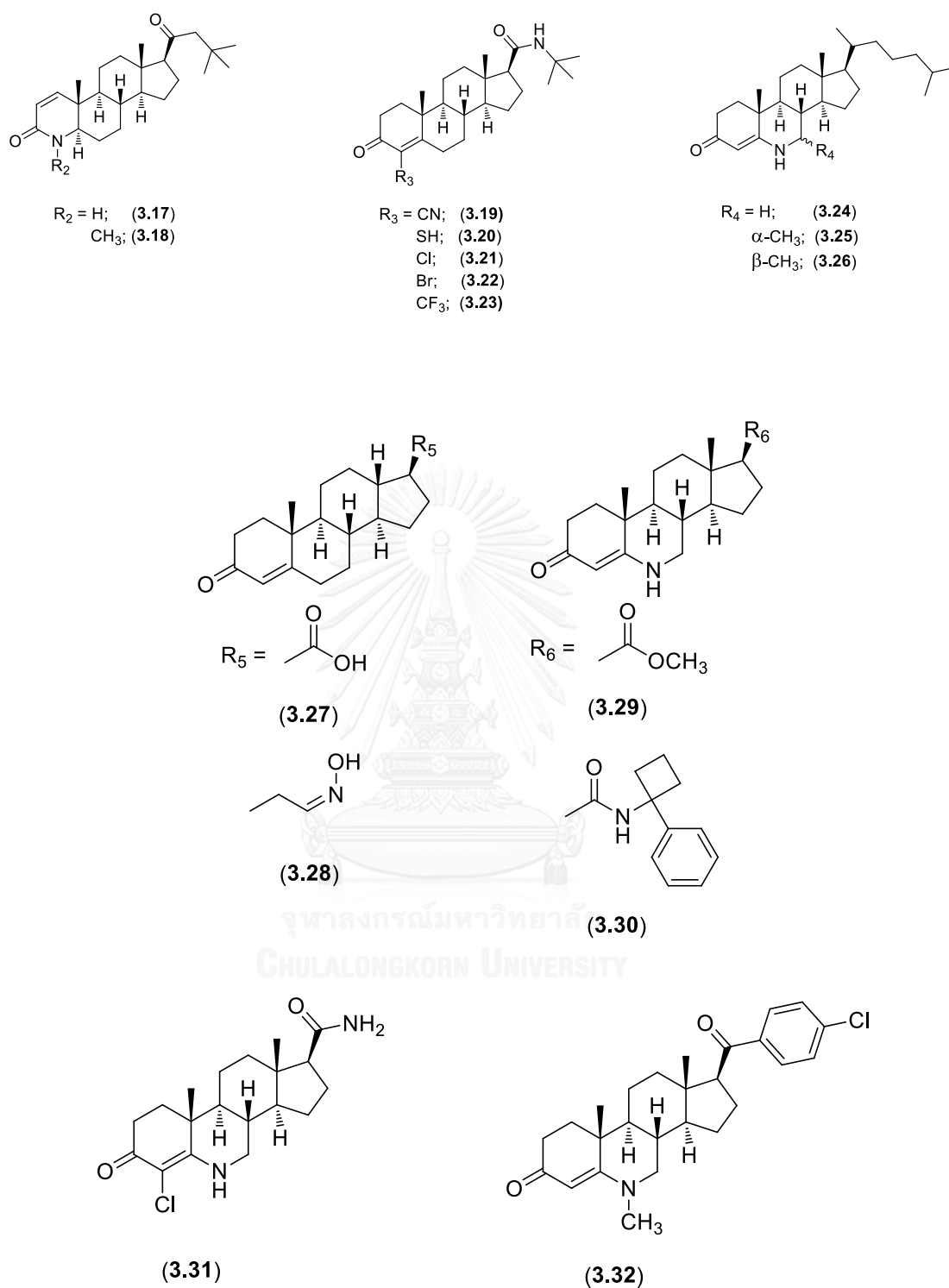
Prediction of the transmembrane site of an *in silico* 5 $\alpha$ -R1 and 5 $\alpha$ -R2 was performed using by Discovery Studio 2.5. The transmembrane site prediction was determined from its amino acid sequence by using a Hidden Markov Model [43].

### 3.2.5 Docking study of known 5 $\alpha$ -R inhibitors

A series of 27 known steroidal 5 $\alpha$ -R inhibitors [13, 44] were studied *via* molecular docking operated by Autodock Vina. Each inhibitor was docked into the predicted active site of the *in silico* 5 $\alpha$ -R/NADPH binary structure of both 5 $\alpha$ -R1 and 5 $\alpha$ -R2. All chemical structures were converted into PDB coordinated files by Open Babel software and the results were analyzed. All interested structures are shown in Figure 8.



**Figure 8** Chemical structures of known 5 $\alpha$ -reductase inhibitors used for docking studies.



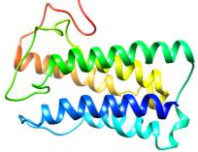
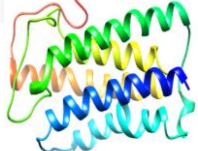
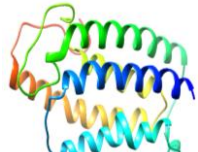
**Figure 8 (Cont.)** Chemical structures of known  $5\alpha$ -reductase inhibitors used for docking studies.

### 3.3 Results and discussion

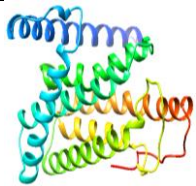
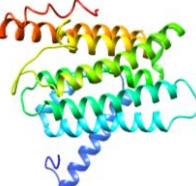
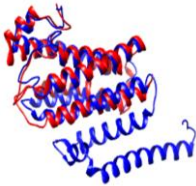
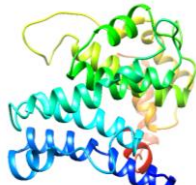
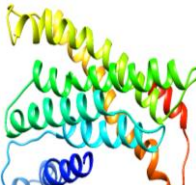
#### 3.3.1 Predicted three-dimensional structure of 5 $\alpha$ -R1 and 5 $\alpha$ -R2

The *in silico* structures of 5 $\alpha$ -R1 and 5 $\alpha$ -R2 were generated by several homology web based servers. As the results shown in **Tables 8** and **9**, the predicted three-dimensional structures of 5 $\alpha$ -R1 and 5 $\alpha$ -R2 were obtained from 8 web based servers, including SWISS-MODEL, Phyre, I-TASSER, SP4, CPHModels, FFAS, Robetta and mGenThreader. Each web based servers performed homologous model prediction with different algorithm and different template proteins by automatic selection mode.

**Table 8** Resulting *in silico* 5 $\alpha$ -R1 structures from web based servers

Entry	Server name	Homology model	Template <sup>a</sup>	Sequence identity (%)	Sequence similarity (%)
1	SWISS-MODEL	 Residue 82-257	4A2N	17.9	39.6
2	Phyre (normal modeling mode)	 Residue 81-256	4A2N	17.5	39.2
3	Phyre (intensive modeling mode)	 Residue 81-256	4A2N	12.5	27.9

**Table 8** (Cont.) Resulting *in silico* 5 $\alpha$ -R1 structures from web based servers

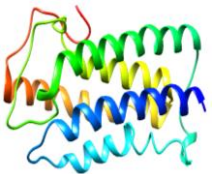
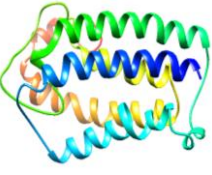
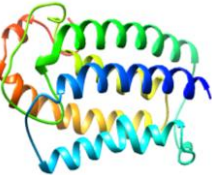
Entry	Server name	Homology model	Template <sup>a</sup>	Sequence identity (%)	Sequence similarity (%)
4	I-TASSER	 Residue 1-259	4A2N	16.0	36.4
5	I-TASSER (exclude homologous templates 60%)	 Residue 1-259	4A2N	16.0	36.4
6	I-TASSER (exclude homologous templates 100%)	 Residue 1-259	4A2N	16.0	36.4
7	SP4	 Residue 1-259	3A00	9.9	21.1
8	CPHModels	 Residue 12-236	2QPE	14.5	25.1

**Table 8** (Cont.) Resulting *in silico* 5 $\alpha$ -R1 structures from web based servers

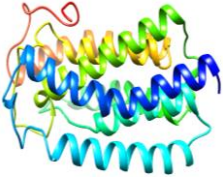
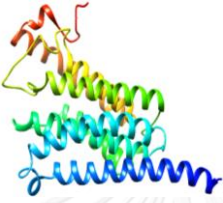
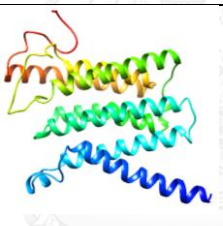
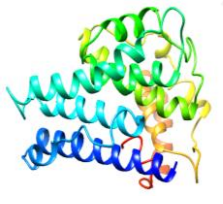
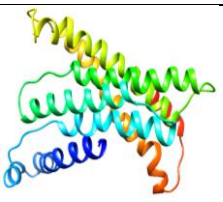
Entry	Server name	Homology model	Template <sup>a</sup>	Sequence identity (%)	Sequence similarity (%)
9	FFAS	NA <sup>b</sup>	4A2N	NA	NA
10	Robetta	NA <sup>b</sup>	4A2N	NA	NA
11	mGen Threader	NA <sup>b</sup>	4LEP	NA	NA

<sup>a</sup> 4A2N = Isoprenylcysteine carboxymethyl transferase Chain B (resolution 3.40); 3A00 = Oligo alginate lyase Chain A (resolution 2.11); 2QPE = Cytochrome c oxidase subunit 1 Chain A (resolution 2.90); 4LEP = Oligopeptide symporter POT Chain A (resolution 3.20) <sup>b</sup> NA refers to not available homology model due to incompatible algorithm

**Table 9** Resulting *in silico* 5 $\alpha$ -R2 structures from web based servers

Entry	Server name	Homology model	Template <sup>a</sup>	Sequence identity (%)	Sequence similarity (%)
1	SWISS-MODEL	 Residue 77-251	4A2N	16.1	43.9
2	Phyre (normal modeling mode)	 Residue 77-251	4A2N	16.1	43.9
3	Phyre (intensive modeling mode)	 Residue 77-251	4A2N	14.2	38.4

**Table 9** (Cont.) Resulting *in silico* 5 $\alpha$ -R2 structures from web based servers

Entry	Server name	Homology model	Template <sup>a</sup>	Sequence identity (%)	Sequence similarity (%)
4	I-TASSER	 Residue 1-254	4A2N	14.2	38.4
5	I-TASSER (exclude homologous templates 60%)	 Residue 1-254	4A2N	14.2	38.4
6	I-TASSER (exclude homologous templates 100%)	 Residue 1-254	4A2N	14.2	38.4
7	SP4	 Residue 1-254	3AF1	19.6	38.4
8	CPHModels	 Residue 7-231	2QPE	15.0	26.7



**Table 9** (Cont.) Resulting *in silico* 5 $\alpha$ -R2 structures from web based servers

Entry	Server name	Homology model	Template <sup>a</sup>	Sequence identity (%)	Sequence similarity (%)
9	FFAS	NA <sup>b</sup>	4A2N	NA	NA
10	Robetta	NA <sup>b</sup>	4A2N	NA	NA
11	mGen Threader	NA <sup>b</sup>	3WC3	NA	NA

<sup>a</sup> 4A2N = Isoprenylcysteine carboxylmethyl transferase Chain B (resolution 3.40); 3A00 = Oligo alginate lyase Chain A (resolution 2.11); 2QPE = Cytochrome c oxidase subunit 1 Chain A (resolution 2.90); 4LEP = Oligopeptide symporter POT Chain A (resolution 3.20) <sup>b</sup> NA refers to not available homology model due to incompatible algorithm

The resulting *in silico* three-dimensional structures of 5 $\alpha$ -R1 and 5 $\alpha$ -R2 were obtained from several web based servers as shown in **Tables 8** and **9**, respectively. The sequence identities and similarities between template proteins and query sequences were compared to select the best homologous representative. As a result, SWISS-MODEL server was the best choice for homology simulation because it generated the highest sequence similarity in both 5 $\alpha$ -R1 and 5 $\alpha$ -R2 cases (**Table 8**, entry 1 and **Table 9**, entry 1). Therefore, the predicted 5 $\alpha$ -R1 and 5 $\alpha$ -R2 structures from SWISS-MODEL server were chosen as the surrogates of 5 $\alpha$ -R1 and 5 $\alpha$ -R2 for the next study [45, 46]. In addition, some web based servers were performed with more than 1 functional mode such as Phyre and I-TASSER to get the optimum homology calculation. Briefly, Phyre normal modeling mode produces a set of potential 3D models based on fold recognition method, while Phyre intensive modeling mode produces a set of 3D models based on *ab initio* method [47]. In the case of I-TASSER, the exclude homologous templates 60% and 100% modes are the predictions that exclude all templates in the I-TASSER library having sequence identities more than 60% and 100% to the query protein, respectively [48]. In this study, the template homologous proteins were crossed identified by Discovery Studio 2.5. Due to the low sequence identity and similarity, several homology modeling software failed to generate the homologous model (**Table 8**, entries 9-11 and **Table 9**, entries 9-11). The

quality of template proteins was considered based upon their reported resolution. The lower resolution number refers the higher quality of the crystal structure of protein and vice versa.

Furthermore, we performed the comparison of sequence identities and similarities of each template proteins consisting of 4A2N, 3A0O, 2QPE and 4LEP with the sequences of 5 $\alpha$ -R1 and 5 $\alpha$ -R2 to confirm the best template for homology models. This experiment was performed using discovery studio 2.5 and the results were depicted in **Table 10** and **11** showing the results for 5 $\alpha$ -R1 and 5 $\alpha$ -R2, respectively.

**Table 10** Comparison of sequence identities and similarities between 5 $\alpha$ -R1 sequences and the template sequences

Template <sup>a</sup>	5 $\alpha$ -R1		
	Resolution	Sequence identity (%)	Sequence similarity (%)
4A2N	3.4	16.0	36.4
3A0O	2.11	10.2	22.5
2QPE	2.9	12.5	27.9
4LEP	3.2	13.6	30.6

<sup>a</sup> 4A2N = Isoprenylcysteine carboxylmethyl transferase Chain B; 3A0O = Oligo alginate lyase Chain A; 2QPE = Cytochrome c oxidase subunit 1 Chain A; 4LEP = Oligopeptide symporter POT Chain A.

**Table 11** Comparison of sequence identities and similarities between 5 $\alpha$ -R2 sequences and the template sequences

Template <sup>a</sup>	5 $\alpha$ -R2		
	Resolution	Sequence identity (%)	Sequence similarity (%)
4A2N	3.4	14.2	38.4
3AF1	2.5	19.6	38.4
2QPE	2.9	12.5	27.9
3WC3	31.5	13.0	29.2

<sup>a</sup> 4A2N = Isoprenylcysteine carboxylmethyl transferase Chain B; 3A00 = Oligo alginate lyase Chain A; 2QPE = Cytochrome c oxidase subunit 1 Chain A; 4LEP = Oligopeptide symporter POT Chain A.

The results from the above mentioned models were evaluated for their quality by the sequence alignment method to obtain sequence identities and similarities based on the corresponding template protein. As the results, 5 $\alpha$ -R1 showed the highest sequence match with isoprenylcysteine carboxyl methyltransferase chain B (ICMT, PDB: 4A2N) with 36.4% similarity. In the case of 5 $\alpha$ -R2, both isoprenylcysteine carboxyl methyltransferase chain B (ICMT, PDB: 4A2N) and pantothenate kinase chain A (PDB: 3AF1) possessed the highest sequence similarity at the same level (38.4%). These results implied both suitable template protein and practical online-based protocol for the best homologous model of 5 $\alpha$ -R1 and 5 $\alpha$ -R2. However, we observed lower than 30% sequence similarity from SP4 and CPHModels, which referred to the unacceptable homologue structures due to the alignment difficulty [39]. Thus, ICMT was served as the most appropriate template for both 5 $\alpha$ -R1 and 5 $\alpha$ -R2 using SWISS-MODEL protocol. The resulting *in silico* structures of 5 $\alpha$ -R1 and 5 $\alpha$ -R2 are demonstrated in **Table 8** entry 1 and **Table 9** entry 1, respectively.

An isoprenylcysteine carboxyl methyltransferase (ICMT, PDB: 4A2N) was automatically selected by SWISS-MODEL algorithm as a sequence protein template for comparative modeling. This membrane-bound enzyme catalyzes the final process of C-terminal CAAX motif after prenylation of the cysteine residue and endoproteolysis of -AAX motif (C refers to cysteine, A refers to an aliphatic amino acid, and X refers to

any amino acid). The amino acid sequence of 5 $\alpha$ -R1 and 5 $\alpha$ -R2 were aligned with ICMT (Figure 9). Even though, relatively low sequence identity and similarity between 5 $\alpha$ -R1 and ICMT were of 16.6 % and 36.8 %, respectively, in addition to identity and similarity between 5 $\alpha$ -R2 and ICMT were obtained, 14.1% and 40.0%, respectively. The ICMT appeared to be a reasonable homologous template, since it is a membrane-associated enzyme similar to 5 $\alpha$ -R1 and 5 $\alpha$ -R2 [49]. Therefore, the primary  $\alpha$ -helix shapes of these 3 enzymes presumably were equivalent.

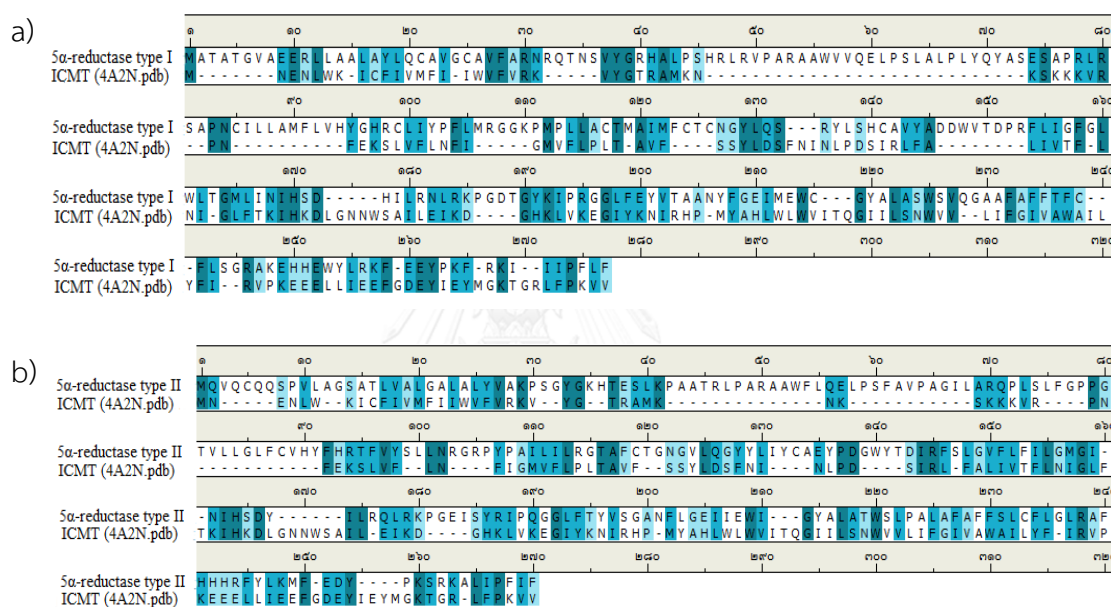


Figure 9 a) Sequence alignment between 5 $\alpha$ -R1 and isoprenylcysteine carboxyl methyltransferase b) Sequence alignment between 5 $\alpha$ -R2 and isoprenylcysteine carboxyl methyltransferase

Previously, 5 $\beta$ -R has been reported as a template for 5 $\alpha$ -R1 and 5 $\alpha$ -R2 [37] and used as an alternative protein structure for virtual screening of 5 $\alpha$ -R2 inhibitors, since these three stereospecific steroid reductases required NADPH as a cofactor to initiate their catalytic action [36, 50] and finasteride was an inhibitor of those enzymes [51]. To validate the quality of our *in silico* 5 $\alpha$ -R model, sequence alignment between 5 $\alpha$ -R1 and 5 $\beta$ -R (PDB: 3G1R) provided 13.3% and 35.3%, while 5 $\alpha$ -R2 and 5 $\beta$ -R

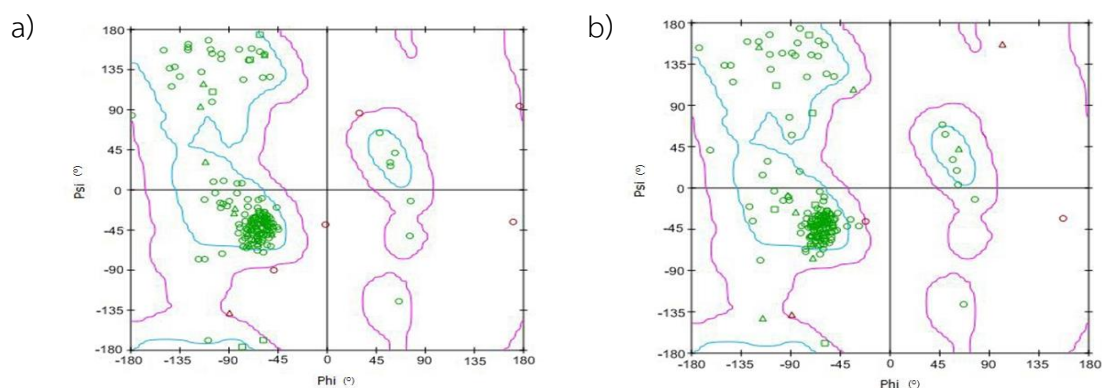
provided 18.1% and 38.0% of protein sequence identity and similarity, respectively (Table 12). The results demonstrated that ICMT had higher sequence similarity with 5 $\alpha$ -R1 and 5 $\alpha$ -R2 than 5 $\beta$ -R. According to sequence similarity and membrane-bound physical property, ICMT was selected as a template protein for building the homologous structures of 5 $\alpha$ -R1 and 5 $\alpha$ -R2 in this study [45, 46].

**Table 12** Sequence alignment of 5 $\alpha$ -R1 and 5 $\alpha$ -R2 with isoprenylcysteine carboxyl methyltransferase (ICMT) and 5 $\beta$ -reductase

Enzyme	5 $\alpha$ -R1		5 $\alpha$ -R2	
	%identity	%similarity	%identity	%similarity
ICMT	16.6	36.8	14.1	40.0
5 $\beta$ -reductase	13.3	35.3	18.1	38.0

### 3.3.2 Ramachandran Plot

The derived comparative structure of 5 $\alpha$ -R1 and 5 $\alpha$ -R2 were verified for the theoretical visualize backbone dihedral angles of amino acid residues in protein structure by Ramachandran method (Figure 10) [52]. The diagram illustrated the dihedral angles (Phi and Psi) of each amino acid residue. The result showed 89.3% (5 $\alpha$ -R1) and 91.1% (5 $\alpha$ -R2) of all amino acid residues were located in an allowed region, which was the area inside blue and pink line. This result suggested that the  $\alpha$ -helix shape of the *in silico* 5 $\alpha$ -R1 and 5 $\alpha$ -R2 was relatively similar to its template, ICMT [45, 46].



Green spots are amino acid residues in an allowed region. Red spots are amino acid residues in a disallowed region. Hard sphere is an area in blue line and overlap area is an area in pink line

**Figure 10** a) Ramachandran plot of *in silico* 5 $\alpha$ -R1 structure b) Ramachandran plot of *in silico* 5 $\alpha$ -R2 structure

### 3.3.3 Catalytic pocket and transmembrane site

The NADPH (**3.4**), T (**3.1**), 5 $\alpha$ -DHT (**3.2**), finasteride (**3.5**), and dutasteride (**3.6**) (**Figure 6** and **7**), which are cofactor, substrates, and known 5 $\alpha$ -R inhibitors were sequentially docked into the derived *in silico* 5 $\alpha$ -R1 and 5 $\alpha$ -R2 structures to identify the active sites and necessary amino acid interactions. The NADPH was firstly docked into the protein structure, following the previous proposed mechanism, which indicated that the binary complex of 5 $\alpha$ -R and NADPH was formed at the beginning of catalytic cycle [53, 54]. Then, a ligand (substrate or inhibitor) approached the active site and formed a ternary complex leading to an irreversible inhibition [1].

First, docking of NADPH into the *in silico* 5 $\alpha$ -R1 structures showed  $\Delta G$  of -9.3 kcal/mol and consisted of the hydrogen bonding interactions with Tyr95, Tyr102, Arg176, Asn198, Tyr199, and Arg232. (**Table 13**) Furthermore, T (**3.1**), 5 $\alpha$ -DHT (**3.2**), finasteride (**3.5**), and dutasteride (**3.6**) to the enzyme- NADPH binary complex provided  $\Delta G$  of -4.4, -4.2, -5.8, and -4.4 kcal/mol, respectively. Each ligand had resembling hydrogen bond interactions with Tyr95 at a carbonyl moiety at C3.

Second, docking of NADPH into the *in silico* 5 $\alpha$ -R2 structures displayed  $\Delta G$  of -8.8 kcal/mol and consisted of the hydrogen bonding interactions with Tyr91, Arg94, Tyr107, Arg114, Arg171, Asn193, and Tyr235 (**Table 14**). Furthermore, docking of T (**3.1**), 5 $\alpha$ -DHT (**3.2**), finasteride (**3.5**), and dutasteride (**3.6**) to the enzyme- NADPH binary complex provided  $\Delta G$  of -4.5, -4.8, -5.3, and -7.3 kcal/mol, respectively. Each ligand had resembling hydrogen bond interactions with Ser99 at a carbonyl moiety at C3. Interestingly, dutasteride (**3.6**) contained the extra hydrogen bonding interaction with Arg114 at fluorinated substituent on C17.

**Table 13** Docking studies of the *in silico* 5 $\alpha$ -R1 with NADPH and ligands

Compounds	$\Delta G$ (kcal/mol)	Hydrogen bonding interactions with amino acid
NADPH ( <b>3.4</b> )	-9.3	Tyr95, Tyr102, Arg176, Asn198, Tyr199, and Arg232
Testosterone ( <b>3.1</b> )	-4.4	Tyr95
5 $\alpha$ -dihydrotestosterone ( <b>3.2</b> )	-4.2	Tyr95
Finasteride ( <b>3.5</b> )	-4.4	Tyr95
Dutasteride ( <b>3.6</b> )	-5.8	Tyr95

Each ligand was docked into an *in silico* 5 $\alpha$ -R1-NADPH binary complex

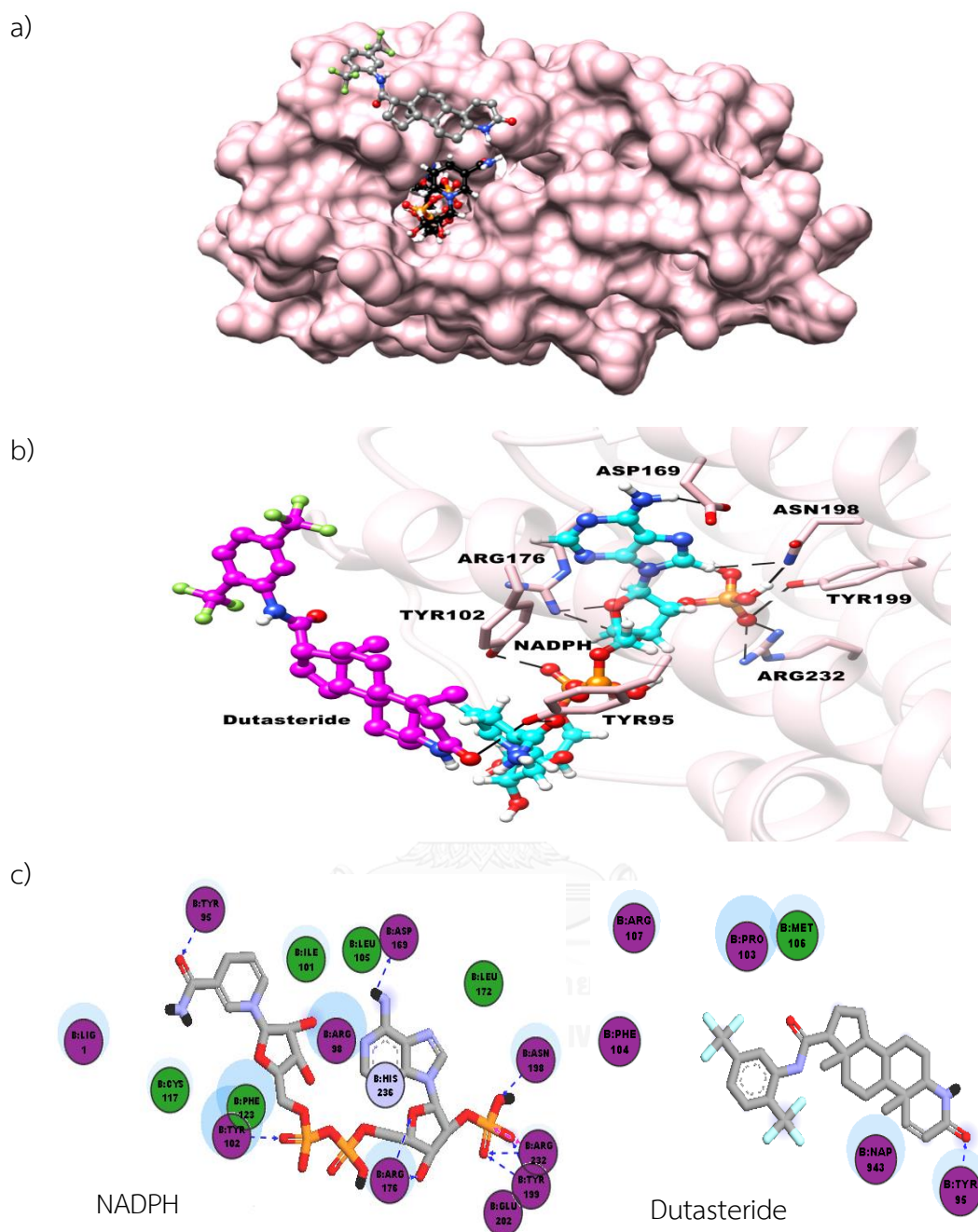
**Table 14** Docking studies of the *in silico* 5 $\alpha$ -R2 with NADPH and ligands

Compounds	$\Delta G$ (kcal/mol)	Hydrogen bonding interactions with amino acid
NADPH ( <b>3.4</b> )	-8.8	Tyr91, Arg94, Tyr107, Arg114, Arg171, Asn193 and Tyr235
Testosterone ( <b>3.1</b> )	-4.5	Ser99
5 $\alpha$ -dihydrotestosterone ( <b>3.2</b> )	-4.8	Ser99
Finasteride ( <b>3.5</b> )	-5.3	Ser99
Dutasteride ( <b>3.6</b> )	-7.3	Ser99, Arg114

Each ligand was docked into an *in silico* 5 $\alpha$ -R2-NADPH binary complex

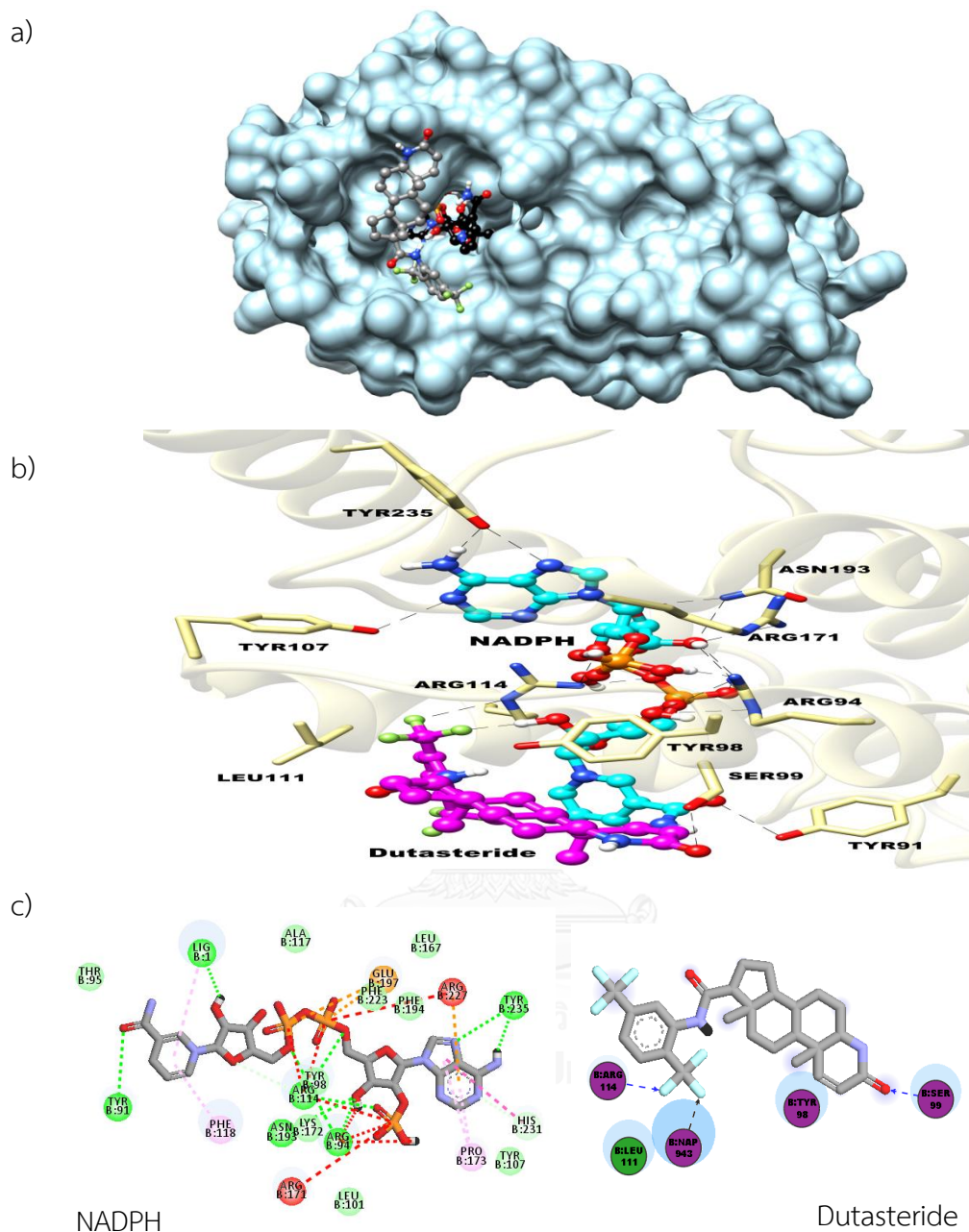
From the results shown in **Tables 13** and **14**, dutasteride (**3.6**) showed the highest negative binding energy. Thus, it was selected to illustrate the binding interactions at the catalytic site of the **5 $\alpha$ -R1** and **5 $\alpha$ -R2**. The three-dimensional complex structure of **5 $\alpha$ -R1** and **5 $\alpha$ -R2** with cofactor NADPH and dutasteride as a ligand are shown in **Figures 11a** and **12a**, respectively. In addition, the derived ternary complex clearly showed the binding region of NADPH and dutasteride, which were located adjacent to each other. Interestingly, our docking results showed that NADPH resided inside the *in silico* structure of **5 $\alpha$ -R1** and **5 $\alpha$ -R2** and dutasteride was stayed nearly on the surface of the enzyme structure (**Figure 11b** and **12b**, respectively), which corresponded to the catalytic action of the membrane-associated enzyme [1]. Beside hydrogen bonds, the NADPH and dutasteride were also stabilized by van der Waals and polar interactions contributed from the residues in green and purple circles, respectively. Therefore, the predicted catalytic region of **5 $\alpha$ -R1** was composed of Arg98, Tyr95, Ile101, Tyr102, Leu105, Cys117, Phe123, Leu172, Arg176, Asn198, Tyr199, Arg232, and His236 interacting with NADPH and Met106, Tyr95, Pro103, Phe104, and Arg107 interacting with dutasteride (**Figure 11c**). For **5 $\alpha$ -R2**, the calculated catalytic region of **5 $\alpha$ -R2** consisted of Phe118, Phe194, Phe223 and Pro173 interacting with NADPH and Leu111, Tyr98, Ser99, and Arg114 interacting with dutasteride (**Figure 12c**).





Blue dash lines are hydrogen acceptor; black dash lines are hydrogen donor; light blue surface areas represent hydrophobic interactions.

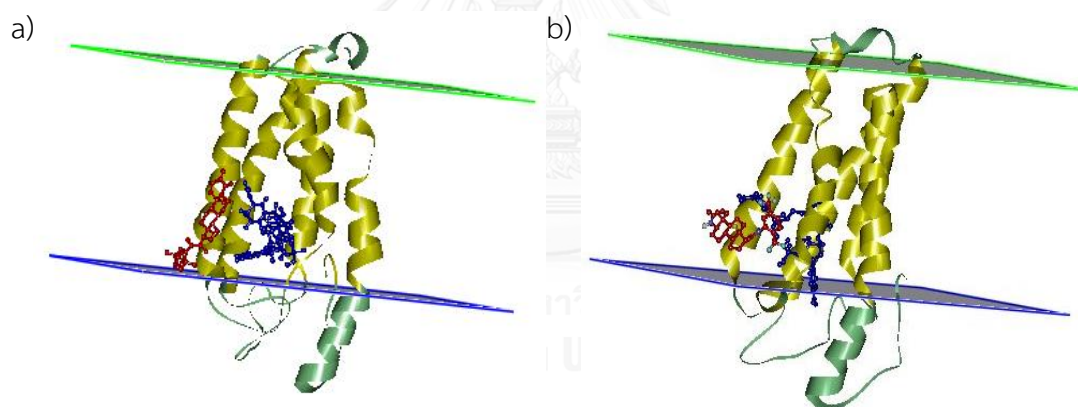
**Figure 11** Ternary complex of the *in silico* 5 $\alpha$ -R1 with NADPH and dutasteride; a) 3D complex structure of 5 $\alpha$ -R1, NADPH and dutasteride b) 3D-diagram displaying a catalytic site; c) 2D-diagram displaying the binding interactions [46]



Blue dash lines are hydrogen acceptor; green dash lines are hydrogen acceptor; light pink dash lines are  $\pi$ -alkyl interaction; dark pink dash lines are  $\pi$ - $\pi$  T-shaped interaction; red dash lines are unfavorable donor-donor; black dash lines are hydrogen donor; light blue surface areas represent hydrophobic interactions.

**Figure 12** Ternary complex of the *in silico* 5 $\alpha$ -R2 with NADPH and dutasteride; a) 3D complex structure of 5 $\alpha$ -R2, NADPH and dutasteride b) 3D-diagram displaying a catalytic site; c) 2D-diagram displaying the binding interactions [45]

The transmembrane calculation indicated that majority of the *in silico* structures of both 5 $\alpha$ -R1 and 5 $\alpha$ -R2 were a transmembrane protein (**Figure 13**). Almost the entire structure of NADPH (blue structure) was attached inside the membrane region (yellow area) and T (red structure) was partially bound at the membrane area and leaned on the outer surface. Our results were related to the previous explanation, which the 5 $\alpha$ -R1 and 5 $\alpha$ -R2 are membrane-associated enzymes that are composed of high amount of hydrophobic amino acids to facilitate the spanning in the lipid bilayer membrane. Once T entered through cell membrane, a part of 5 $\alpha$ -R1 and 5 $\alpha$ -R2 that spread inside the cell firstly formed a complex with NADPH and the adjacent part of enzyme that spanned in the cell membrane embodied with T. Then, 5 $\alpha$ -DHT was slowly released inside the cell and conjugated with the androgen receptor [1, 12].



Yellow and green area refer to the membrane and cytosol region, respectively. NADPH and dutasteride are displayed in blue and red, respectively.

**Figure 13** Transmembrane prediction; a) *in silico* 5 $\alpha$ -R1 b) *in silico* 5 $\alpha$ -R2

The NADPH conjugated binary complex of the *in silico* 5 $\alpha$ -R was employed for docking studies of 28 known steroidal 5 $\alpha$ -R inhibitors (**Figure 8**), including T (**3.1**), 5 $\alpha$ -DHT (**3.2**), finasteride (**3.5**), and dutasteride (**3.6**). The selected steroidal 5 $\alpha$ -reductase inhibitors were composed of two types of steroidal cores, based on structure of ring A. Compounds **3.5-3.18** were  $\Delta^1$ -3-keto-4-azasteroids, which had the double bond

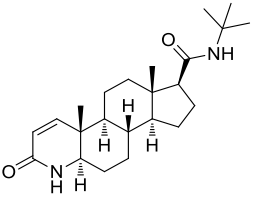
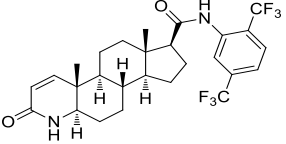
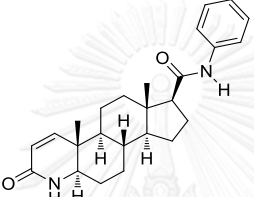
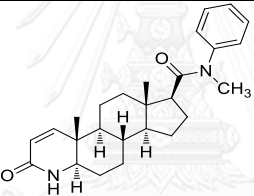
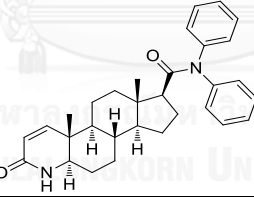
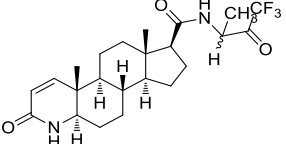
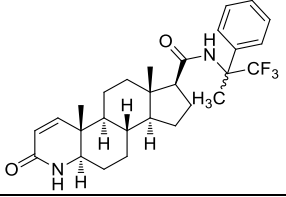
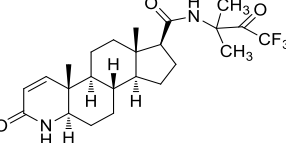
between C1 and C2, while compounds **3.19-3.32** were  $\Delta^4$ -3-ketosteroids, which contained a double bond between C4 and C5 instead.

### 3.3.4 Docking studies of $5\alpha$ -R1 with known $5\alpha$ -R inhibitors

The docking studies of  $5\alpha$ -R1 with known  $5\alpha$ -R inhibitors were performed to verify and confirm the catalytic site, as previously described. The docking results displayed the binding energy ( $\Delta G$ ) ranging from -4.2 to -5.8 kcal/mol. All inhibitors showed  $\Delta G$  values that were not significantly different from T (-4.4 kcal/mol), (**Table 15**). Furthermore, the group of  $\Delta^1$ -3-keto-4-azasteroids (**Table 15**, entries 1 - 14) showed better binding interactions than  $\Delta^4$ -3-keto-4-azasteroids of the comparative enzyme structure.



**Table 15** Docking studies of the *in silico* 5 $\alpha$ -R1 with known 5 $\alpha$ -R inhibitors

Entry	Compounds	Structure	$\Delta G$ (kcal/mol)	Interaction with amino acid
1	Finasteride (3.5)		-4.4	Tyr95
2	Dutasteride (3.6)		-5.8	Tyr95
3	(3.7)		-4.9	Tyr95
4	(3.8)		-5.0	Tyr95
5	(3.9)		-5.1	NADPH
6	FCE27837 (3.10)		-5.1	NADPH
7	FCE28260 (3.11)		-5.2	Tyr95
8	(3.12)		-5.2	Tyr95

**Table 15** (Cont.) Docking studies of the *in silico* 5 $\alpha$ -R1 with known 5 $\alpha$ -R inhibitors

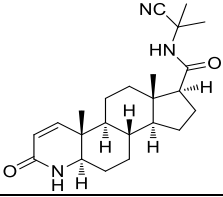
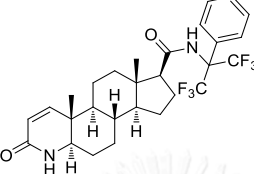
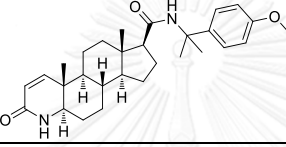
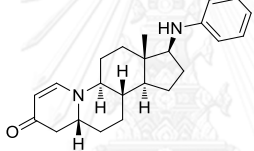
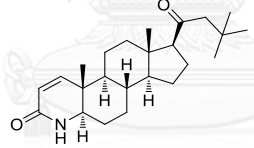
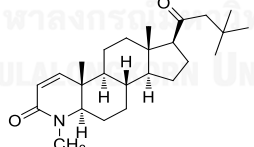
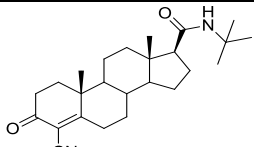
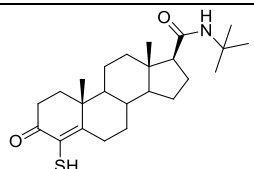
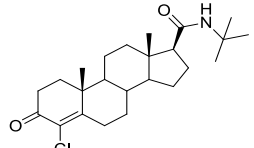
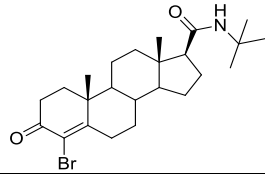
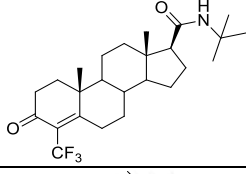
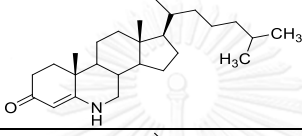
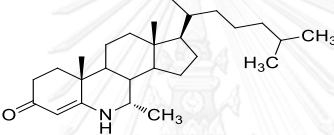
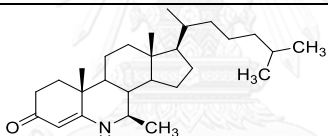
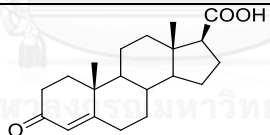
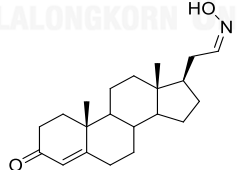
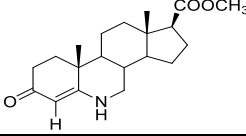
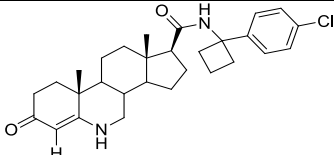
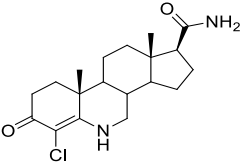
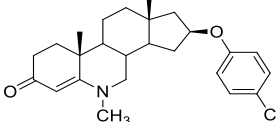
Entry	Compounds	Structure	$\Delta G$ (kcal/mol)	Interaction with amino acid
9	CGP53153 (3.13)		-4.7	Tyr95
10	PNU157706 (3.14)		-5.2	Tyr95
11	Lapisteride (3.15)		-5.1	Tyr102
12	(3.16)		-4.9	-
13	(3.17)		-5.2	Tyr95
14	(3.18)		-5.1	Tyr95
15	(3.19)		-5.0	Tyr95
16	(3.20)		-5.0	-
17	(3.21)		-4.5	Tyr95

Table 15 (Cont.) Docking studies of the *in silico* 5 $\alpha$ -R1 with known 5 $\alpha$ -R inhibitors

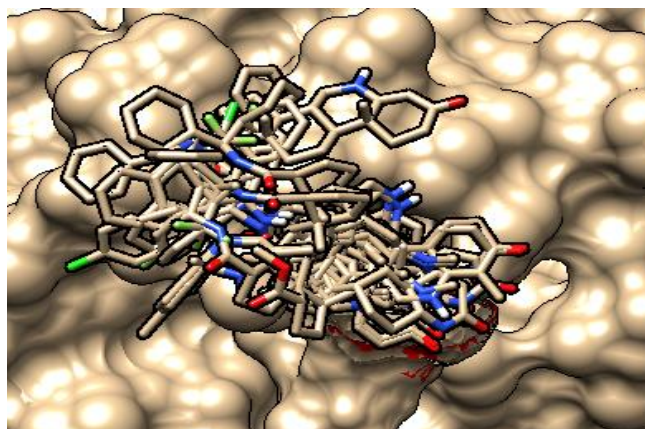
Entry	Compounds	Structure	$\Delta G$ (kcal/mol)	Interaction with amino acid
18	(3.22)		-4.4	Tyr95
19	(3.23)		-4.9	Tyr95
20	(3.24)		-4.5	-
21	(3.25)		-4.6	Tyr95
22	(3.26)		-4.5	Tyr95
23	(3.27)		-4.3	Tyr95
24	(3.28)		-5.0	-
25	(3.29)		-4.6	-
26	(3.30)		-5.2	Tyr95

**Table 15** (Cont.) Docking studies of the *in silico* 5 $\alpha$ -R1 with known 5 $\alpha$ -R inhibitors

Entry	Compounds	Structure	$\Delta G$ (kcal/mol)	Interaction with amino acid
27	(3.31)		-4.2	Tyr95
28	(3.32)		-4.6	NADPH

From the  $\Delta G$  results shown in **Table 15**, dutasteride (Entry 2) exhibited the best protein-ligand binding affinity at -5.8 kcal/mol. Interestingly, most of steroidal compounds in this study including dutasteride had hydrogen bonding interaction with Tyr 95 at C3 position. The binding energies ( $\Delta G$ ) of steroidal compounds were relatively similar. Some steroidal compounds such as finasteride (**3.5**), (**3.21**), (**3.22**), (**3.24**), (**3.25**), (**3.26**), (**3.27**), (**3.29**), (**3.31**) and (**3.32**) showed binding affinity resemble with T (**3.1**) (-4.4 kcal/mol), which implied that these compounds may have lower binding capability compared to dutasteride (**3.6**). The superimposition of all interesting ligands confirmed the predicted catalytic site of the *in silico* 5 $\alpha$ -R1, which were located at the same region (**Figure 14**) [46].



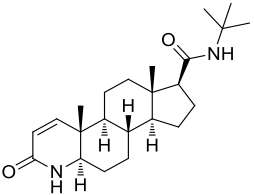
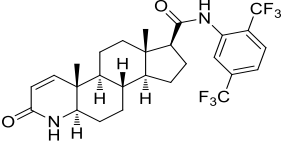
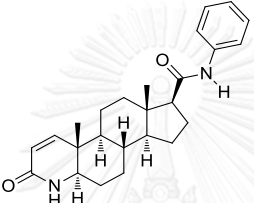
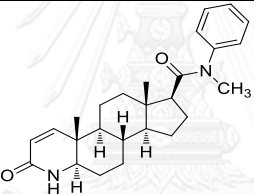
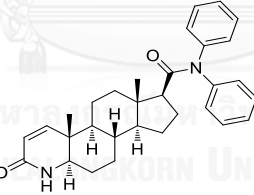
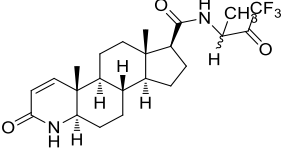
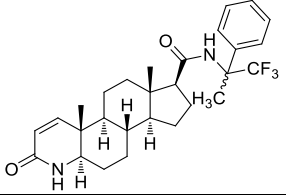
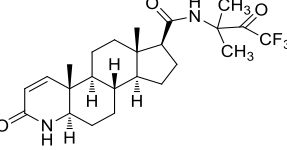


**Figure 14** Superimposition of steroidal compounds to verify the active sites of  $5\alpha$ -R1

### 3.3.5 Docking studies of $5\alpha$ -R2 with known $5\alpha$ -R inhibitors

Docking studies of  $5\alpha$ -R2 with known  $5\alpha$ -R inhibitors (3.5-3.32) demonstrated the binding energy ( $\Delta G$ ) that ranging from -4.6 to -7.8 kcal/mol (Table 16). All inhibitors showed  $\Delta G$  lower than that of T (-4.5 kcal/mol), which implied the competitive inhibition between T and inhibitors. Our results were in agreement with a previously reported publication [13]. In addition, the group of  $\Delta^1$ -3-keto-4-azasteroids (Table 16, entries 1 - 14) displayed better binding interactions with the comparative enzyme structure.

**Table 16** Docking studies of the *in silico* 5 $\alpha$ -R2 with known 5 $\alpha$ -R inhibitors

Entry	Compounds	Structure	$\Delta G$ (kcal/mol)	Interaction with amino acid
1	Finasteride (3.5)		-5.3	Ser99
2	Dutasteride (3.6)		-7.3	Ser99, Arg114, NADPH
3	(3.7)		-5.7	Ser99
4	(3.8)		-6.1	Ser99
5	(3.9)		-7.8	Ser99
6	FCE27837 (3.10)		-7.1	Ser99, NADPH
7	FCE28260 (3.11)		-6.9	Ser99, Arg114, NADPH
8	(3.12)		-7.3	Ser99, NADPH

**Table 16** (Cont.) Docking studies of the *in silico* 5 $\alpha$ -R2 with known 5 $\alpha$ -R inhibitors

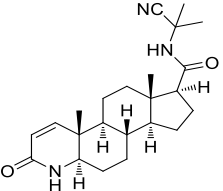
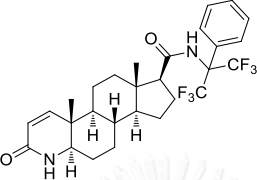
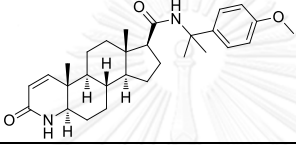
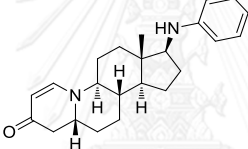
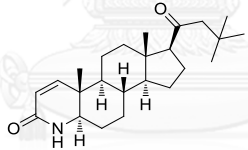
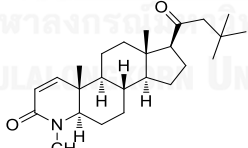
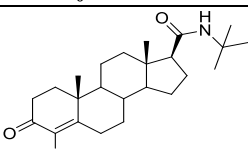
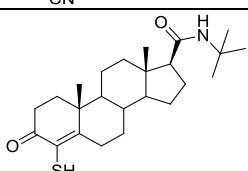
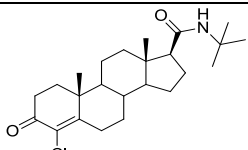
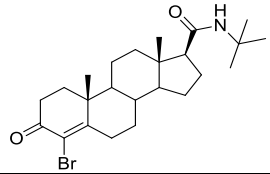
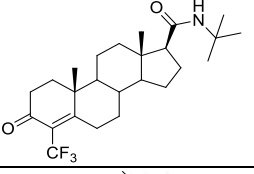
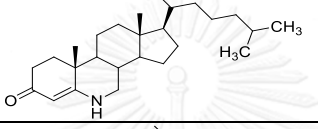
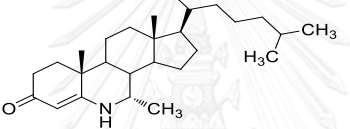
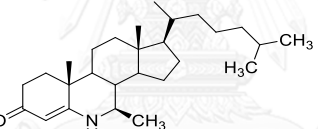
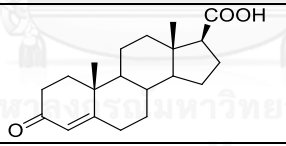
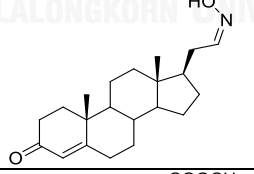
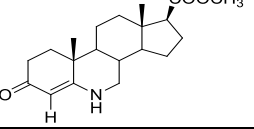
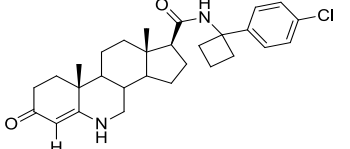
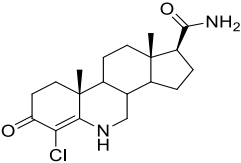
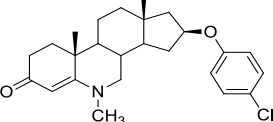
Entry	Compounds	Structure	$\Delta G$ (kcal/mol)	Interaction with amino acid
9	CGP53153 (3.13)		-5.9	Ser99, NADPH
10	PNU157706 (3.14)		-7.6	Ser99
11	Lapisteride (3.15)		-7.5	Ser99
12	(3.16)		-5.8	-
13	(3.17)		-5.7	Ser99
14	(3.18)		-5.7	Ser99
15	(3.19)		-5.3	Ser99
16	(3.20)		-5.9	Ser99
17	(3.21)		-5.1	Ser99

Table 16 (Cont.) Docking studies of the *in silico* 5 $\alpha$ -R2 with known 5 $\alpha$ -R inhibitors

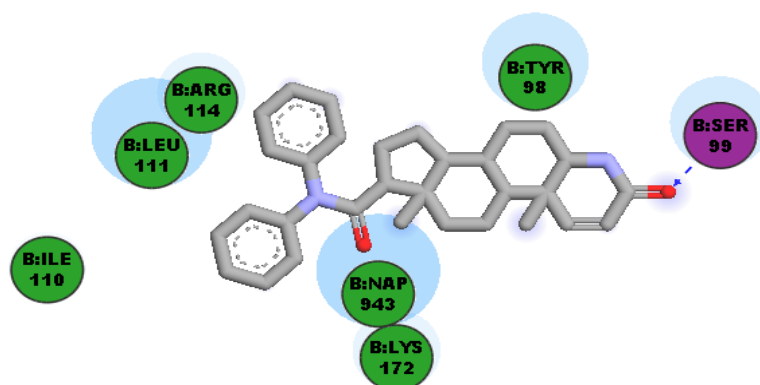
Entry	Compounds	Structure	$\Delta G$ (kcal/mol)	Interaction with amino acid
18	(3.22)		-4.6	Ser99
19	(3.23)		-5.8	Ser99
20	(3.24)		-4.9	Ser99
21	(3.25)		-5.5	Ser99
22	(3.26)		-4.6	Ser99
23	(3.27)		-4.9	Ser99
24	(3.28)		-5.7	Lys172, NADPH
25	(3.29)		-4.6	Ser99
26	(3.30)		-5.6	Ser99

**Table 16** (Cont.) Docking studies of the *in silico* 5 $\alpha$ -R2 with known 5 $\alpha$ -R inhibitors

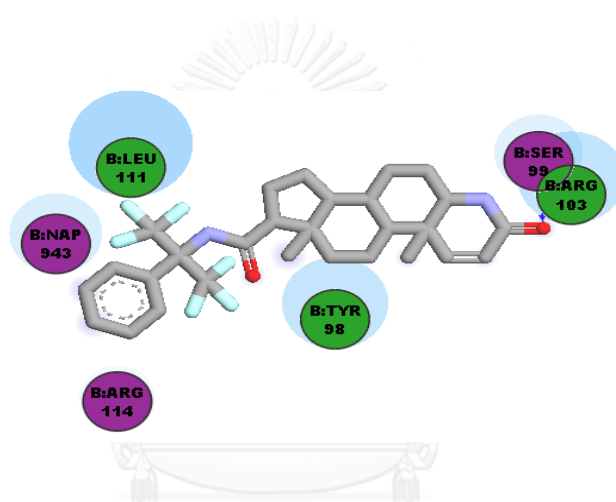
Entry	Compounds	Structure	$\Delta G$ (kcal/mol)	Interaction with amino acid
27	(3.31)		-5.7	Tyr98, NADPH
28	(3.32)		-6.2	Ser99

From the  $\Delta G$  results shown in **Table 16**, compound **3.9**, PNU157706 (**3.14**), and lapisteride (**3.15**) were the best top three inhibitors showing the highest negative protein-ligand binding affinity (-7.8, -7.6, and -7.5, respectively). Compound **3.9** was stabilized by catalytic residues; Tyr98, Ser99, Ile110, Leu111, Arg114, Lys172, and NADPH (**Figure 15a**). PNU157706 (**3.14**) was stabilized by catalytic residues; Tyr98, Ser99, Leu111, Arg113, Arg114, and NADPH (**Figure 15b**). Lapisteride (**3.15**) was stabilized by Tyr98, Ser99, Leu101, Arg103, Leu111, Arg114, Gly115, Lys172, and NADPH (**Figure 15c**). The results showed that compound **3.9**, PNU157706 (**3.14**), and lapisteride (**3.15**) had the hydrogen bond interactions at C3 with Ser99, which was similar to dutasteride. However, the bulky phenyl group on the amide substituents at C17 of these three inhibitors showed only hydrophobic interactions, while the bulky phenyl group of dutasteride showed hydrogen bond interactions with catalytic residues Arg114 and NADPH. Therefore, the main predicted catalytic sites involved Ser99 and Arg114 for hydrophilic and hydrophobic interactions, respectively. Moreover, our docking results agreed with a previous reported 3D-QSAR experiment that indicated that the steric field at C17 was crucial for hydrophobic interactions with the enzyme active site [50]. Superimposition of all interested ligands also confirmed the predicted catalytic site of the *in silico* 5 $\alpha$ -R2, which were located at the same region (**Figure 16**) [45].

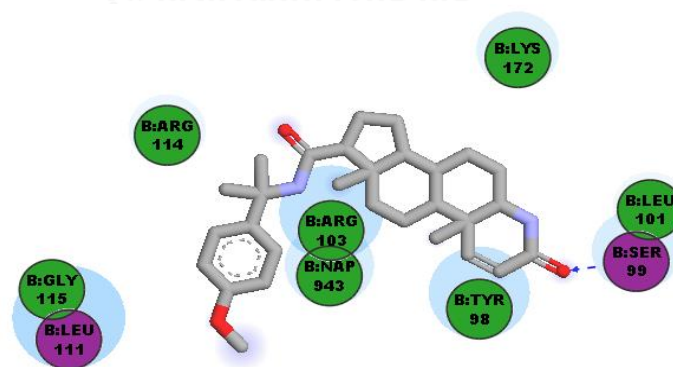
a)



b)



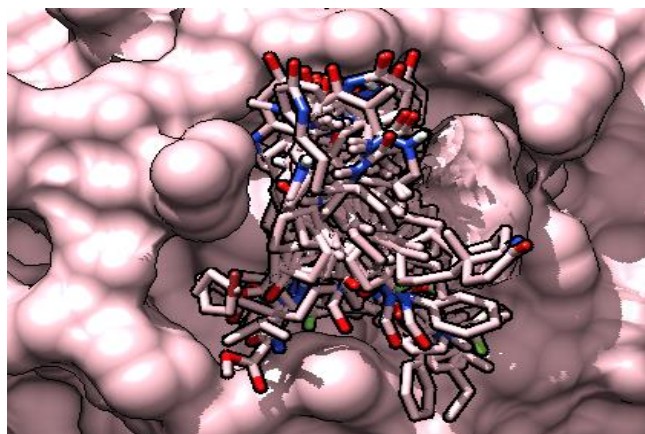
c)



Blue dash lines are hydrogen acceptor. Light blue surface areas represent hydrophobic interactions.

**Figure 15** 2D-diagram displayed the binding interactions of  $5\alpha$ -R2 with ligands;

a) compounds **3.9** b) PNU157706 (**3.14**) c) lapisteride (**3.15**)

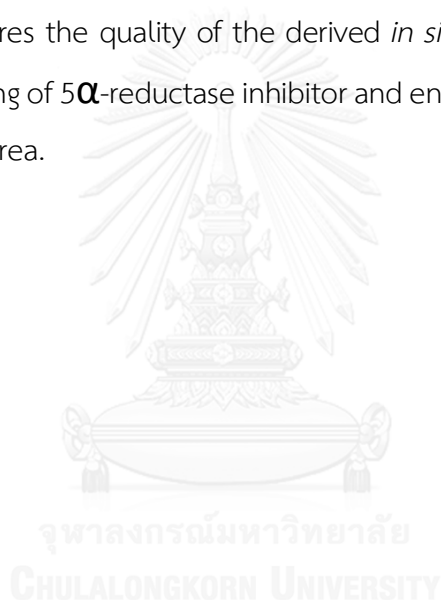


**Figure 16** Superimposition of steroidal compounds to verify the active sites of  $5\alpha$ -R2

### 3.4 Conclusions

In this study, the *in silico* three-dimensional  $5\alpha$ -R1 and  $5\alpha$ -R2 were built by the homology modeling using SWISS-MODEL. The isoprenylcysteine carboxyl methyltransferase (ICMT, PDB code: 4A2N) was automatically selected by SWISS-MODEL as a homologous protein template for both  $5\alpha$ -R1 and  $5\alpha$ -R2 simulations, based on their identical transmembrane protein nature. The predicted structure of  $5\alpha$ -R1 and  $5\alpha$ -R2 were confirmed by Ramachandran plot. Regarding our protocol, NADPH was firstly docked into the *in silico* structure of  $5\alpha$ -R1 and  $5\alpha$ -R2, since it is a cofactor and necessary for  $5\alpha$ -R function. With predicted  $5\alpha$ -R1 structure, NADPH showed  $\Delta G$  of -9.3 kcal/mol and the hydrogen bonding interactions at Tyr95, Tyr102, Arg176, Asn198, Tyr199, and Arg232. In the case of  $5\alpha$ -R2, NADPH displayed  $\Delta G$  of -8.8 kcal/mol and the hydrogen bonding interactions with Tyr91, Arg94, Tyr107, Arg114, Arg171, Asn193, and Tyr235. After that, docking of T,  $5\alpha$ -DHT, finasteride and dutasteride were conducted with the resulting enzyme-NADPH binary complex. Dutasteride provided the highest negative binding energy and was selected to illustrate the binding network with the calculated  $5\alpha$ -R structures. We observed  $\Delta G$  of -5.8 kcal/mol and the hydrogen bonding interactions at Tyr95 with  $5\alpha$ -R1 structure. Additionally, we observed  $\Delta G$  of -7.3 kcal/mol with the hydrogen bond interactions at Ser99 and Arg114 with  $5\alpha$ -R2 structure. Transmembrane calculation depicted that the

*in silico* 5 $\alpha$ -R1 and 5 $\alpha$ -R2 are the transmembrane enzymes. Docking studies of 28 known 5 $\alpha$ -reductase inhibitors were operated using Autodock Vina. In the study of 5 $\alpha$ -R1, dutasteride exhibited the highest negative  $\Delta G$  of -5.5 kcal/mol and the other steroidal compounds showed relatively similar binding energy. With 5 $\alpha$ -R2, compounds **3.9**, **3.11**, and **3.15** presented the highest negative  $\Delta G$  of -7.8, -7.6, and -7.5, respectively. Interestingly, these three inhibitors contain the bulky phenyl groups on the amide at C17. Our results were in agreement with areported 3D-QASR study that described the importance of the bulky phenyl substituent as the crucial point for the hydrophobic interactions. In summary, the docking of 28 known 5 $\alpha$ -reductase inhibitors clearly assures the quality of the derived *in silico* 5 $\alpha$ -R1 and 5 $\alpha$ -R2 for the further virtual screening of 5 $\alpha$ -reductase inhibitor and enables to employ for the future study in the related area.





## Chapter IV

### Molecular Docking of Avicequinone C and Analogs

#### Contents

- 4.1 Introduction
  - 4.1.1 Ligand-based drug design
  - 4.1.2 Structure-based drug design
  - 4.1.3 Molecular docking
  - 4.1.4 Example of computational aided drug design researches
- 4.2 Materials and methods
- 4.3 Results and discussion
  - 4.3.1 Docking studies of 5 $\alpha$ -R1
  - 4.3.2 Docking studies of 5 $\alpha$ -R2
- 4.4 Conclusions

## 4.1 Introduction

Drug discovery is a process of searching for a new medicine for curing a particular disease. The traditional methods of drug discovery have been relied on a trial-and-error procedure by evaluating biological activities of some interesting compounds via *in vitro* or *in vivo* assays and analyze their potency against specific treatment. To date, computational technique known as computational aided drug design has been generally used to expedite the drug discovery process. The calculated program rapidly provides the prediction of biological activity of the compounds of interest. As a result, computer-aided drug design helps to establish a series of new drug candidates with more specific, faster research, with lower cost and higher successful rate than the traditional strategy [55]. There are 2 main types of computational aided drug design, which are ligand-based drug design and structure-based drug design.

### 4.1.1 Ligand-based drug design

Ligand-based drug design is a process that depends on the knowledge of a set of compounds, which have similar structure and pharmacological activity. These compounds are used to analyze the essential functional group or pharmacophore, which is a functional group that crucially bind to the protein target. In other word, a model of the biological target is built based on the knowledge of what binds to it, and this model is used to design new compounds that potentially interact with the molecular target in a similar manner as the original template compounds. This method is employed in the quantitative structure-activity relationship (QSAR) study, which is the study of a relationship between calculated properties of compounds and the experimental data of biological activity, which results in the prediction of the biological activity of new druggable analogs [56].

#### 4.1.2 Structure-based drug design

Structure-based drug design is a method that depends on the knowledge of three-dimensional structure of the biological target, which is obtained from X-ray crystallography or NMR spectroscopy. If a structure of biological target has not been reported, the three-dimensional structure can be predicted by homology modeling [56].

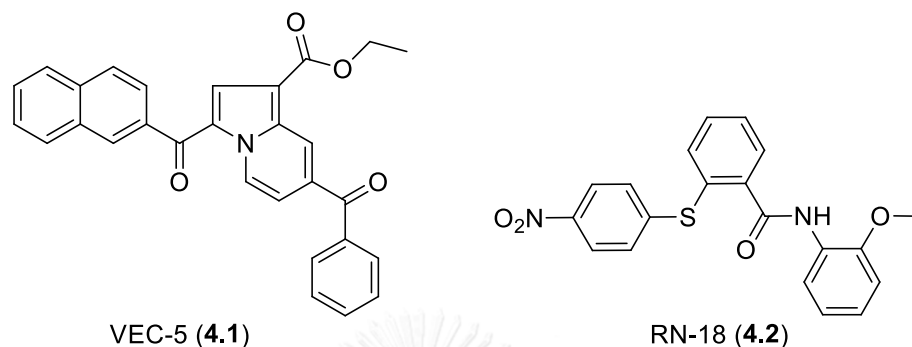
#### 4.1.3 Molecular docking

Molecular docking is one of the methods in structural molecular biology that uses for the prediction of biological property by searching the binding interaction between a compound (ligand) and a known three-dimensional structure of target protein. Molecular docking is commonly utilized in drug discovery, involving structure activity relationship studies, lead optimization, virtual screening, prediction of mutagenesis studies, pharmacological mechanism studies and combinatorial library design [57]. Molecular docking can provide the predicted information regarding the structural interaction between the ligand and the target enzyme as the binding energy ( $\Delta G$ ). The lower number of  $\Delta G$  refers to the stronger interaction between the ligand and the target enzyme [57].

#### 4.1.4 Example of computational aided drug design researches

To date, there are many researches that describe the discovery of new bioactive compounds and the study of biological mechanisms of the interesting diseases by using computational aided drug design. For instance, VEC5 and RN18 (**Figure 17**) were discovered and identified to inhibit viral infectivity factor (Vif), which is an essential target for the treatment HIV infection by the *in silico* studies [58]. After the first report of oseltamivir-resistance virus strain, homology modeling was employed in the study of drug resistance against chicken influenza virus (H5N1) neuraminidase [59]. Homology modeling of mammalian cytochrome P450, which involved in

metabolism of many medicines was conducted from published crystal structures of bacteria cytochrome P450 to study the key residues, enzyme-substrate interactions, analysis of inhibitors and site-directed mutagenesis [60].



**Figure 17** Structures of HIV inhibitors: VEC5 and RN8

According to a previous result, avicequinone C showed  $5\alpha$ -R1 inhibitory activities in human hair dermal papilla cells [5]. It is believed that naphthoquinones potentially possess  $5\alpha$ -R1 inhibitory activities, and the carbonyl groups of quinone potentially are essential for  $5\alpha$ -R1 inhibition. In this research, molecular docking studies of *in silico* three-dimensional structures of  $5\alpha$ -R1 and  $5\alpha$ -R2 were performed on avicequinone C and analogs to identify the key functional groups that involve in the catalytic sites of  $5\alpha$ -R and as a screening for the new  $5\alpha$ -R inhibitors having naphthoquinone moiety. Furthermore, some other natural naphthoquinones were included in our docking simulations.

## 4.2 Materials and methods

Avicequinone C and analogs were designed based upon simple synthetic accessibility. All the derivatives were furanonaphthoquinone with various furan side chain. In addition, some natural naphthoquinones were selected based on commercial availability. Our study involved three commercial natural naphthoquinones including 1,4-dihydroxyanthraquinone, 2-hydroxy-1,4-naphthoquinone, and lapachol. Moreover,

2,5-dihydroxy-1,4-benzoquinone and 4-hydroxycoumarin were added into our study as the example of the compounds lacking of benzene ring and quinone moieties, respectively. The two non-naphthoquinone compounds could confirm the importance of naphthoquinone moiety as an essential pharmacophore for 5 $\alpha$ -R inhibitory activity.

Structure of naphthoquinones were written by ChemBioDraw Ultra 12.0 and converted into PDB coordinated files by Open Babel software. Docking simulations were performed by Autodock Vina (Trott and Olson, 2010). Then, each ligand was docked into the resulting *in silico* NADPH and 5 $\alpha$ -R1 binary complex with the grid box near the position of NADPH (center x=0.487, center y=36.43, and center z=96.802) and the grid box sizes are size x=38, size y=18, and size z=16. In the case of 5 $\alpha$ -R2, each ligand was docked into the resulting *in silico* NADPH and 5 $\alpha$ -R2 binary complex with the grid box near the position of NADPH (center x=4.403, center y=51.086, and center z=113.368) and the grid box sizes are size x=18, size y=32, and size z=22. Both 5 $\alpha$ -R1 and 5 $\alpha$ -R2 were performed 100 docking number. Finally, the results were analyzed.

### 4.3 Results and discussion

#### 4.3.1 Docking studies of 5 $\alpha$ -R1

The docking studies of 5 $\alpha$ -R1 with avicequinone C and analogs were provided in **Table 17**. The docking results displayed the binding energy ( $\Delta G$ ) ranging from -3.7 to -5.8 kcal/mol. T (entry 1), the 5 $\alpha$ -R substrate and dutasteride (entry 2), and finasteride (entry 3), the known 5 $\alpha$ -R2 inhibitor showed  $\Delta G$  of -4.4, -5.8 and -4.4 kcal/mol, respectively. These 3 steroid compounds were employed in this experiment as references for comparison of the protein-ligand binding. The docking study indicated that they had the same hydrogen bond interactions with Tyr95 at a carbonyl group of steroid ring. In addition, dutasteride possessed the lowest binding energy, which refers to the best fit at the active pocket of 5 $\alpha$ -R1 that required NADPH as a cofactor. Next, a series of furanonaphthoquinone such as avicequinone C (entry 4), WNK-6 (entry 5), WNK-1 (entry 6), WNK-3 (entry 7), WNK-4 (entry 8), and WNK-7 (entry 9) had  $\Delta G$  of -5.5,

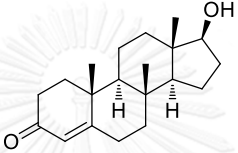
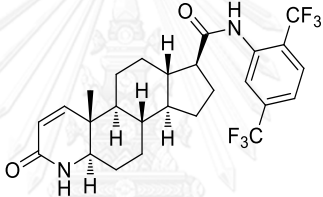
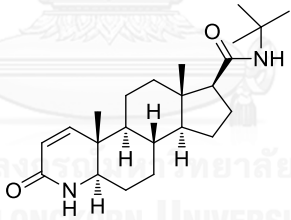
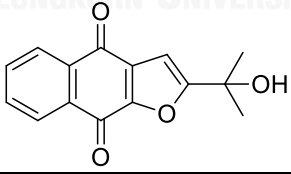
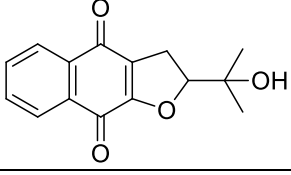
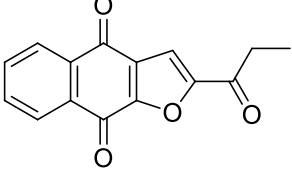
-5.4, -5.1, -4.9, -5.2 and -4.6 kcal/mol, respectively. Avicequinone C displayed the best docking energies that were closest to the reference compounds. All furanonaphthoquinone presented the same hydrogen bond interactions with Tyr95 similar to testosterone, dutasteride, and finasteride. Avicequinone C and WNK-6 displayed hydrogen bond interactions with Tyr95 at the hydroxyl group (-OH) of the alkyl group attached to the furan and dihydrofuran ring, respectively. WNK-1, WNK-3, and WNK-4 showed the hydrogen bond interactions with Tyr95 at ketone group of the side chain attached to the furan or dihydrofuran ring. Interestingly, avicequinone C, WNK-1 and WNK-4 had the additional hydrogen bond interactions with Gln131 through the ketone group of quinone ring. WNK-7 was the least favor furanonaphthoquinone that had lowest binding affinity to 5 $\alpha$ -R1, probably due to the lack of substituent at furan ring. It demonstrated hydrogen bond interactions with Tyr95 at ketone group of quinone ring. Comparing between furan and dihydrofuran motifs, the docking energies obtained from the compounds having furan motif (avicequinone C, WNK-1, and WNK-4) were slightly better than those of the compounds having dihydrofuran motif (WNK-6, and WNK-3). Moreover, the docking energy obtained from the compounds with alcohol or ketone substituent were not significantly different. One conclusion could be drawn from the docking study of furanonaphthoquinone that the substituent at furan or dihydrofuran ring was important for the binding activity to 5 $\alpha$ -R1 catalytic pocket.

Natural naphthoquinones included 1,4-dihydroxyanthraquinone (entry 10), lapachol (entry 11) and 2-hydroxy-1,4-naphthoquinone (entry 12) had  $\Delta G$  of -5.3, -4.4, -4.3, respectively. They showed hydrogen bond interactions with Tyr95 through the ketone group. In addition, 2-hydroxy-1,4-naphthoquinone (entry 12) also had hydrogen bond interactions with NADPH at hydroxyl group.

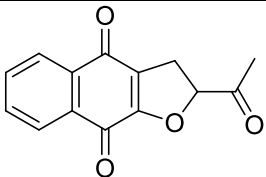
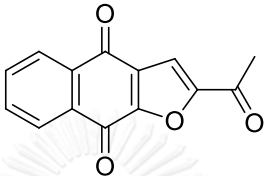
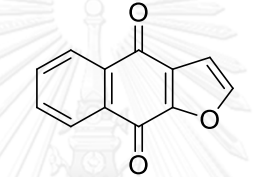
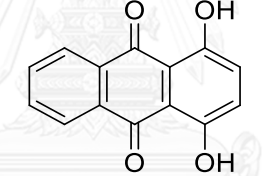
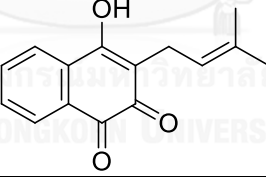
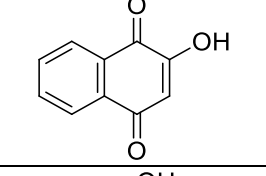
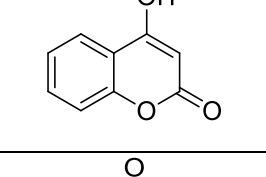
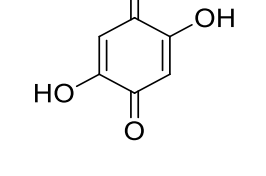
Two non-naphthoquinones including 4-hydroxycoumarin (entry 13) and 2,5-dihydroxy-1,4-naphthoquinone (entry 14) had  $\Delta G$  of -4.5 and -3.7 kcal/mol, respectively. They had hydrogen bond interactions with Tyr95 through ketone group. Besides, 4-hydroxycoumarin (entry 13) had hydrogen bond interactions with NADPH at hydroxyl group. Lacking of quinone ring but remaining of aromatic ring such as 4-

hydroxycoumarin (entry 13) and lacking of aromatic but remaining quinone such as 2,5-dihydroxy-1,4-benzoquinone (entry 14) showed significant drop of binding interaction at 5 $\alpha$ -R1 catalytic pocket. Thus, the naphthoquinone skeleton was essential for biological activity for 5 $\alpha$ -R1.

**Table 17** Docking studies of 5 $\alpha$ -R1 with avicequinone C and analogs

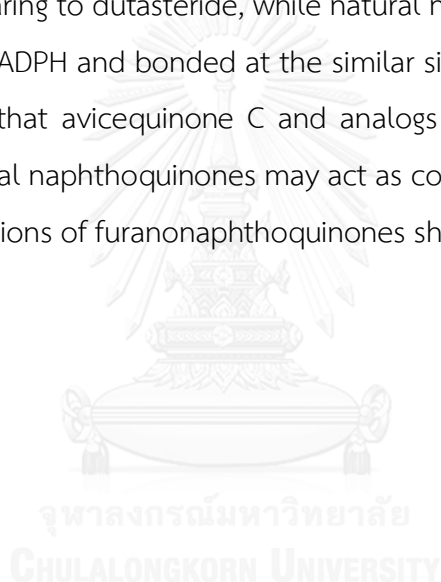
Entry	Compound	Structure	$\Delta G$ (kcal/mol)	Interaction with amino acid
1	Testosterone (4.3)		-4.4	Tyr95
2	Dutasteride (4.4)		-5.8	Tyr95
3	Finasteride (4.5)		-4.4	Tyr95
4	Avicequinone C (WNK-5, 4.6)		-5.5	Tyr95, NADPH
5	WNK-6 (4.7)		-5.4	Tyr95, NADPH
6	WNK-1 (4.8)		-5.1	Tyr95, Gln131 NADPH

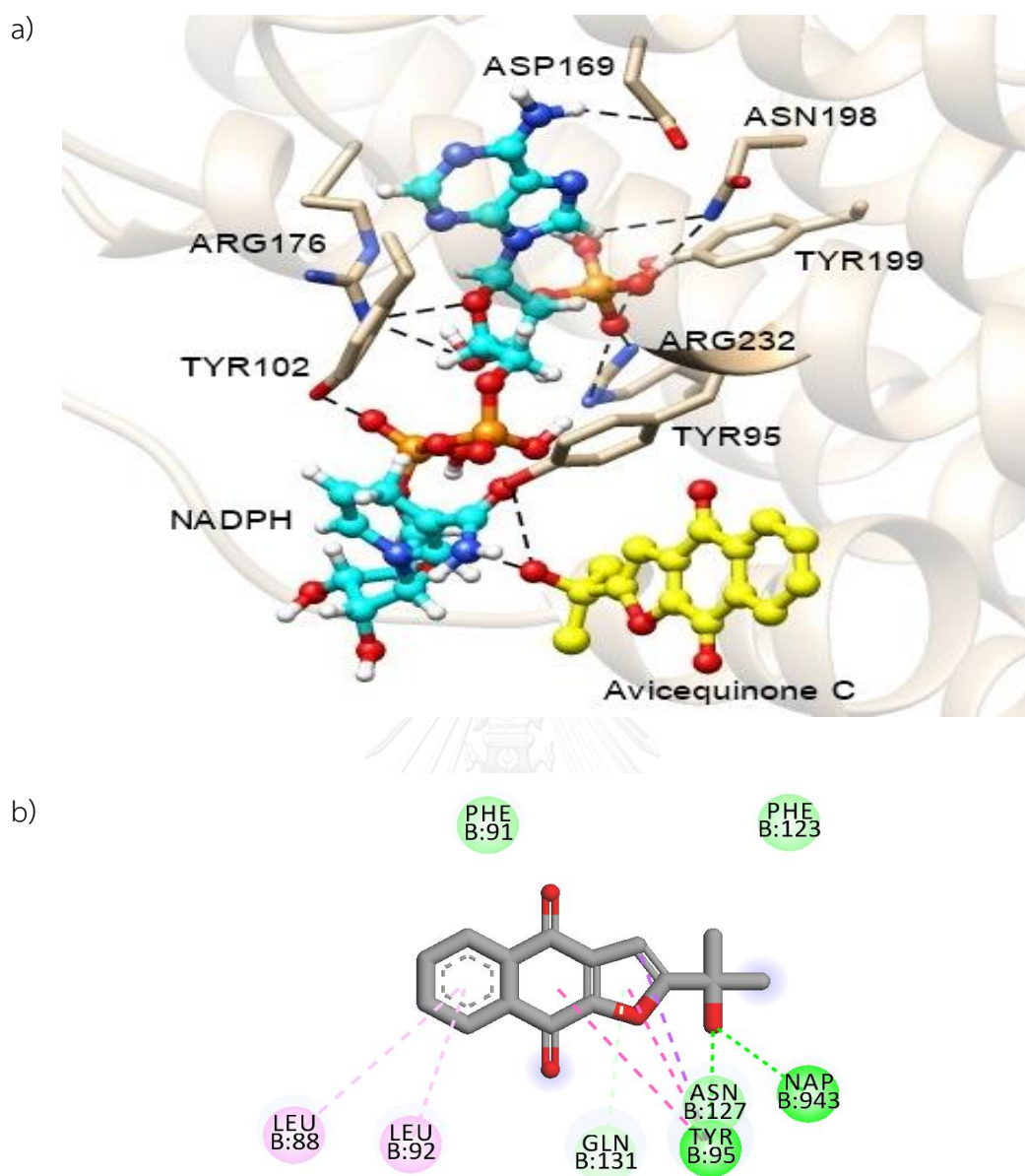
**Table 17** (Cont.) Docking studies of 5 $\alpha$ -R1 with avicequinone C and analogs

Entry	Compound	Structure	$\Delta G$ (kcal/mol)	Interaction with amino acid
7	WNK-3 (4.9)		-4.9	Tyr95, NADPH
8	WNK-4 (4.10)		-5.2	Tyr95, Gln131 NADPH
9	WNK-7 (4.11)		-4.6	Tyr95
10	1,4-dihydroxy Anthraquinone (4.12)		-5.3	Tyr95
11	Lapachol (4.13)		-4.4	Tyr95
12	2-Hydroxy-1,4- naphthoquinone (4.14)		-4.3	Tyr95, NADPH
13	4- Hydroxycoumari n (4.15)		-4.5	Tyr95, NADPH
14	2,5-Dihydroxy- 1,4- benzoquinone (4.16)		-3.7	Tyr95



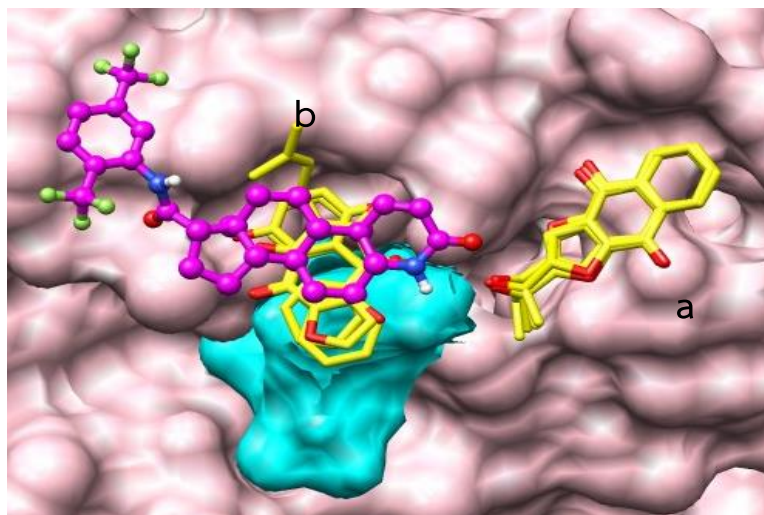
From the  $\Delta G$  results shown in **Table 17**, among all naphthoquinones, avicequinone C (**4.6** entry 4) exhibited the best protein-ligand binding affinity at -5.5 kcal/mol, which was similar to the binding energy level of dutasteride. The results suggest the development of avicequinone C as a promising  $5\alpha$ -R1 inhibitor. The catalytic site of the *in silico*  $5\alpha$ -R1 with NADPH and avicequinone is shown in **Figure 18**. We observed that avicequinone C had hydrogen bond interactions with NADPH. However, the superimposition of all interesting compounds illustrated that the binding sites of avicequinone C and analogs and a set of natural naphthoquinones were significantly different (**Figure 19**). Surprisingly, avicequinone C and analogs had different binding region, comparing to dutasteride, while natural naphthoquinones were closely resided adjacent to NADPH and bonded at the similar site of T and dutasteride. Thus, we could speculate that avicequinone C and analogs may act as non-competitive inhibitors, while natural naphthoquinones may act as competitive inhibitors. However, the mechanism of actions of furanonaphthoquinones should be further studied in the *in vitro* experiments.





Green dash lines are hydrogen acceptor. Light pink dash lines are  $\pi$ -alkyl interaction. Dark pink dash lines are  $\pi$ - $\pi$  T-shaped interaction. Purple dash lines are  $\pi$ - $\sigma$  interaction. Light purple surface areas represent hydrophobic interactions.

**Figure 18** Ternary complex of the *in silico* 5 $\alpha$ -R1 with NADPH and avicequinone C a) 3D-diagram displayed a catalytic site; c) 2D-diagram displayed the binding interactions



Blue surface areas represent NADPH; Magenta structure represents dutasteride; Yellow structures represent a) avicequinone C and analogs and b) natural naphthoquinones.

**Figure 19** Superimposition of dutasteride, avicequinone C and analogs and natural naphthoquinones with  $5\alpha$ -R1

#### 4.3.2 Docking studies of $5\alpha$ -R2

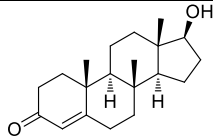
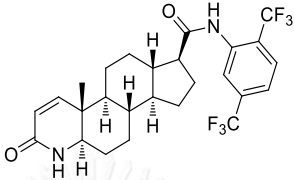
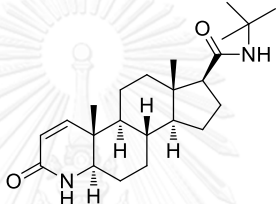
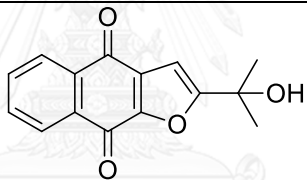
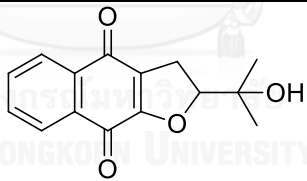
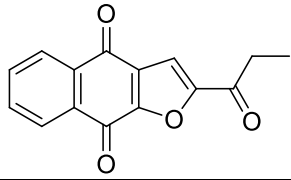
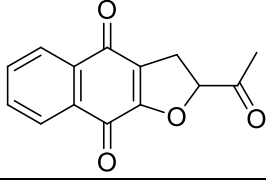
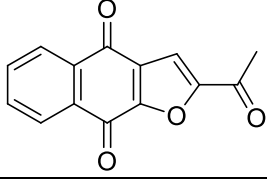
The docking studies of  $5\alpha$ -R2 with avicequinone C and analogs are provided in **Table 18**. The docking results displayed the binding energy ( $\Delta G$ ) ranging from -4.5 to -7.3 kcal/mol. T (entry 1), the  $5\alpha$ -R substrate and dutasteride (entry 2), and finasteride (entry 3), the known  $5\alpha$ -R2 inhibitor showed  $\Delta G$  of -4.5, -7.3 and -5.3 kcal/mol, respectively. These 3 steroid compounds were employed in this experiment as the references to compare the protein-ligand binding. The docking studies indicated that they had the same hydrogen bond interactions with Ser99 at a carbonyl group of steroid ring. In addition, dutasteride possessed the lowest binding energy, which refers to the best fit at the active pocket of  $5\alpha$ -R2 required composed of NADPH as a cofactor. Next, a series of furanonaphthoquinone such as avicequinone C (entry 4), WNK-6 (entry 5), WNK-1 (entry 6), WNK-3 (entry 7), WNK-4 (entry 8), and WNK-7 (entry 9) had  $\Delta G$  of -6.3, -6.2, -6.2, -5.2, -6.1 and -5.4 kcal/mol, respectively. Avicequinone C (entry 4) displayed the best docking energies. All furanonaphthoquinone presented the same hydrogen bond interactions with NADPH. Moreover, all furanonaphthoquinones except

WNK-6 showed hydrogen bond interactions with Tyr98. Avicequinone C and WNK-6 displayed hydrogen bond interactions with NADPH at hydroxyl group (-OH) that connected to furan and dihydrofuran ring, respectively. WNK-1, WNK-3, and WNK-4 showed hydrogen bond interactions with Tyr98 through ketone of quinone ring. WNK-7 was the least favor furanonaphthoquinone, with binding to 5 $\alpha$ -R2, possibly due to the lack of substituent at furan ring. Interestingly, the docking energy obtained from the compounds having alcohol substituent and ketone substituent were not significantly different. However, the substituent at furan or dihydrofuran ring was essential for the binding activity to 5 $\alpha$ -R2 catalytic pocket.

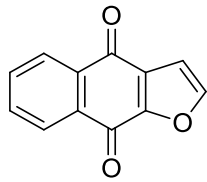
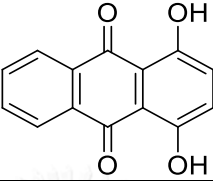
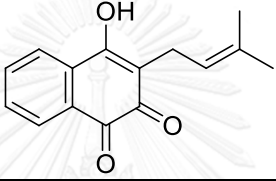
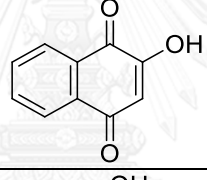
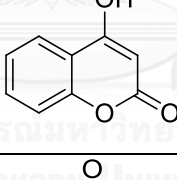
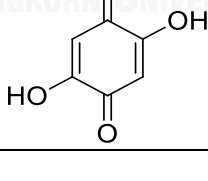
Natural naphthoquinones including 1,4-dihydroxyanthraquinone (entry 10), lapachol (entry 11) and 2-hydroxy-1,4-naphthoquinone (entry 12) had  $\Delta G$  of -6.0, -6.2, -5.6, respectively. 1,4-dihydroxyanthraquinone (entry 10), lapachol (entry 11) had hydrogen bond interactions with Lys172 through the ketone group. Remarkably, 2-hydroxy-1,4-naphthoquinone (entry 12) had hydrogen bond interactions with Tyr98 and Arg114 at ketone group.

Two non-naphthoquinones including 4-hydroxycoumarin (entry 13) and 2,5-dihydroxy-1,4-naphthoquinone (entry 14) had  $\Delta G$  of -5.3 and -4.6 kcal/mol, respectively. 4-hydroxycoumarin (entry 13) had hydrogen bond interactions with NADPH at ketone group. It also had hydrogen bond interactions with NADPH at hydroxyl group. While, 2,5-dihydroxy-1,4-naphthoquinone (entry 14) had hydrogen bond interactions with Lys172 at ketone group. The decreased of binding interaction of 4-hydroxycoumarin (entry 13) and 2,5-dihydroxy-1,4-naphthoquinone (entry 14) showed the importance of naphthoquinone as an significant pharmacophore for binding activity of 5 $\alpha$ -R2.

**Table 18** Docking studies of 5 $\alpha$ -R2 with avicequinone C and analogs

Entry	Compound	Structure	$\Delta G$ (kcal/mol)	Interaction with amino acid
1	Testosterone (4.3)		-4.5	Ser99
2	Dutasteride (4.4)		-7.3	Ser99, Arg114, NADPH
3	Finasteride (4.5)		-5.3	Ser99
4	Avicequinone C (WNK-5, 4.6)		-6.3	Tyr98, Lys172, NADPH
5	WNK-6 (4.7)		-6.2	Lys172, Arg114, NADPH
6	WNK-1 (4.8)		-6.2	Tyr98, NADPH
7	WNK-3 (4.9)		-5.2	Tyr98, NADPH
8	WNK-4 (4.10)		-6.1	Tyr98, Arg114, NADPH

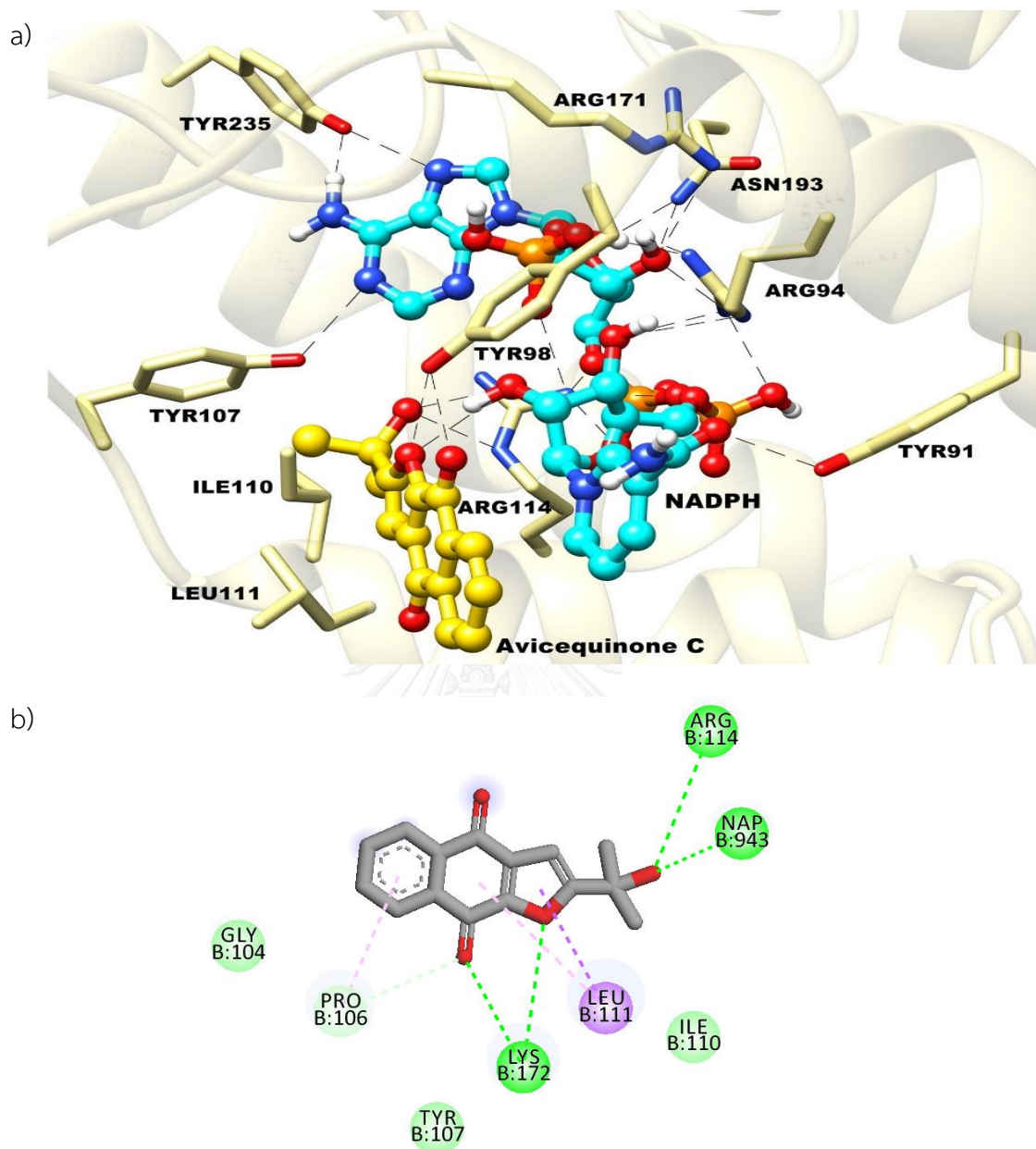
**Table 18** (Cont.) Docking studies of 5 $\alpha$ -R2 with avicequinone C and analogs

Entry	Compound	Structure	$\Delta G$ (kcal/mol)	Interaction with amino acid
9	WNK-7 (4.11)		-5.4	Tyr98, Arg114, NADPH
10	1,4-dihydroxy Anthraquinone (4.12)		-6.0	Arg114, Lys172, NADPH
11	Lapachol (4.13)		-6.2	Arg114, Lys172, NADPH
12	2-Hydroxy-1,4- naphthoquinone (4.14)		-5.6	Tyr98, Arg114, Leu111, Lys172, NADPH
13	4- Hydroxycoumarin (4.15)		-5.3	Lys172, NADPH
14	2,5-Dihydroxy- 1,4-benzoquinone (4.16)		-4.6	Tyr98, Lys172

From the  $\Delta G$  results shown in **Table 18**, among all naphthoquinone structures, avicequinone C (entry 4) exhibited the best protein-ligand binding affinity at -6.3 kcal/mol. To compare binding energy of Avicequinone C (entry 4) with 5 $\alpha$ -R substrate (T) and known inhibitors (finasteride and dutasteride), we observed that avicequinone C (entry 4) had  $\Delta G$  higher than dutasteride (entry 2) that had  $\Delta G$  of -7.3 kcal/mol. However, avicequinone C (entry 4) exhibited significant lower  $\Delta G$  than testosterone (entry 1) and finasteride (entry 3), which showed  $\Delta G$  of -4.5 and -5.3 kcal/mol,

respectively. These results support the development of avicequinone C as potential  $5\alpha$ -R2 inhibitor. Interestingly, avicequinone C had hydrogen bond interactions with Tyr98, Pro106, Lys172 and NADPH, which were different from T, finasteride and dutasteride (**Figure 20**). The superimposition of all interested compounds along with dutasteride at the catalytic site of the *in silico*  $5\alpha$ -R2 with NADPH confirmed the similar binding interaction of dutasteride, avicequinone C and analogs and natural naphthoquinones (**Figure 21**). Furanonaphthoquinones and natural naphthoquinones similarly resided adjacent to NADPH and bonded at the similar region of dutasteride. However, the hydrogen bond interaction with amino acid residues were different. Thus, molecular dynamics simulations should be proceeded in the future study in order to validate specific predicted interaction of the compounds in the series.

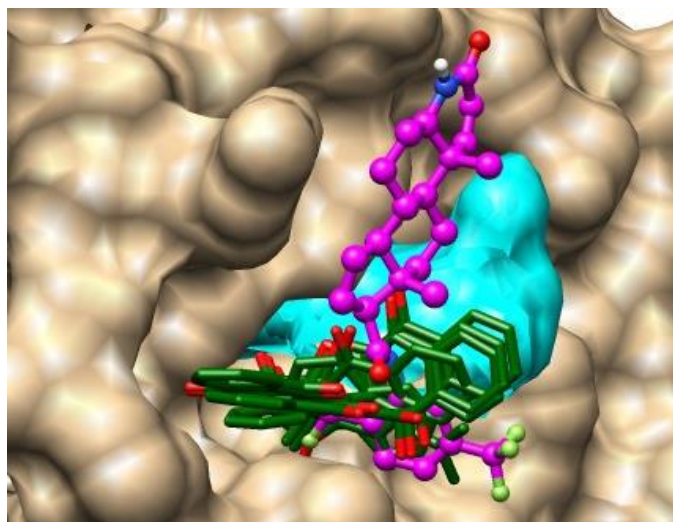




Green dash lines are hydrogen acceptor. Pink dash lines are  $\pi$ -alkyl interaction. Purple dash lines are  $\pi$ - $\sigma$  interaction. Light purple surface areas represent hydrophobic interactions.

**Figure 20** Ternary complex of the *in silico* 5 $\alpha$ -R2 with NADPH and avicequinone C a) 3D-diagram displayed a catalytic site; c) 2D-diagram displayed the binding interactions





Blue surface areas represent NADPH; Magenta structure represents dutasteride;  
Dark green structures represent furanonaphthoquinones and natural naphthoquinones.

**Figure 21** Superimposition of dutasteride, avicequinone C and analogs and natural naphthoquinones with  $5\alpha$ -R2

#### 4.4 Conclusions

Docking simulations of the enzyme-NADPH binary complex *in silico*  $5\alpha$ -R1 and  $5\alpha$ -R2 structures with avicequinone C and analogs and other natural naphthoquinones were performed using Autodock Vina. Based on our observation, Tyr95 was the key amino acid residue for  $5\alpha$ -R1, while Tyr98 and Lys172 were the key amino acid residues for  $5\alpha$ -R2. Among all the naphthoquinones, avicequinone C possessed the lowest binding energy in both *in silico*  $5\alpha$ -R1 and  $5\alpha$ -R2 structures, which supported the further development as potential  $5\alpha$ -R inhibitor. The naphthoquinone moiety was confirmed as an essential pharmacophore controlling binding interaction between selected compounds and  $5\alpha$ -R protein structure. Importantly, superimposition of dutasteride, avicequinone C and analogs and natural naphthoquinones with  $5\alpha$ -R1 showed different binding interactions between avicequinone C and analogs and natural naphthoquinones. This finding is important for the future studies toward  $5\alpha$ -R inhibiting assay.

## Chapter V

### Synthesis of Avicequinone C and Analogs

#### Contents

- 5.1 Introduction
- 5.2 Material and methods
- 5.3 Synthesis of avicequinone C and analogs
  - 5.3.1 Synthesis of 2-propionyl naphtho[2,3-b]furan-4,9-dione (**5.8**, WNK-1)
  - 5.3.2 Synthesis of 2-acetyl-2,3-dihydronaphtho[2,3-b]furan-4,9-dione (**5.10**, WNK-3)
  - 5.3.3 Synthesis of 2-acetyl naphtho[2,3-b]furan-4,9-dione (**5.11**, WNK-4)
  - 5.3.4 Synthesis of avicequinone C (**5.2**, WNK-5)
  - 5.3.5 Synthesis of 2-(2-hydroxypropan-2-yl)-2,3-dihydronaphtho[2,3-b]furan-4,9-dione (**5.12**, WNK-6)
  - 5.3.6 Synthesis of naphtho[2,3-b]furan-4,9-dione (**5.14**, WNK-7)
- 5.4 Spectroscopic data of synthetic avicequinone C and analogs
  - 5.4.1 2-Propionyl naphtho[2,3-b]furan-4,9-dione (**5.8**, WNK-1)
  - 5.4.2 2-Acetyl-2,3-dihydronaphtho[2,3-b]furan-4,9-dione (**5.10**, WNK-3)
  - 5.4.3 2-Acetyl naphtho[2,3-b]furan-4,9-dione (**5.11**, WNK-4)
  - 5.4.4 Avicequinone C (**5.2**, WNK-5)
  - 5.4.5 2-(2-Hydroxypropan-2-yl)-2,3-dihydronaphtho[2,3-b]furan-4,9-dione (**5.12**, WNK-6)
  - 5.4.6 Naphtho[2,3-b]furan-4,9-dione (**5.14**, WNK-7)
- 5.5 Results and discussion
- 5.6 Conclusions

## 5.1 Introduction

Avicequinone C (**5.2**), a natural furanonaphthoquinone, was first discovered from *Avicennia alba* in 2000 [61] and it was recently isolated from *Avicennia marina* in 2014 [5]. This compound showed various biological activities (**Table 19**) including antimicrobial, antiproliferative and 5 $\alpha$ -reductase inhibitory activities [5, 62].

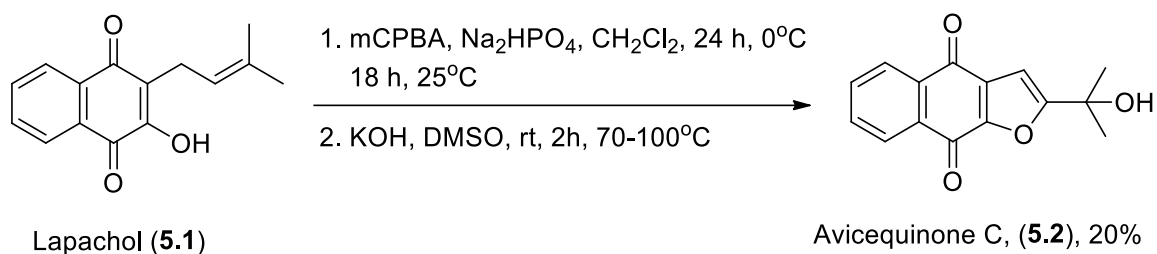
**Table 19** Reported biological activities of avicequinone C

Activities	Bioassay	Concentration ( $\mu\text{g/ml}$ )
Antiproliferative activity	Antiproliferative activity against L-929 (mouse fibroblasts)	$\text{GI}_{50} = 0.8$
	Antiproliferative activity against human K562 (human chronic myeloid leukemia) cells	$\text{GI}_{50} = 1.1$
Cytotoxic activity	Cytotoxic activity against the HeLa (human cervix carcinoma) cell line	$\text{CC}_{50} = 3.2$
Antimicrobial activity	Antimicrobial activity against vancomycin-resistant <i>Enterococcus faecalis</i> 1528 by micro-broth dilution method	MIC = 50
	Antimicrobial activity against <i>Mycobacterium fortuitum</i> B by micro-broth dilution method	MIC = 12.5
	Antimicrobial activity against <i>Mycobacterium vaccae</i> IMET 10670 by micro-broth dilution method	MIC = 6.2

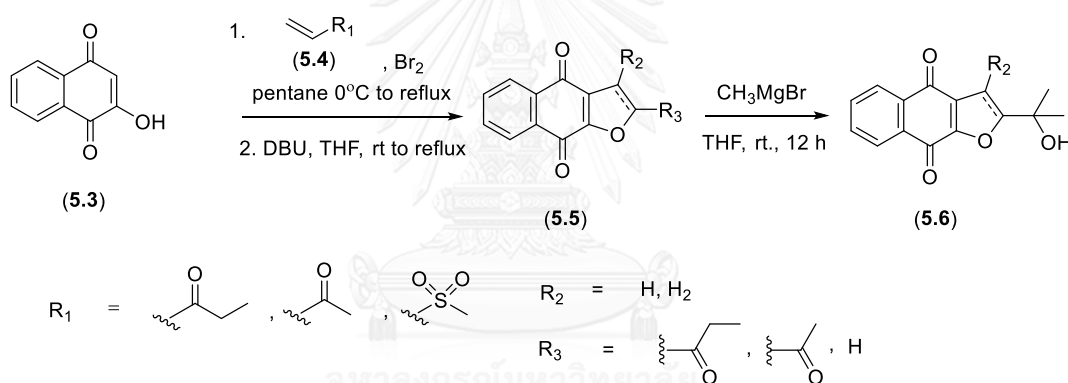
**Table 19** (Cont.) Reported biological activities of avicequinone C

Activities	Bioassay	Concentration ( $\mu\text{g/ml}$ )
Antimicrobial activities	Antimicrobial activity against <i>Mycobacterium smegmatis</i> SG 987 by micro-broth dilution method	MIC = 6.25
	Antimicrobial activity against <i>Candida albicans</i> BNSY 212 by micro-broth dilution method	MIC = 12.5
	Antimicrobial activity against <i>Mycobacterium aurum</i> SB 66 by micro-broth dilution method	MIC = 6.25
	Antimicrobial activity against methicillin-resistant <i>Staphylococcus aureus</i> by micro-broth dilution method	MIC = 6.25
5 $\alpha$ -reductase inhibitory activities	Human hair dermal papilla cell	IC <sub>50</sub> = 9.94

The synthesis of avicequinone C was first reported in 2011 by employing lapachol as the starting material (**Figure 22**). The synthesis involved epoxide formation and cyclization to afford avicequinone C in 20% yield [63].

**Figure 22** Synthesis of avicequinone C from lapachol

In this chapter, the preparation of avicequinone C and analogs was elaborated. The selected analogs of avicequinone C were chosen based on  $\Delta G$  values, which were obtained from molecular docking studies in Chapter 4. In general, our synthetic protocol involved 2-step transformations, which were cyclization *via* nucleophilic substitution to construct a furan ring [64] and alkylation *via* Grignard's reaction to form an alcohol side chain [65]. Under this strategy, 2-hydroxy-1,4-naphthoquinone (**5.3**) was used as the starting material and was treated with several vinylogous reagents such as pen-1-en-3-one, methyl vinyl ketone and methyl vinyl sulfone to obtain furanonaphthoquinone (**5.5**) (**Figure 23**). Next, the resulting furanonaphthoquinone (**5.5**) reacted with methyl magnesium bromide ( $\text{CH}_3\text{MgBr}$ ) to give the corresponding alcohol of the desired product **5.6**.



**Figure 23** Synthesis of avicequinone C and analogs

## 5.2 Material and methods

Reactions were carried out in oven-dried glassware and magnetically stirred under inert atmosphere using syringe tube equipped with argon or nitrogen balloon. Room temperature was  $25^\circ\text{C}$ , unless otherwise stated. Commercial solvents and reagents were used as received, unless otherwise explained. Anhydrous solvents were dried over  $4\text{\AA}$  molecular sieves. Brine refers to a saturated aqueous solution of sodium chloride. All reactions were monitored by thin layer chromatography (TLC) using aluminium silica gel 60 F254 (Merck). Bands were visualized by UV activity at  $254\text{ nm}$ .

Flash column chromatography was performed using 60Å silica gel (230-400 mesh, 0.040-0.063 mm) as a stationary phase. All solvents such as ethyl acetate, dichloromethane and hexane were distilled before using. IR spectra were measured on a Fourier Transform Infrared Spectrometer, PerkinElmer from Scientific and Technological Research Equipment Center, Chulalongkorn University.  $^1\text{H}$  and  $^{13}\text{C}$  NMR spectra were obtained on a Bruker Avance DPX-300 FT-NMR spectrometer.  $^1\text{H}$ -NMR chemical shifts ( $\delta$ ) and coupling constants ( $J$ ) were given in ppm and Hz, respectively. Deuterated chloroform ( $\text{CDCl}_3$ ) served as an internal standard for both  $^1\text{H}$  and  $^{13}\text{C}$  NMR spectra at 7.26 and 77.0 ppm, respectively. Mass spectra were recorded on a microTOF Bruker Daltonics mass spectrometer of Department of Chemistry, Faculty of Science, Mahidol University. Abbreviations were defined as follows; THF: tetrahydrofuran and DBU: 1,8-Diazabicycloundec-7-ene.

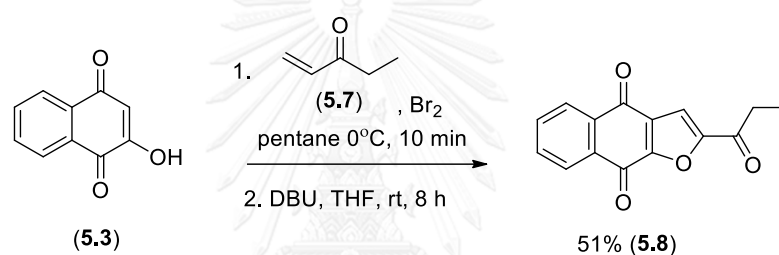
### 5.3 Synthesis of avicequinone C and analogs

#### 5.3.1 Synthesis of 2-propionylnaphtho[2,3-b]furan-4,9-dione (**5.8**, WNK-1)

To a stirred solution of pen-1-en-3-one (**5.7**, MW = 84.06 g/mol, 2.5 equiv, 7.18 mmol, 0.609 ml) in pentane 5.8 ml was added a solution of bromine (MW = 159.83 g/mol, 2.6 equiv, 7.46 mmol, 0.3 ml) in pentane 2.9 ml at  $-15^\circ\text{C}$  (NaCl mixed ice bath). The reaction was stirred for 10 minutes. After 10 minutes, all volatiles were evaporated under reduced pressure to yield crude 1,2-dibromopentan-2-one, which was further used in the next step without purification.

Next, 2-hydroxy-1,4-naphthoquinone (**5.3**, MW = 174.15 g/mol, 1 equiv., 2.87 mmol, 500 mg) was weighted into a 50 ml oven dried-rounded bottom flask and dissolved in THF 14.37 ml. DBU (MW = 152.24 g/mol, 3.7 equiv, 10.62 mmol, 1.595 ml) was added resulting a red solution. The reaction was stirred at  $0^\circ\text{C}$  (ice bath) for 20 minutes under nitrogen atmosphere. A freshly prepared solution of 1,2-dibromopentan-2-one in THF 3 ml was added. After addition, the ice bath was immediately removed. The reaction mixture was gradually warmed up to room temperature and stirred for 5 hours. Another portion of DBU (MW = 152.24 g/mol, 0.52

equiv, 1.49 mmol, 0.2175 ml) was added. The reaction mixture was continuously stirred for 3 hours at room temperature. The reaction was quenched by addition of aqueous ammonium chloride. The reaction mixture was extracted with chloroform (25 ml x 3 times). The organic extracts were combined, washed with water and saturated sodium chloride, dried over anhydrous  $\text{Na}_2\text{SO}_4$ , filtered and evaporated under reduced pressure to obtain a crude product. Purification of the crude reaction by silica gel column chromatography using ethyl acetate/hexane (1:1) provided 2-propionynaphtho[2,3-b]furan-4,9-dione (**5.8**) (**Figure 24**) Under this condition, 2-propionynaphtho[2,3-b]furan-4,9-dione (**5.8**) was obtained as the major product in 258.5 mg (51%) as a yellow solid [64].



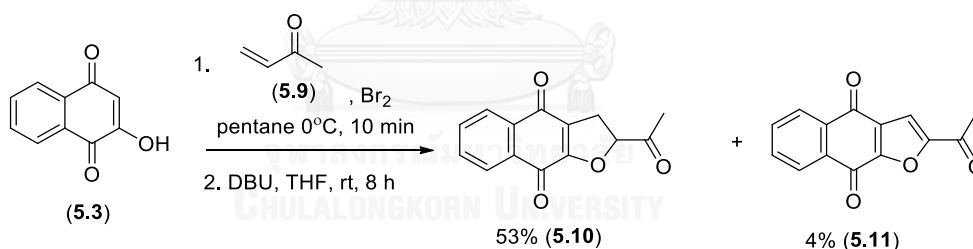
**Figure 24** Synthesis of 2-propionynaphtho[2,3-b]furan-4,9-dione (**5.8**, WNK-1)

### 5.3.2 Synthesis of 2-acetyl-2,3-dihydronaphtho[2,3-b]furan-4,9-dione (**5.10**, WNK-3)

To a stirred solution of methyl vinyl ketone (**5.9**, MW = 70.09 g/mol, 2.5 equiv, 7.18 mmol, 0.609 ml) in pentane 5.8 ml was added a solution of bromine (MW = 159.83 g/mol, 2.6 equiv, 7.46 mmol, 0.3 ml) in pentane 2.9 ml at  $-15^\circ\text{C}$  (NaCl mixed ice bath). The reaction mixture was stirred for 10 minutes. After 10 minutes, all volatiles were evaporated under reduced pressure to yield crude 1,2-dibromobutan-2-one, which was further used in the next step without purification.

Next, 2-hydroxy-1,4-naphthoquinone (**5.3**, MW = 174.15 g/mol, 1 equiv., 2.87 mmol, 500 mg) was weighted into a 50 ml oven dried-rounded bottom flask and dissolved in THF 14.37 ml. DBU (MW = 152.24 g/mol, 3.7 equiv, 10.62 mmol, 1.595 ml) was added resulting a red solution. The reaction was stirred at  $0^\circ\text{C}$  (ice bath) for 20

minutes under nitrogen atmosphere. A freshly prepared solution of 1,2-dibromobutan-2-one in THF 3 ml was added. After addition, the ice bath was immediately removed. The reaction mixture was gradually warmed up to room temperature and stirred for 5 hours. Another portion of DBU (MW = 152.24 g/mol, 0.52 equiv, 1.49 mmol, 0.2175 ml) was added. The reaction was continuously stirred for 3 hours at room temperature. The reaction was quenched by addition of aqueous ammonium chloride. The reaction mixture was extracted with chloroform (25 ml  $\times$  3 times). The organic extracts were combined, washed with water and saturated sodium chloride, dried over anhydrous  $\text{Na}_2\text{SO}_4$ , filtered and evaporated under reduced pressure to obtain a crude product. Purification of the crude reaction by silica gel column chromatography using dichloromethane/hexane (4:1) provided 2-acetyl-2,3-dihydronaphtho[2,3-b]furan-4,9-dione (**5.10**) (**Figure 25**). Under this condition, 2-acetyl-2,3-dihydronaphtho[2,3-b]furan-4,9-dione (**5.10**) was obtained as the major product in 262.6 mg (53%) as a yellow solid and 2-acetylnaphtho[2,3-b]furan-4,9-dione (**5.11**) was obtained as a minor product in 21.8 mg (4%) as a yellow solid [64].



**Figure 25** Synthesis of 2-acetyl-2,3-dihydronaphtho[2,3-b]furan-4,9-dione (**5.10**, WNK-3)

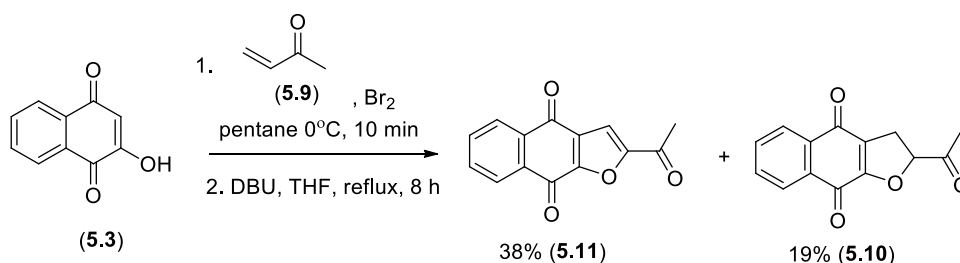
### 5.3.3 Synthesis of 2-acetylnaphtho[2,3-b]furan-4,9-dione (**5.11**, WNK-4)

To a stirred solution of methyl vinyl ketone (**5.9**, MW = 70.09 g/mol, 2.5 equiv, 7.18 mmol, 0.609 ml) in pentane 5.8 ml was added a solution of bromine (MW = 159.83 g/mol, 2.6 equiv, 7.46 mmol, 0.3 ml) in pentane 2.9 ml at  $-15^\circ\text{C}$  (NaCl mixed ice bath). The reaction was stirred for 10 minutes. After 10 minutes, all volatiles were evaporated



under reduced pressure to yield crude 1,2-dibromobutan-2-one, which was further used in the next step without purification.

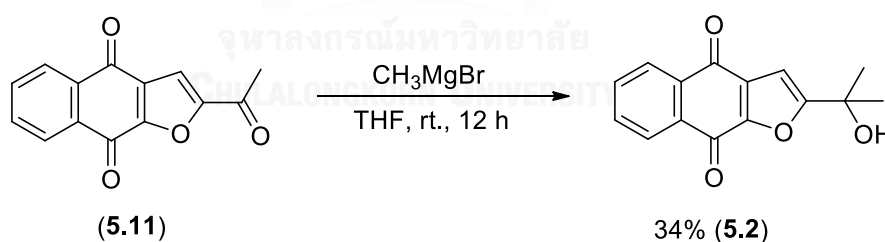
Next, 2-hydroxy-1,4-naphthoquinone (**5.3**, MW = 174.15 g/mol, 1 equiv., 2.87 mmol, 500 mg) was weighted into a 50 ml oven dried-rounded bottom flask and dissolved in THF 14.37 ml. DBU (MW = 152.24 g/mol, 3.7 equiv, 10.62 mmol, 1.595 ml) was added resulting a red solution. The reaction was stirred at 0°C (ice bath) for 20 minutes under nitrogen atmosphere. A freshly prepared solution of 1,2-dibromobutan-2-one in THF 3 ml was added. After addition, the ice bath was immediately removed. The reaction mixture was gradually warmed up and heated at 70°C to reflux for 5 hours. Another portion of DBU (MW = 152.24 g/mol, 0.52 equiv, 1.49 mmol, 0.2175 ml) was added. The reaction was continuously refluxed and stirred for 3 hours. The reaction was quenched by addition of aqueous ammonium chloride. The reaction mixture was extracted with chloroform (25 ml x 3 times). The organic extracts were combined, washed with water and saturated sodium chloride, dried over anhydrous Na<sub>2</sub>SO<sub>4</sub>, filtered and evaporated under reduced pressure to obtain a crude product. Purification of the crude reaction by silica gel column chromatography using dichloromethane/hexane (4:1) provided 2-acetylnaphtho[2,3-b]furan-4,9-dione (**5.11**) (Figure 26). Under this condition, 2-acetylnaphtho[2,3-b]furan-4,9-dione (**5.11**) was obtained as the major product in 191.3 mg (38%) as a yellow solid and 2-acetyl-2,3-dihydronaphtho[2,3-b]furan-4,9-dione (**5.10**) was obtained as a minor product in 97mg (19%) as a yellow solid [64].



**Figure 26** Synthesis of 2-acetylnaphtho[2,3-b]furan-4,9-dione (**5.11**, WNK-4)

### 5.3.4 Synthesis of avicequinone C (**5.2**, WNK-5)

2-acetylnaphtho[2,3-b]furan-4,9-dione (WNK-4, **5.11**, MW = 240.21 g/mol, 1 equiv, 0.208 mmol, 50 mg) was weighted into a 50 ml oven dried-rounded bottom flask and dissolved in THF 20 ml. The reaction mixture was stirred at room temperature under argon atmosphere.  $\text{CH}_3\text{MgBr}$  (MW 119.24 = g/mol, 6 equiv, 1.249 mmol, 0.1 ml) was added to the reaction mixture. The reaction mixture was stirred at room temperature for 6 hours. After completion, the reaction mixture was quenched by the addition of aqueous hydrochloric acid (2 N, 15 ml) and stirred at room temperature for 30 minutes. The reaction mixture was evaporated under reduced pressure until about 10 ml of reaction mixture remained. Then 5 ml of DI water was added. The reaction mixture was extracted with ethyl acetate (35 ml  $\times$  2 times) and washed with saturated sodium chloride 20 ml. The organic layers were collected, dried over anhydrous  $\text{Na}_2\text{SO}_4$  and filtered. The reaction mixtures were evaporated to obtain crude compound. Purification by silica gel column chromatography using ethyl acetate/hexane (3:7) provided avicequinone C (**5.2**). Under this condition, avicequinone C (**5.2**) was obtained as the major product in 17.2 mg (34%) as a brown solid (**Figure 27**) [65].

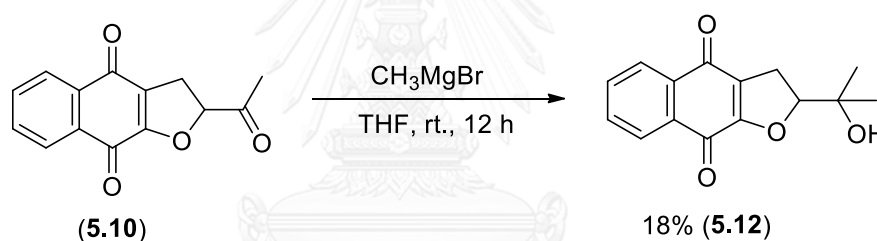


**Figure 27** Synthesis of avicequinone C (**5.2**, WNK-5)

### 5.3.5 Synthesis of 2-(2-hydroxypropan-2-yl)-2,3-dihydronaphtho[2,3-b]furan-4,9-dione (**5.12**, WNK-6)

2-acetyl-2,3-dihydronaphtho[2,3-b]furan-4,9-dione (WNK-3, **5.10**, MW = 242.22 g/mol, 1 equiv, 0.206 mmol, 50 mg) was weighted into a 50 ml oven dried-rounded bottom flask and dissolved in THF 20 ml. The reaction was stirred at room temperature

under argon atmosphere.  $\text{CH}_3\text{MgBr}$  (MW 119.24 = g/mol, 6 equiv, 1.249 mmol, 0.1 ml) was added to the reaction mixture. The reaction mixture was stirred at room temperature for 6 hours. After the reaction complete, the reaction mixture was quenched by the addition of aqueous hydrochloric acid (2 N, 15 ml) and stirred at room temperature for 30 minutes. The reaction mixture was evaporated until about 10 ml of reaction mixture was remained. Then 5 ml of DI water was added. The reaction mixture was extracted with ethyl acetate (35 ml  $\times$  2 times) and washed with saturated sodium chloride 20 ml. The organic layers were collected, dried over anhydrous  $\text{Na}_2\text{SO}_4$  and filtered. The reaction mixture was evaporated to obtain crude compound. Purification by silica gel column chromatography using ethyl acetate/hexane (3:7) provided WNK-6 (**5.12**). Under this condition, WNK-6 (**5.12**) was obtained as the major product in 8.81 mg (18%) as a yellow solid (**Figure 28**) [65].

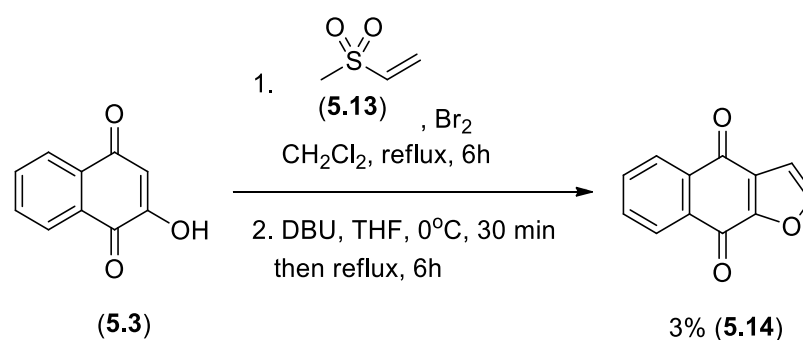


**Figure 28** Synthesis of 2-(2-hydroxypropan-2-yl)-2,3-dihydro[2,3-b]naphtho[4,9-dione] (**5.12**, WNK-6)

### 5.3.6 Synthesis of naphtho[2,3-b]furan-4,9-dione (**5.14**, WNK-7)

Methyl vinyl sulfone (**5.13**, MW 106.14 g/mol, 1.0 equiv, 4.71 mmol, 500 mg) was weighted into a 50 ml oven dried-rounded bottom flask and dissolved in dichloromethane (10 ml). The reaction mixture was stirred at room temperature under argon atmosphere. Bromine (MW 79.9 g/mol, density 3.1028 g/ml, 1.5 equiv, 7.07 mmol, 0.18 ml) was slowly added into the reaction mixture. The yellow solution turned to dark orange solution. The reaction mixture was heated to reflux at 50°C for 6 hours. After 6 hours, the reaction was monitored by TLC and no starting material remained. The reaction mixture was concentrated to yield a sticky residue. The

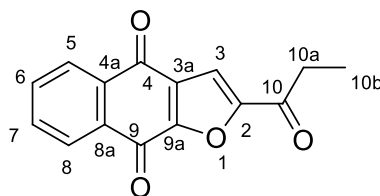
resulted residue was dissolved in THF (20ml) and the solution was cooled at 0°C in an ice-bath under argon atmosphere. DBU (MW 152.24 g/mol, density 1.018 g/ml, 1.5 equiv, 7.07 mmol, 1.06 ml) was slowly added dropwise over 20 minutes. The reaction mixture was stirred for 30 minutes at 0°C in an ice-bath under argon atmosphere. 2-hydroxy-1,4-naphthoquinone (**5.3**, MW 174.15 g/mol, 1.0 equiv, 4.71 mmol, 820.2 mg) was added and another portion of DBU (MW 152.24 g/mol, density 1.018 g/mL, 1.5 equiv, 7.07 mmol, 1.06 ml) was slowly added dropwise over 20 minutes. The reaction mixture was stirred for 30 minutes at 0°C in an ice-bath under argon atmosphere. The ice-bath was removed and the reaction was warmed up to room temperature. The reaction mixture was heated to reflux at 70°C for 6 hours. The reaction was then concentrated in vacuum. The residue was dissolved in dichloromethane (100 ml), washed with water 100 ml, followed by ammonium chloride (100 ml). The organic layer was separated and the aqueous layer was extracted with dichloromethane (50 ml x 3 times). The combined organic layers were dried over sodium sulfate and concentrated to obtain a crude product. The crude product was purified over silica gel column chromatography using dichloromethane/hexanes (3:1) as eluent provided naphtho[2,3-b]furan-4,9-dione (**5.14**). Under this condition, naphtho[2,3-b]furan-4,9-dione (**5.14**) was obtained as the major product in 16.4 mg (3%) as a pale yellow solid (**Figure 29**) [66].



**Figure 29** Synthesis of naphtho[2,3-b]furan-4,9-dione (**5.14**, WNK-7)

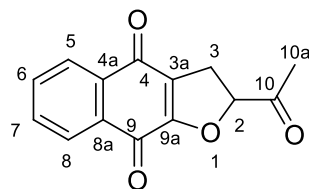
## 5.4 Spectroscopic data of synthetic avicequinone C and analogs

### 5.4.1 2-Propionylnaphtho[2,3-b]furan-4,9-dione (5.8, WNK-1)

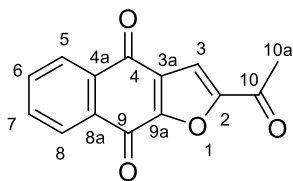


(5.8)

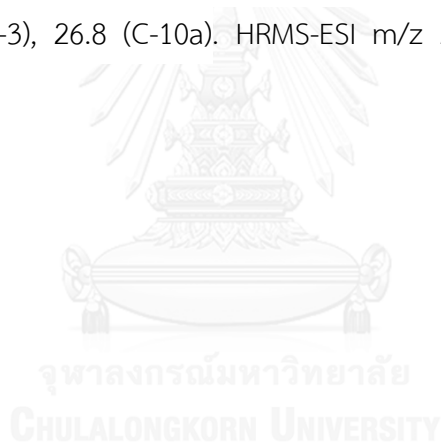
2-propionylnaphtho[2,3-b]furan-4,9-dione : 258.5 mg (51%); orange solid.  $R_f$  0.77 [EtOAc:hexane (1:1)]. IR (KBr) 3385, 3115, 2978, 2878, 1698, 1672, 1579, 1567, 1354, 1219, 958, 721  $\text{cm}^{-1}$ ;  $^1\text{H-NMR}$  ( $\text{CDCl}_3$ , 300 MHz)  $\delta$  8.26 (1H, m, 5-H), 8.23 (1H, m, 8-H), 7.81 (1H, m, 6-H), 7.81 (1H, m, 7-H), 7.61 (1H, s, 3-H), 3.06 (2H, q,  $J = 7.5, 14.7$  Hz, 10-Ha), 1.26 (3H, t,  $J = 7.2$  Hz, 10-Hb);  $^{13}\text{C-NMR}$  ( $\text{CDCl}_3$ , 300 MHz)  $\delta$  190.8 (C-10), 179.8 (C-4), 173.9 (C-9), 155.4 (C-9a), 152.7 (C-2), 134.4 (C-7), 134.3 (C-6), 133.1 (C-8a), 132.6 (C-4a), 130.7 (C-3a), 127.3 (C-5), 127.3 (C-8), 112.0 (C-3), 32.6 (C-10a), 7.4 (C-10b). HRMS-ESI  $m/z$  277.0464 ( $[\text{M}+\text{Na}]^+$ , calcd for  $\text{C}_{15}\text{H}_{10}\text{O}_4\text{Na}^+$  277.0471)

5.4.2 2-Acetyl-2,3-dihydronaphtho[2,3-b]furan-4,9-dione (**5.10**, WNK-3)**(5.10)**

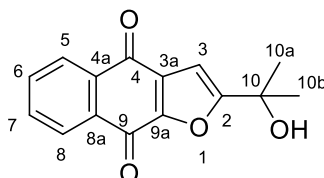
2-acetyl-2,3-dihydronaphtho[2,3-b]furan-4,9-dione : 262.6 mg (53%); yellow solid.  $R_f$  0.72 [Dichloromethane:hexane (4:1)]. IR (KBr) 3093, 2949, 2860, 1737, 1682, 1652, 1631, 1591, 1395, 1375, 1361, 1242, 1195, 963, 722  $\text{cm}^{-1}$ ;  $^1\text{H-NMR}$  ( $\text{CDCl}_3$ , 300 MHz)  $\delta$  8.08 (1H, m, 5-H), 8.08 (1H, m, 8-H), 7.72 (1H, m, 6-H), 7.72 (1H, m, 7-H), 5.27 (1H, t,  $J = 9.6$  Hz, 2-H), 3.42 (2H, dd,  $J = 2.1, 10.8$  Hz 3-H), 2.39 (3H, s, 10-Ha);  $^{13}\text{C-NMR}$  ( $\text{CDCl}_3$ , 300 MHz)  $\delta$  204.6 (C-10), 181.7 (C-4), 177.2 (C-9), 159.2 (C-9a), 134.4 (C-7), 133.3 (C-6), 132.8 (C-4a), 131.4 (C-8a), 126.4 (C-8), 126.2 (C-5), 123.8 (C-3a), 87.1 (C-2), 30.1 (C-3), 26.5 (C-10a); Carbonyl groups of quinone at C-4 and C-9 were based on reported data [67]. HRMS-ESI  $m/z$  281.0223 ( $[\text{M}+\text{K}]^+$ , calcd for  $\text{C}_{14}\text{H}_{10}\text{O}_4\text{K}^+$  281.0211)

5.4.3 2-Acetylnaphtho[2,3-b]furan-4,9-dione (**5.11**, WNK-4)**(5.11)**

2-acetylnaphtho[2,3-b]furan-4,9-dione : 191.3mg (38%); yellow solid.  $R_f$  0.43 [Dichlormethane:hexane (4:1)]. IR (KBr) 3113, 3014, 2854, 1690, 1674, 1581, 1359, 1285, 1259, 1224, 1197, 977, 875, 717  $\text{cm}^{-1}$ ;  $^1\text{H-NMR}$  ( $\text{CDCl}_3$ , 300 MHz)  $\delta$  8.26 (1H, m, 5-H), 8.25 (1H, m, 8-H), 7.81 (1H, m, 6-H), 7.81 (1H, m, 7-H), 7.61 (1H, s, 3-H), 2.67 (3H, s, 10-Ha);  $^{13}\text{C-NMR}$  ( $\text{CDCl}_3$ , 300 MHz)  $\delta$  187.5 (C-10), 179.7 (C-4), 173.9 (C-9), 155.5 (C-9a), 152.9 (C-2), 134.4 (C-6), 134.3 (C-7), 133.1 (C-8a), 132.6 (C-4a), 130.7 (C-3a), 127.4 (C-8), 127.2 (C-5), 112.3 (C-3), 26.8 (C-10a). HRMS-ESI  $m/z$  263.0321 ( $[\text{M}+\text{Na}]^+$ , calcd for  $\text{C}_{14}\text{H}_8\text{O}_4\text{Na}^+$  263.0315)



5.4.4 2-(2-Hydroxypropan-2-yl)naphtha[2,3-b]furan-4,9-dione (Avicquinone C,  
5.2, WNK-5)

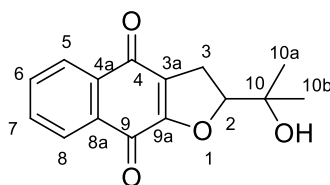


(5.2)

2-(2-hydroxypropan-2-yl)naphtha[2,3-b]furan-4,9-dione : 17.2 mg (34%); brown solid.  $R_f$  0.23 [Chloroform:hexane (4:1)]. IR (KBr) 3532, 3388, 3178, 3121, 2986, 2926, 1682, 1665, 1586, 1376, 1231, 1165, 1154, 968, 954, 724  $\text{cm}^{-1}$ ;  $^1\text{H-NMR}$  ( $\text{CDCl}_3$ , 300 MHz)  $\delta$  8.21 (1H, m, 5-H), 8.18 (1H, m, 8-H), 7.75 (1H, m, 6-H), 7.75 (1H, m, 7-H), 6.82 (1H, s, 3-H), 1.69 (3H, s, 10-Ha), 1.69 (3H, s, 10-Hb);  $^{13}\text{C-NMR}$  ( $\text{CDCl}_3$ , 300 MHz)  $\delta$  180.8 (C-4), 173.4 (C-9), 167.9 (C-9a), 151.8 (C-2), 133.9 (C-7), 133.8 (C-6), 133.0 (C-8a), 132.5 (C-4a), 131.3 (C-3a), 126.9 (C-5), 127.0 (C-8), 102.6 (C-3), 69.4 (C-10), 29.7 (C-10b), 28.8 (C-10a). HRMS-ESI  $m/z$  279.0635 ( $[\text{M}+\text{Na}]^+$ , calcd for  $\text{C}_{15}\text{H}_{12}\text{O}_4\text{Na}^+$  279.0628)

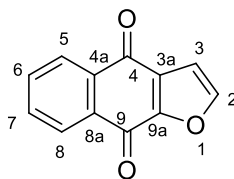


5.4.5 2-(2-Hydroxypropan-2-yl)-2,3-dihydronaphtho[2,3-b]furan-4,9-dione  
(5.12, WNK-6)



(5.12)

2-(2-hydroxypropan-2-yl)-2,3-dihydronaphtho[2,3-b]furan-4,9-dione : 8.81 mg (18%); yellow solid.  $R_f$  0.68 [EtOAc:hexane (3:7)]. IR (KBr) 3436, 2925, 2854, 1686, 1655, 1632, 1597, 1464, 1376, 1200, 1079, 970  $\text{cm}^{-1}$ ;  $^1\text{H-NMR}$  ( $\text{CDCl}_3$ , 300 MHz)  $\delta$  8.08 (1H, m, 5-H), 8.08 (1H, m, 8-H), 7.70 (1H, m, 6-H), 7.70 (1H, m, 7-H), 4.85 (1H, t,  $J = 9.9$  Hz, 2-H), 3.17 (2H, d,  $J = 9.9$  Hz, 3-H), 1.40 (3H, s, 10-Hb), 1.28 (3H, s, 10-Ha);  $^{13}\text{C-NMR}$  ( $\text{CDCl}_3$ , 300 MHz)  $\delta$  182.2 (C-4), 177.7 (C-9), 159.9 (C-9a), 134.2 (C-4a), 133.0 (C-6), 133.0 (C-7), 131.5 (C-8a), 126.3 (C-8), 126.1 (C-5), 125.0 (C-3a), 71.7 (C-10), 92.1 (C-2), 29.7 (C-3), 25.8 (C-10a), 24.1 (C-10b); Carbonyl groups of quinone at C-4 and C-9 were based on reported data [67]. HRMS-ESI  $m/z$  281.0793 ( $[\text{M}+\text{Na}]^+$ , calcd for  $\text{C}_{15}\text{H}_{14}\text{O}_4\text{Na}^+$  281.0784)

5.4.6 Naptho[2,3-b]furan-4,9-dione (**5.14**, WNK-7)**(5.14)**

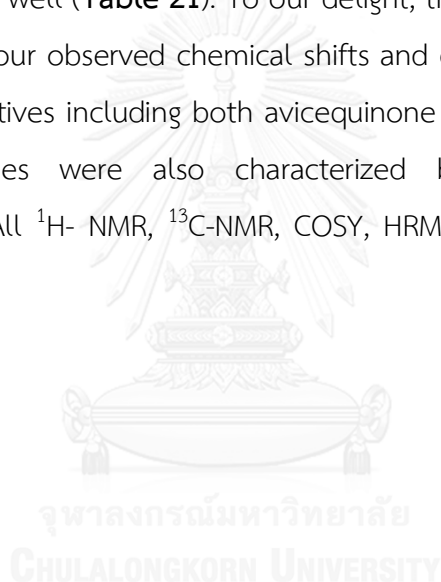
Naptho[2,3-b]furan-4,9-dione : 16.4 mg (3%); pale yellow solid.  $R_f$  0.42 [Dichloromethane:hexane (3:1)]. IR (KBr) 3142, 2853, 1683, 1585, 1566, 1478, 1365, 1206, 1182, 952, 714  $\text{cm}^{-1}$ ;  $^1\text{H-NMR}$  ( $\text{CDCl}_3$ , 300 MHz)  $\delta$  8.22 (1H, m, 5-H), 8.22 (1H, m, 8-H), 7.77 (1H, m, 6-H), 7.77 (1H, m, 7-H), 7.77 (1H, d,  $J = 1.5$  Hz, 2-H), 7.01 (1H, d,  $J = 1.5$  Hz, 3-H);  $^{13}\text{C-NMR}$  ( $\text{CDCl}_3$ , 300 MHz)  $\delta$  180.6 (C-4), 173.6 (C-9), 152.7 (C-9a), 148.6 (C-2), 132.5 (C-4a), 134.0 (C-7), 133.9 (C-6), 133.2 (C-8a), 130.5 (C-3a), 127.1 (C-8), 127.0 (C-5), 108.7 (C-3). HRMS-ESI  $m/z$  221.0212 ( $[\text{M}+\text{Na}]^+$ , calcd for  $\text{C}_{12}\text{H}_6\text{O}_3\text{Na}^+$  221.0215)

## 5.5 Results and discussion

Regarding our synthetic strategies, avicequinone C (WNK-5) and analogs (WNK-1, WNK-3, WNK-4, WNK-6 and WNK-7) were prepared from 2-hydroxy-1,4-naphthoquinone (**5.3**). First, the corresponding vinyl ketone (or sulfone) was *in situ* brominated by bromine to obtain 1, 2 dibromoketone (or sulfone) intermediate. Subsequent one-pot cyclization under basic condition yielded corresponding furanonaphthoquinones (WNK-1, WNK-3, WNK-4 and WNK-7) depending on reaction temperature. Second, the ketone pendent of the resulting furanonaphthoquinone WNK-3 and WNK-4 were reacted with methyl magnesium bromide to produce tertiary alcohol yielding avicequinone C (WNK-5) and its dihydro-furanonaphthoquinone WNK-6. Avicequinone C (WNK-5) and analogs WNK-1, WNK-3, WNK-4, and WNK-6 were obtained in moderated yields (18-53%). Interestingly, yield of 2-acetylnaptho[2,3-b]furan-4,9-dione (**5.11**, WNK-4) was improved by increasing of reaction temperature to reflux. In addition, WNK-7 was the only furanonaphthoquinone derivative that was synthesized from methyl vinyl sulfone (**5.13**) and had no ketone substituent. Under

this condition, WNK-7 was obtained in low yield (less than 5%). The optimization was necessary to improve the overall yield and it will be further studied in the future.

In addition, avicequinone C (WNK-5) and analogs (WNK-1, WNK-3, WNK-4, WNK-6 and WNK-7) were a series of known furanonaphthoquinone that were found either from natural sources or chemical syntheses [68-72]. Thus, the chemical structure of synthetic avicequinone C (WNK-5) was confirmed based upon the reported spectroscopic data [5]. Herein, the reported 1D-NMR data and our current 1D-NMR data of synthetic avicequinone C were compared as shown in **Table 20**. Furthermore, WNK-7, which was named as avicequinone B [73], was also confirmed with reported spectroscopic data as well (**Table 21**). To our delight, the published  $^1\text{H}$ - and  $^{13}\text{C}$ -NMR data were similar to our observed chemical shifts and coupling constants measuring from synthetic derivatives including both avicequinone B and C. The other synthetic furanonaphthoquinones were also characterized based on avicequinone C spectroscopic data. All  $^1\text{H}$ - NMR,  $^{13}\text{C}$ -NMR, COSY, HRMS, IR and mass spectra were depicted in Appendix.



**Table 20** NMR spectral data of WNK-5 (in CDCl<sub>3</sub>) and avicequinone C (in CDCl<sub>3</sub>)

Position	<sup>1</sup> H δ ppm (mult., <i>J</i> in Hz)		<sup>13</sup> C (δ ppm)		
	Avicequinone C Jain <i>et al.</i> , 2014 [5]	WNK-5	Avicequinone C Jain <i>et al.</i> , 2014 [5]	WNK-5	Δδ
1	-	-	-	-	-
2	-	-	151.8	151.8	0.0
3	6.82 (s)	6.82 (s)	102.6	102.6	0.0
3a	-	-	131.3	131.3	0.0
4	-	-	180.8	180.8	0.0
4a	-	-	133.1	132.5	0.6
5	8.21 (m)	8.21 (m)	126.9	126.9	0.0
6	7.75 (m)	7.75 (m)	133.9	133.8	0.1
7	7.75 (m)	7.75 (m)	133.7	133.9	0.2
8	8.16 (m)	8.18 (m)	126.8	127.0	0.2
8a	-	-	132.5	133.0	0.5
9	-	-	173.4	173.4	0.0
9a	-	-	167.9	167.9	0.0
10	-	-	69.4	69.4	0.0
10a	1.69 (s)	1.69 (s)	28.8	28.8	0.0
10b	1.69 (s)	1.69 (s)	28.8	29.7	0.9

**Table 21** NMR spectral data of WNK-7 (in CDCl<sub>3</sub>) and avicequinone B (in CDCl<sub>3</sub>)

Position	<sup>1</sup> H δ ppm (mult., <i>J</i> in Hz)		<sup>13</sup> C (δ ppm)		
	Avicequinone B Tseng <i>et al.</i> , 2010 [73]	WNK-7	Avicequinone B Tseng <i>et al.</i> , 2010 [73]	WNK-7	Δδ
1	-	-	-	-	-
2	7.77 (d., 1.6 )	7.77 (d, 1.5)	148.6	148.6	0.0
3	7.01 (d., 1.6)	7.01 (d, 1.5)	108.7	108.7	0.0
3a	-	-	130.5	130.5	0.0
4	-	-	180.6	180.6	0.0
4a	-	-	132.5	132.5	0.0
5	8.22 (m)	8.22 (m)	127.0	127.0	0.0
6	7.77 (m)	7.77 (m)	133.9	133.9	0.0
7	7.77 (m)	7.77 (m)	134.0	134.0	0.0
8	8.22 (m)	8.22 (m)	127.1	127.1	0.0
8a	-	-	133.2	133.2	0.0
9	-	-	173.6	173.6	0.0
9a	-	-	152.7	152.7	0.0

All avicequinone C and analogs were obtained as a yellow solid, which was a general physical property of naphthoquinone. The key IR signals of the resulting furanonaphthoquinones consisted of ketone, aromatic, and hydroxyl group stretching as sharp signal at 1651.73-1698.22 cm<sup>-1</sup>, moderate signal at 1570.86-1590.78 cm<sup>-1</sup>, and broad signal at 3435.59 cm<sup>-1</sup>, respectively. The characteristic <sup>1</sup>H- and <sup>13</sup>C-NMR signals of furanonaphthoquinones were assigned. The proton at C-5, C-6, C-7 and C-8 of aromatic ring appeared at 7.10-8.81 ppm, which corresponded to aromatic carbons at 127.0-134.2 ppm. The methyl protons were shown at 1.71-2.39 ppm, which corresponded to methyl carbons at 26.5-28.8 ppm. The quinone carbonyl carbons at C-4 and C-9 showed signals at 180.8 and 179.3 ppm, respectively. Moreover, the proton

at C-2 and C-3, which corresponded to the methylene moiety in WNK-3 and WNK-6 showed chemical shifts at 5.27 and 3.42 ppm as triplet and doublet, respectively.

## 5.6 Conclusions

Avicquinone C and 5 analogs including WNK-1, WNK-3, WNK-4, WNK-6 and WNK-7 were successfully synthesized from 2-hydroxy-1,4-naphthoquinone (**5.3**) by following the reported reactions involving cyclization *via* nucleophilic substitution to form a furan ring [64] and alkylation *via* Grignard's reaction to install an alcohol side chain [65]. As a result, avicquinone C (WNK-5, **5.2**) was obtained in 34% (17.2 mg). WNK-1 (**5.8**) was afforded in 51% (258.5 mg). WNK-3 (**5.10**) was obtained in 53% (262.6 mg). WNK-4 (**5.11**) was gotten in 38% (191.3 mg). WNK-6 (**5.12**) was afforded in 18% (8.81 mg). WNK-7 (**5.14**) was obtained in 3% (16.4 mg). Each compound was fully characterized by NMR analysis. The observed high resolution mass data of each derivative agreed with its calculated mass. Avicquinone C and 5 analogs were further studied for the 5 $\alpha$ -reductase inhibitory activities in HaCaT cell line.



## Chapter VI

### Evaluation of 5 $\alpha$ -Reductase Inhibitory Activity *via* HaCaT Cell-line Assay

#### Contents

- 6.1 Introduction
- 6.2 Material and methods
  - 6.2.1 Culturing of HaCaT cells
  - 6.2.2 Cytotoxicity of avicequinone C and analogs and natural naphthoquinones against HaCaT cell line
  - 6.2.3 5 $\alpha$ -reductase inhibitory activity of avicequinone C and analogs and natural naphthoquinones by HaCaT cell-based assay
- 6.3 Results and discussion
  - 6.3.1 Cytotoxic evaluation of avicequinone C and analogs and natural naphthoquinones against HaCaT cell line
  - 6.3.2 Standard curve of 5 $\alpha$ -DHT
  - 6.3.3 Analysis of 5 $\alpha$ -reductase inhibitory activity of avicequinone C and analogs and natural naphthoquinones using HaCaT cell-based assay
  - 6.3.4 IC<sub>50</sub> value of 2-hydroxy-1,4-naphthoquinone (**6.9**)
- 6.4 Conclusions

## 6.1 Introduction

The bioassays that have been used to evaluate 5 $\alpha$ -reductase (5 $\alpha$ -R) inhibitory activity are separated into 2 categories, cell-free assay system and cell-based assay system. Cell-free assay uses 5 $\alpha$ -R enzymes, which have been isolated from various sources, such as rat prostate, rat liver, rat epididymis, human prostate and transfected cell lines [34]. On the other hand, cell-based assay uses viable whole cells expressing 5 $\alpha$ -R, such as human prostate cancer cell line and transfected rat cell lines [25].

Regarding our previous studies, the cell-based assay using human hair dermal papilla cells (HHDPCs) combined with high performance thin layer chromatography (HPTLC) detection was developed [5]. This result revealed that avicequinone C possessed inhibitory activities toward 5 $\alpha$ -R type 1 (5 $\alpha$ -R1), the isoform of the enzyme found to be expressed by HHDPCs [5]. Practically, the cells were seeded onto a 96-well plate at a cell density of  $1 \times 10^4$  cells/well. After 24 hours, the cells were treated with testosterone (T) in presence of test compounds. After incubating for 48 hours, the medium was collected and the products of the reaction were extracted using ethyl acetate. The organic layer was separated, dried, reconstituted, and analyzed by HPTLC focusing on the presence of T and 5 $\alpha$ -DHT. The study showed that avicequinone C exhibited 5 $\alpha$ -R1 inhibitory activity at  $IC_{50}$  38.8  $\mu$ M [5].

In this research, we used cultured human keratinocytes cell line (HaCaT) instead of HHDPCs as a cell-based assay system to discover new 5 $\alpha$ -R inhibitors. HaCaT cell line is a naturally transformed aneuploidy immortal keratinocyte cell line from adult human skin. HaCaT human keratinocytes has been used *in vitro* as one of the source of T metabolism [74]. The enzyme 5 $\alpha$ -R has been found to be well expressed in HaCaT [75]. Furthermore, the type 1 enzyme, 5 $\alpha$ -R1, has been determined in keratinocytes cultured from infrainfundibulum and epidermis in acne patients [19]. Therefore, inhibition of 5 $\alpha$ -R in HaCaT can also be considered as a target for the treatment of multiple androgen-dependent skin disorders, such as acne, hirsutism and androgenic alopecia. In this work, we proposed to use of HaCaT human keratinocyte to examine



the inhibitory activity of various potential 5 $\alpha$ -R inhibitors, which included all avicequinone C and analogs and natural naphthoquinones.

## 6.2 Material and methods

### 6.2.1 Culturing of HaCaT cells

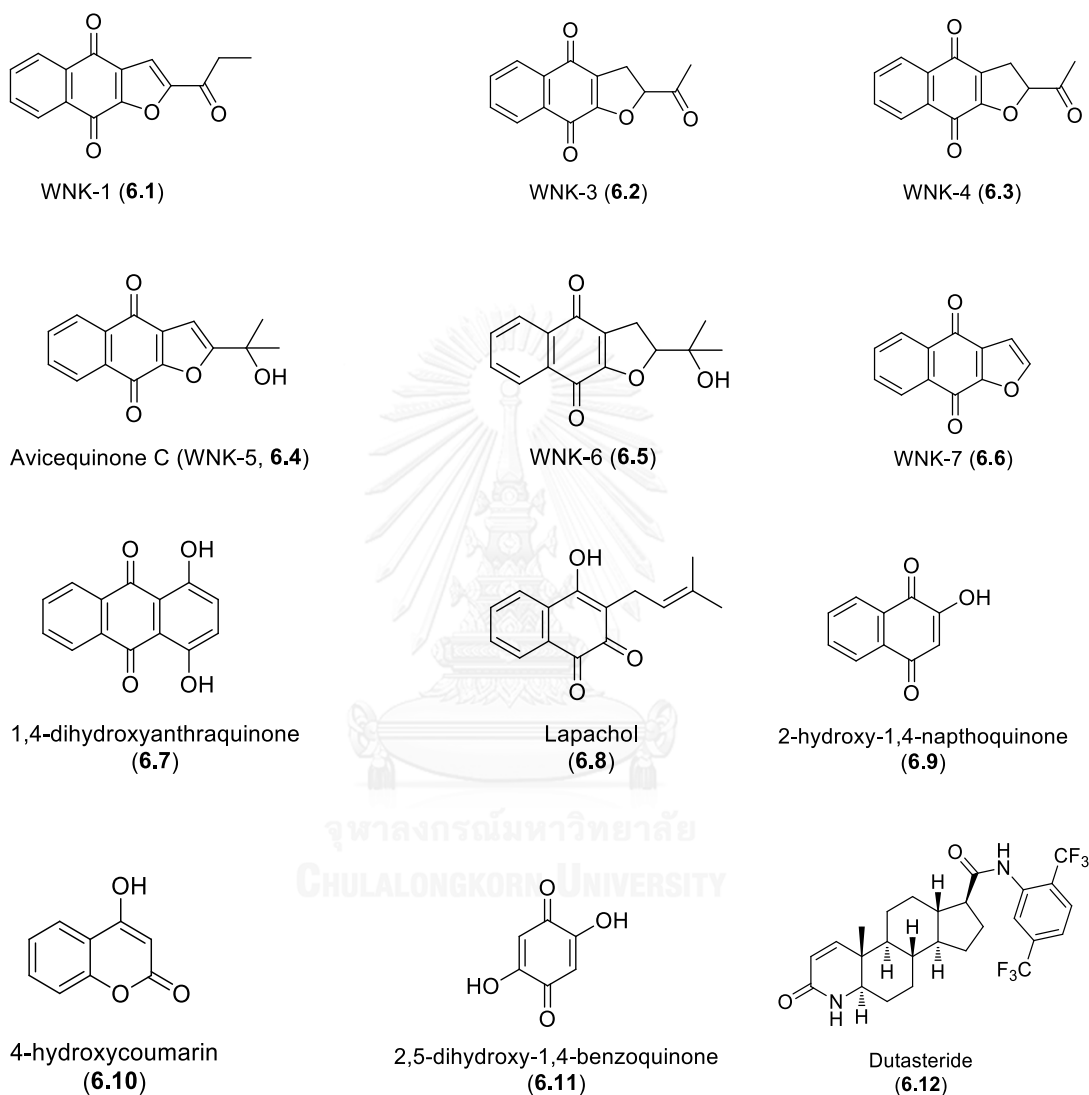
HaCaT cell line were grown in dulbecco's modified medium (DMEM) containing 10% fetal bovine serum (FBS) and 1% antibiotic-antimycotic solution at 37°C in 5% CO<sub>2</sub> in a T-75 flask. The cells were grown until 80% confluency and then subculture was operated.

### 6.2.2 Cytotoxicity of avicequinone C and analogs and natural naphthoquinones against HaCaT cell line

HaCaT cells were seeded at a cell density of  $1 \times 10^4$  cells/well onto a 96-well-plate. After 24 hours, the cells were individually treated with a series of synthetic avicequinone C and analogs including WNK-1 (6.1), WNK-2 (6.2), WNK-4 (6.3), avicequinone C (WNK5, 6.4), WNK-6 (6.5), WNK-7 (6.6); natural naphthoquinones such as 1,4-dihydroxyanthraquinone (6.7), lapachol (6.8), 2-hydroxy-1,4-naphthoquinone (6.9); and two non-naphthoquinones such as 4-hydroxycoumain (6.10) and 2,5-dihydroxy-1,4-benzoquinone (6.11). Dutasteride (6.12) was used as a positive control. The structure of test compounds were shown in **Figure 30**. Each compound was prepared at the concentrations of 5, 10, 20 and 40  $\mu$ M in DEME containing DMSO not more than 1%. DMEM was used as a negative control. Cells were incubated at 37°C in 5% CO<sub>2</sub>. Cell viability was measured after 48 hours of treatment using 1X PrestoBlue<sup>®</sup> in RPMI medium. In the presence of viable cells, PrestoBlue<sup>®</sup> was changed from a non-fluorescent purple color to a fluorescent pink color, which was detected using the Multimode Detector DTX 880 (Beckman Coulter<sup>®</sup>, Indianapolis, USA) by setting a bottom-read absorbance (abs) with an excitation/emission of 570/600 nm. The highest non-toxic concentration was further used as the maximum concentration for measuring

5 $\alpha$ -R1 enzyme activities. The value of % viability were calculated from the following formula:

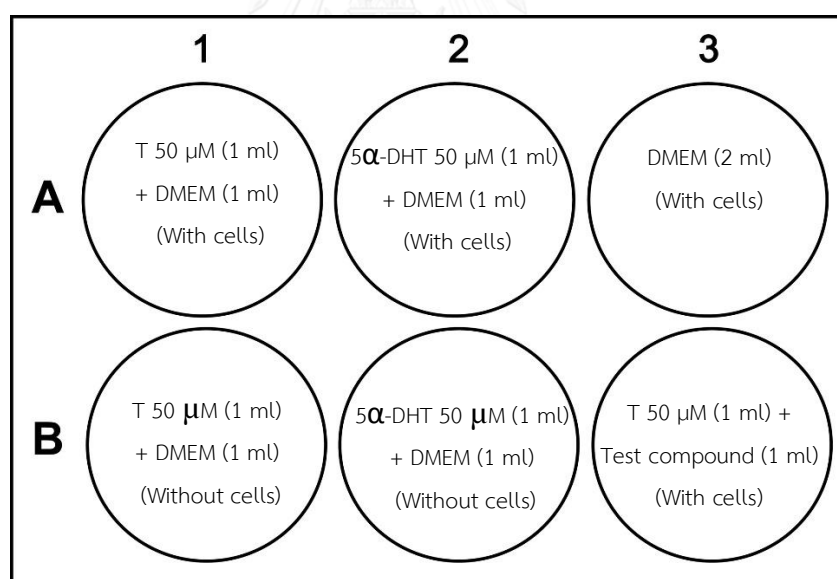
$$\% \text{cell viability} = \frac{(\text{abs of test compounds} - \text{abs of blank})}{(\text{abs of control} - \text{abs of blank})} \times 100$$



**Figure 30** Structures of avicequinone C and analogs (6.1-6.6), natural naphthoquinones (6.7-6.9), non-naphthoquinones (6.10 and 6.11) and dutasteride (6.12)

### 6.2.3 5 $\alpha$ -reductase inhibitory activity of avicequinone C and analogs and natural naphthoquinones by HaCaT cell-based assay

HaCaT were seeded at a cell density of  $2 \times 10^5$  cells/well onto 6-well plates, and allowed to adhere for 24 hours. The internal standards and controls including T (substrate) and 5 $\alpha$ -DHT (product) were then added as shown in **Figure 31**. DMEM (1 ml) was added into each standard and control well. A1 was a negative control. A2, B1, B2 and A3 were a set of internal standards. Dutasteride (**6.12**) was used as a positive control. B3 was prepared as a test well for 5 $\alpha$ -R inhibitory activities investigation. A solution of T (substrate) at 50  $\mu\text{M}$  (1 ml) in DMEM containing 1%DMSO was added in a test well. Cells were treated with test compounds dissolved in DMEM containing not more than 1%DMSO at the non-toxic concentration (1 ml). The overall volume of each well was 2 ml. Each test was repeated in triplicate.



**Figure 31** 6-well plate diagram of HaCaT cell-based assay

After incubating for 48 hours, cell culture medium was extracted by ethyl acetate (2 ml). The remaining T (substrate) and the resulting 5 $\alpha$ -DHT (product) were partitioned from aqueous medium to ethyl acetate. Each ethyl acetate extract was

then dried, reconstituted with 20  $\mu$ l of methanol. Then, 8  $\mu$ l of the resulting methanol solution was spotted onto a TLC Silica gel 60 F<sub>254</sub> aluminum plate using thin layer chromatography sample loader: Camag Linomat 5, Switzerland. The TLC plate was developed using cyclohexane: ethyl acetate: triethanolamine at a ratio 1:1:0.1. The developed TLC plate was dipped in a solution of 42.5% phosphoric acid and heated at 120°C for 20 minutes, for visual detection of 5 $\alpha$ -DHT at 366 nm by thin layer chromatography scanner: Camag TLC Scanner 3, Switzerland. The band intensity of 5 $\alpha$ -DHT product was measured by Image J software and calculated by using the formula:

$$\% \text{inhibition} = \frac{(Ac - At)}{Ac} \times 100$$

Where Ac = Area of 5 $\alpha$ -DHT obtaining from internal control

At = Area of 5 $\alpha$ -DHT obtaining from test compound

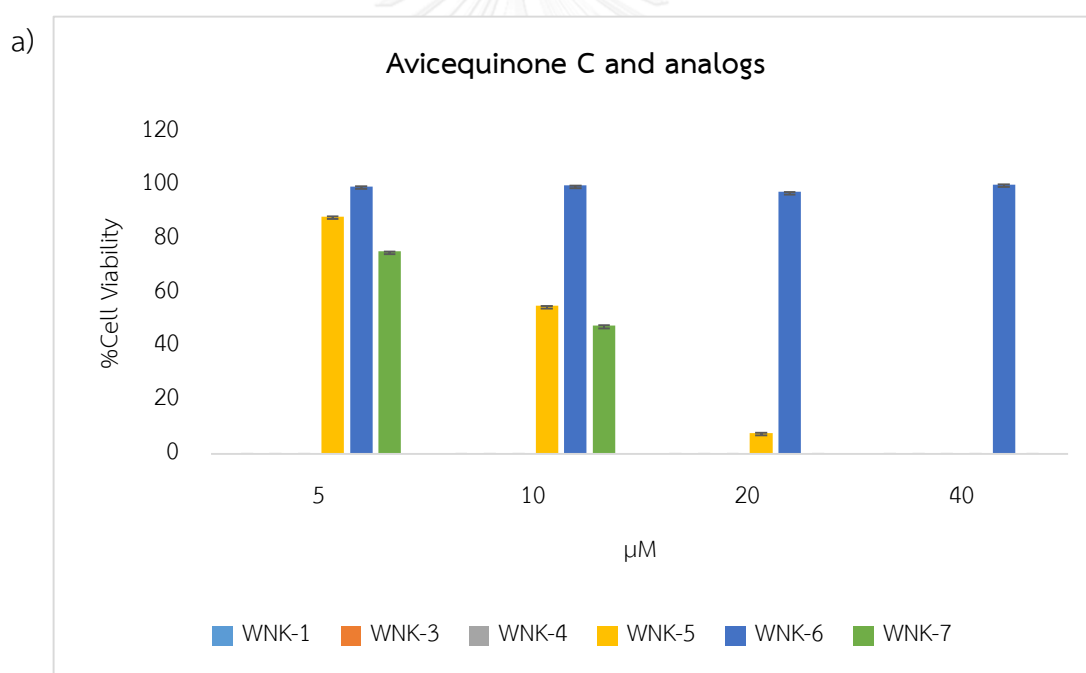
In order to avoid false positive results, cell viability of the attached treated cells was also tested with 1X PrestoBlue<sup>®</sup> reagent in RPMI medium. The test compound that exhibited the highest 5 $\alpha$ -R inhibitory activity was further determined the IC<sub>50</sub> value in molar (M) unit.

### 6.3 Results and discussion

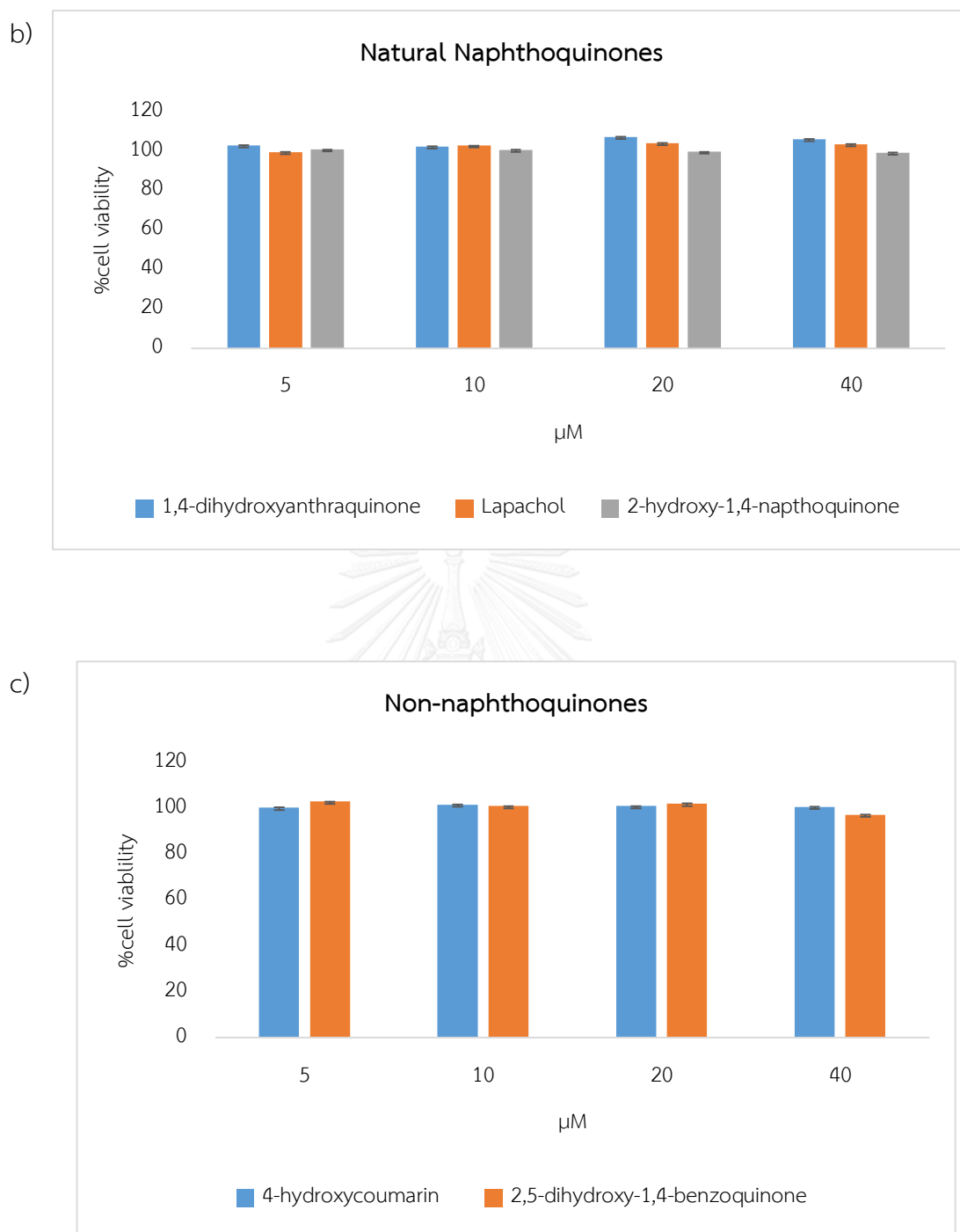
#### 6.3.1 Cytotoxic activity evaluation of avicequinone C and analogs and natural naphthoquinones against HaCaT cell line

To obtain a suitable concentration for evaluating the 5 $\alpha$ -R inhibitory activity of each test compounds including avicequinone C and analogs and natural naphthoquinones along with non-naphthoquinones as shown in **Figure 30**, the cytotoxicity of each compound toward HaCaT cell line were investigated by PrestoBlue<sup>®</sup>. The results of cytotoxicity evaluation of all interesting compounds against HaCaT cell line were illustrated in **Figure 32**. As a result, WNK-1 (**6.1**), WNK-3 (**6.2**) and

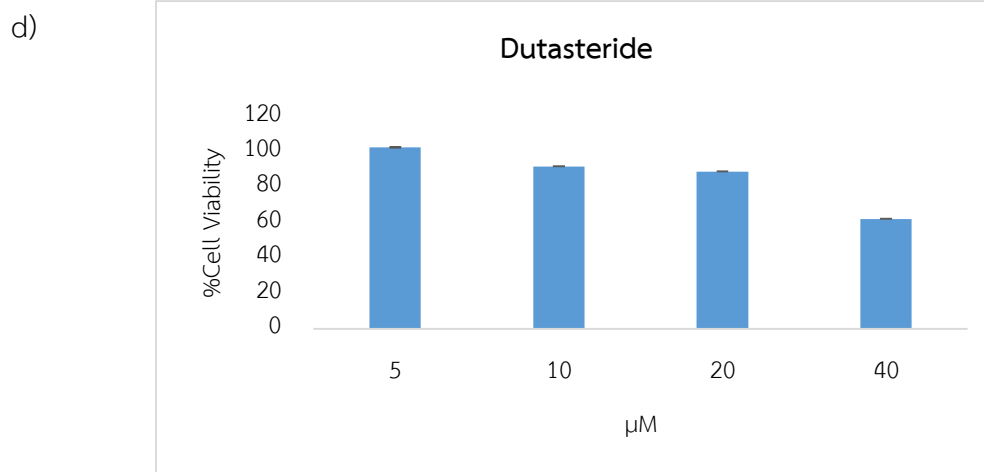
WNK-4 (6.3) were toxic to HaCaT cell line at the concentration less than 5  $\mu\text{M}$ , avicequinone C or WNK-5 (6.4) and WNK-7 (6.6) showed toxicity at the concentration higher than 5  $\mu\text{M}$ . Interestingly, WNK-6 (6.5) showed no toxicity toward HaCaT cell line at 5 to 40  $\mu\text{M}$ . In addition, the natural naphthoquinones and non-naphthoquinones appeared to non-toxic to HaCaT cell line at 5 to 40  $\mu\text{M}$ . Furthermore, dutasteride exhibited toxicity at 40  $\mu\text{M}$ . The compounds that had no cytotoxicity to HaCaT cell line in the range between 5 to 40  $\mu\text{M}$  were selected for further study to determining  $5\alpha\text{-R}$  inhibitory potency. The sub-toxic concentrations against HaCaT cell line were necessary for  $5\alpha\text{-reductase}$  assay. Thus, avicequinone C (6.4) and WNK-7 (6.6) were further studied at the 5  $\mu\text{M}$ , while WNK-6 (6.5), natural naphthoquinones and non-naphthoquinones were selected to study at 10  $\mu\text{M}$ .



**Figure 32** Cytotoxic activity evaluation against HaCaT cell line: a) Avicequinone C and analogs, b) Natural naphthoquinones, c) Non-naphthoquinones, and d) Dutasteride



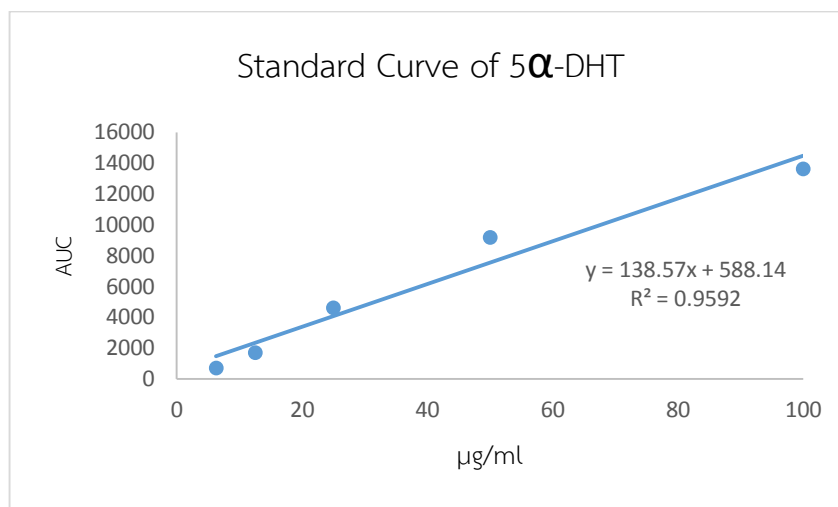
**Figure 32** (Cont.) Cytotoxic activity evaluation against HaCaT cell line: a) Avicequinone C and analogs, b) Natural naphthoquinones, c) Non-naphthoquinones, and d) Dutasteride



**Figure 32** (Cont.) Cytotoxic activity evaluation against HaCaT cell line: a) Avicequinone C and analogs, b) Natural naphthoquinones, c) Non-naphthoquinones, and d) Dutasteride

### 6.3.2 The standard curve of 5 $\alpha$ -DHT

The 5 $\alpha$ -DHT was quantitatively measured to directly evaluate the production of 5 $\alpha$ -DHT during treatment of test compound. Cells were treated with several concentrations of dutasteride following the 5 $\alpha$ -R HaCaT-cell based assay explained above (section 6.2.3). An image of derivatized TLC plate was taken at 366 nm, and then the 5 $\alpha$ -DHT band was quantified by ImageJ software and the correlation coefficient ( $R^2$ ) was calculated. (**Figure 33**)

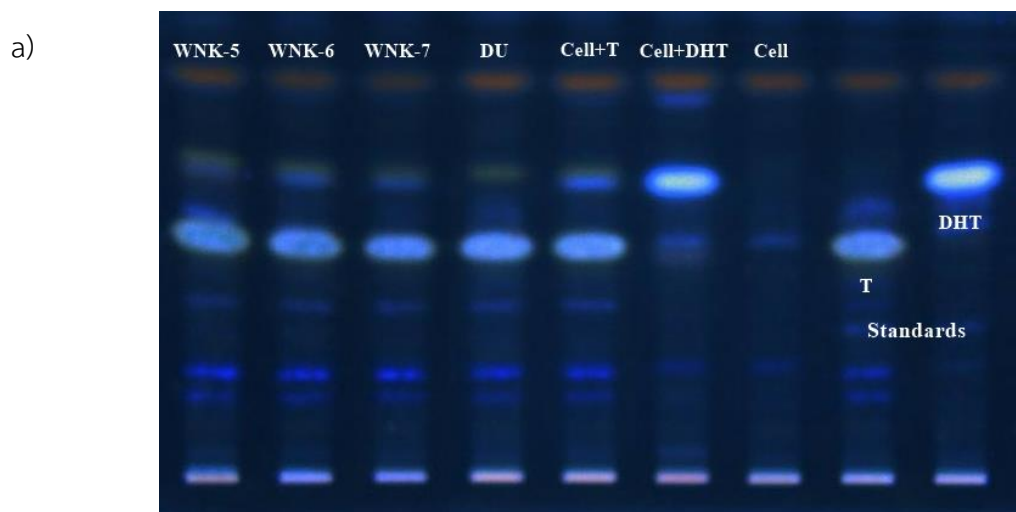


**Figure 33** Standard Curve of 5 $\alpha$ -DHT

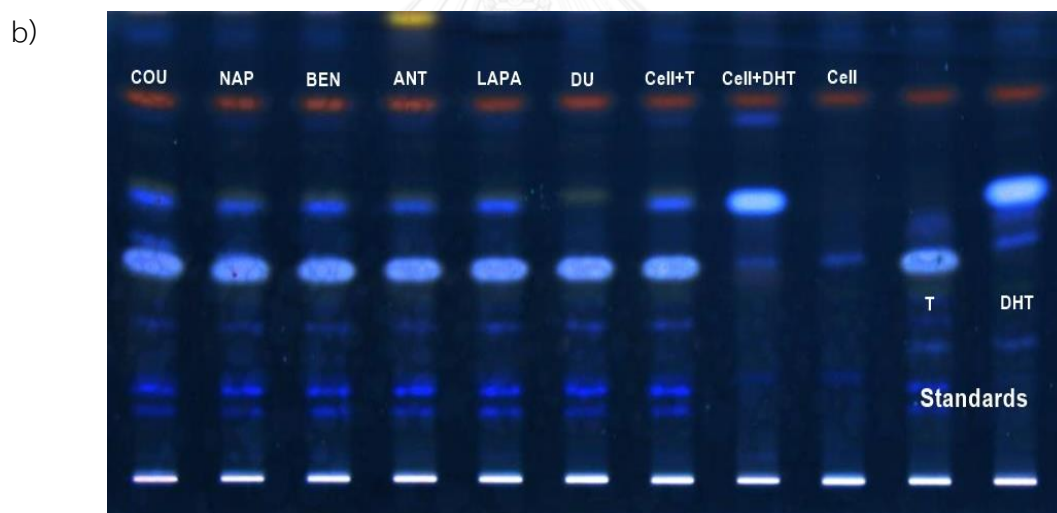
### 6.3.3 Analysis of 5 $\alpha$ -reductase inhibitory activity of avicequinone C and analogs and natural naphthoquinones using HaCaT cell-based assay

The compounds at their non-toxic concentrations were then evaluated for their inhibitory activity of 5 $\alpha$ -R using the HaCaT cell-based assay. As shown in **Figure 34**, each lane indicated the inhibitory potential of each compound. The lane “Cell+T” was the internal control showing the conversion of T to 5 $\alpha$ -DHT, while the lane “T (standard)” was the negative control. Based on HPTLC visualization, the preliminary screening among all the naphthoquinones at the concentration of 10  $\mu$ M in DMEM containing not more than 1%DMSO showed that avicequinone C (WNK-5, **6.4**), WNK-6 (**6.5**), WNK-7 (**6.6**), 1,4-dihydroxyanthraquinone (**6.7**) and 2-hydroxy-1,4-naphthoquinone (**6.9**) exhibited significant 5 $\alpha$ -R inhibitory activity. However, lapachol (**6.8**) and two non-naphthoquinones including 4-hydroxycoumain (**6.10**) and 2,5-dihydroxy-1,4-benzoquinone (**6.11**) were not active enough to inhibit the activity of 5 $\alpha$ -R expressing by HaCaT cell.





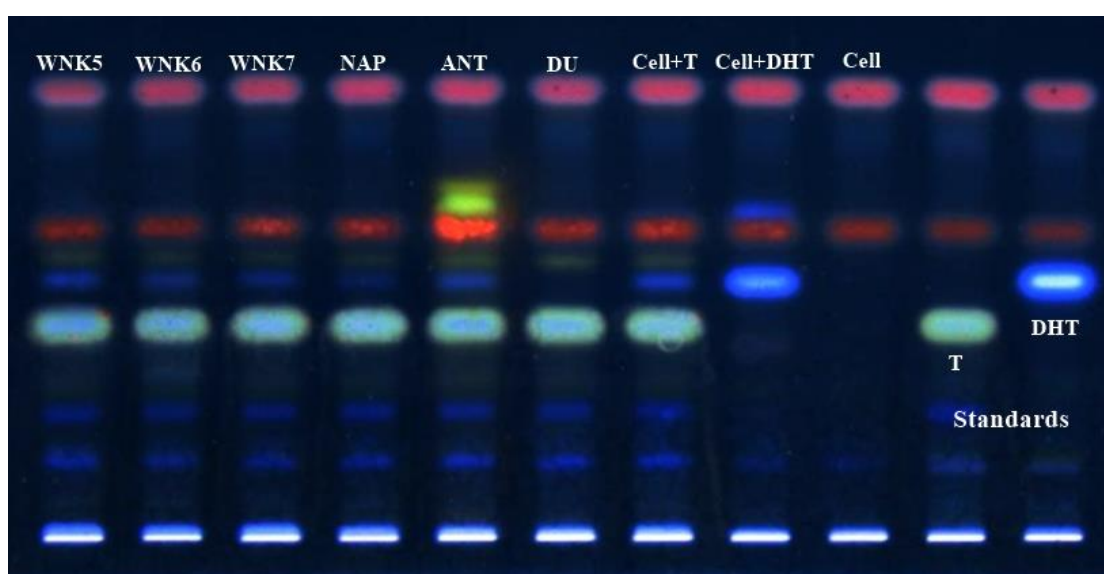
WNK5 (avicequinone C, **6.4**): 5  $\mu$ M, WNK6 (**6.5**): 10  $\mu$ M, WNK-7 (**6.6**): 5  $\mu$ M,  
 DU (Dutasteride, **6.14**): 20  $\mu$ M, Cell+T: Testosterone with HaCaT, Cell+DHT: 5 $\alpha$ -dihydrotestosterone with  
 HaCaT, Cell: HaCaT cell line, T: Testosterone without HaCaT, DHT: 5 $\alpha$ -dihydrotestosterone without HaCaT  
 Mobile Phase: Toluene : Acetone = 4:1 (developing 2 times)



COU (4-hydroxycoumarin, **6.10**): 5  $\mu$ M, NAP (2-hydroxy-1,4-naphthoquinone, **6.9**): 10  $\mu$ M, BEN (2,5-dihydroxy-1,4-  
 benzoquinone, **6.11**): 10  $\mu$ M, ANT (1,4-dihydroxyanthraquinone, **6.7**): 10  $\mu$ M, LAPA (lapachol, **6.8**): 10  $\mu$ M DU  
 (Dutasteride, **6.14**): 20  $\mu$ M, Cell+T: Testosterone with HaCaT, Cell+DHT: 5 $\alpha$ -dihydrotestosterone with HaCaT, Cell:  
 HaCaT cell line, T: Testosterone without HaCaT, DHT: 5 $\alpha$ -dihydrotestosterone without HaCaT  
 Mobile Phase: Toluene : Acetone = 4:1 (developing 2 times)

**Figure 34** Preliminary screening of 5 $\alpha$ -reductase inhibitory activity of test compounds by HPTLC a) Avicequinone C and analogs, b) Natural naphthoquinones and non-naphthoquinones

To find out the best 5 $\alpha$ -R inhibitor among the test compounds, avicequinone C (WNK-5, **6.4**), WNK-6 (**6.5**), WNK-7 (**6.6**), 2-hydroxy-1,4-naphthoquinone (**6.10**) and 1,4-dihydroxyanthraquinone (**6.12**) were further determined the values of %inhibition at maximum concentrations without cytotoxicity by the HaCaT cell-based assay (Figure 35). The results showed that avicequinone C (WNK-5, **6.4**), WNK-6 (**6.5**), WNK-7 (**6.6**), 1,4-dihydroxyanthraquinone (**6.7**) and 2-hydroxy-1,4-naphthquinone (**6.9**) exhibited 42.4%, 60.0%, 67.2%, 47.7%, and 82.7% inhibition, respectively (Table 22).



WNK5 (avicequinone C, **6.4**): 5  $\mu$ M, WNK6 (**6.5**): 40  $\mu$ M, WNK-7 (**6.6**): 5  $\mu$ M,  
 NAP (2-hydroxy-1,4-naphthoquinone, **6.9**): 40  $\mu$ M, ANT (1,4-dihydroxyanthraquinone, **6.7**): 40  $\mu$ M  
 DU (Dutasteride, **6.14**): 20  $\mu$ M, Cell+T: Testosterone with HaCaT, Cell+DHT: 5 $\alpha$ -dihydrotestosterone with HaCaT,  
 Cell: HaCaT cell line, T: Testosterone without HaCaT, DHT: 5 $\alpha$ -dihydrotestosterone without HaCaT  
 Mobile Phase – Cyclohexane : Ethyl acetate : Triethanolamine = 1:1:0.1

**Figure 35** Analysis of %inhibition at maximum concentrations without cytotoxicity of selected compounds by HPTLC

**Table 22** 5 $\alpha$ -Reductase inhibitory activity of selected naphthoquinones toward HaCaT cell-based assay

Compounds	Concentration ( $\mu$ M)	Amount of DHT ( $\mu$ M)	%inhibition $\pm$ SD
Avicquinone C (WNK-5, <b>6.4</b> )	5	85.66	42.4 $\pm$ 6.2
WNK-7 ( <b>6.6</b> )	5	47.48	67.2 $\pm$ 17.3
WNK-6 ( <b>6.5</b> )	40	53.33	60.0 $\pm$ 9.4
1,4-dihydroxyanthraquinone ( <b>6.7</b> )	40	59.36	47.23 $\pm$ 14.25
2-hydroxy-1,4-naphthoquinone ( <b>6.9</b> )	40	7.78	82.7 $\pm$ 14.4

Our results depicted that avicquinone C and analogs such as WNK-6 (**6.5**) and WNK-7 (**6.6**) exhibited moderate 5 $\alpha$ -R inhibitory activities. At the concentration of 5  $\mu$ M, WNK-7 (**6.6**) showed better 5 $\alpha$ -R inhibition that avicquinone C (WNK-5, **6.4**). However, there was a concern regarding the cytotoxicity toward HaCaT cell line at 5  $\mu$ M. The synthetic WNK-6 (**6.5**), which showed equal 5 $\alpha$ -R inhibition to WNK-7, at 40  $\mu$ M, could be considered as a potential 5 $\alpha$ -R inhibitor. However, further optimization of synthetic protocol is required to selectively obtain a single enantiomer of WNK-6 for future studies.

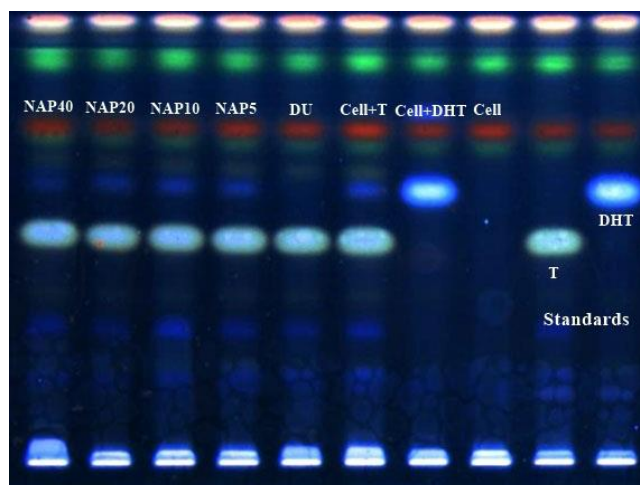
Interestingly, natural naphthoquinones at the concentration of 40  $\mu$ M, 1,4-dihydroxyanthraquinone (**6.7**) and 2-hydroxy-1,4-naphthoquinone (**6.9**) possessed moderate and excellent 5 $\alpha$ -R inhibitory activities, respectively. Thus, 2-hydroxy-1,4-naphthoquinone (**6.9**) could be further studied as a novel candidate for 5 $\alpha$ -reductase inhibitor having satisfied activity and high safe to use. However, 2-hydroxy-1,4-naphthoquinone (**6.9**) showed lower potency than dutasteride (**6.12**).

Besides, we observed that the two non-naphthoquinones such as (4-hydroxycoumarin (**6.10**) and 2,5-dihydroxy-1,4-benzoquinone (**6.11**) did not inhibit the activity of 5 $\alpha$ -R. This finding indicated that naphthoquinone moiety was essential for 5 $\alpha$ -R inhibitory activities. Moreover, avicequinone C analogs having dihydrofuran moiety with tertiary alcohol pendent such as WNK-6 (**6.5**) exhibited low cytotoxicity toward HaCaT cell line in conjugation with excellent 5 $\alpha$ -R inhibitory activity.

Comparing experimental results between *in vitro* and *in silico* 5 $\alpha$ -R inhibitory activities via HaCaT cell-based assay and molecular docking with predicted 5 $\alpha$ -R1, The corresponding issues were found including 1) naphthoquinone moiety was important for 5 $\alpha$ -R inhibitory activities and 2) naphthoquinones showed better inhibitory activities than furanonaphthoquinone based on interactions at catalytic region of predicted 5 $\alpha$ -R1 indicated by testosterone (**Figure 18**, Chapter IV). However, %inhibition and  $\Delta G$  of each compound were not completely matched but resulted in an acceptable range.

#### 6.3.4 IC<sub>50</sub> values of 2-hydroxy-1,4-naphthoquinone (**6.9**)

2-hydroxy-1,4-naphthoquinone (**6.9**), which exhibited significant 5 $\alpha$ -R inhibitory activities was further investigated to determine the IC<sub>50</sub> value in molar unit. Cells were treated with several concentrations of 2-hydroxy-1,4-naphthoquinone (**6.9**). An image of derivatized TLC plate was taken at 366 nm (**Figure 36**), and then the resulting 5 $\alpha$ -DHT band was quantified by ImageJ software. Finally, the IC<sub>50</sub> value and correlation coefficient (R<sup>2</sup>) were calculated (**Figure 37**). We found that 2-hydroxy-1,4-naphthoquinone exhibited 5 $\alpha$ -R inhibitory activity at IC<sub>50</sub> 23.39  $\mu$ M.



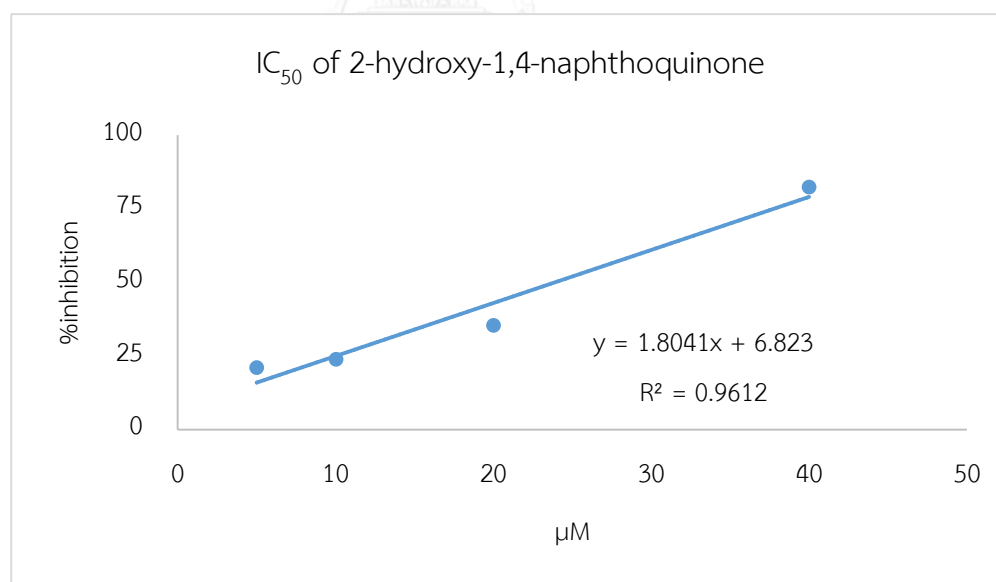
NAP (2-hydroxy-1,4-naphthoquinone, **6.9**): 40, 20, 10, 5  $\mu\text{M}$

DU (Dutasteride, **6.14**): 20  $\mu\text{M}$ , Cell+T: Testosterone with HaCaT, Cell+DHT: Dihydrotestosterone with HaCaT,

Cell: HaCaT cell line, T: Testosterone without HaCaT, DHT: Dihydrotestosterone without HaCaT

Mobile Phase – Cyclohexane : Ethyl acetate : Triethanolamine = 1:1:0.1

**Figure 36** Analysis of  $5\alpha\text{-R}$  inhibitory activity ( $\text{IC}_{50}$ ) of 2-hydroxy-1,4-naphthoquinone by HPTLC



**Figure 37**  $5\alpha\text{-R}$  inhibitory activity ( $\text{IC}_{50}$ ) curve of 2-hydroxy-1,4-naphthoquinone (**6.9**)

## 6.4 Conclusions

In this research, 5 $\alpha$ -R inhibitory activities was evaluated *via* HaCaT cell line assay. In the presence of HaCaT cell, 5 $\alpha$ -R was expressed and T was reduced to 5 $\alpha$ -DHT. Dutasteride was used as negative control. Avicquinone C and synthetic analogs modified at furan motif, natural naphthoquinones and non-naphthoquinones were employed in this study. The results showed that WNK-1 (**6.1**), WNK-3 (**6.2**) and WNK-4 (**6.3**) were toxic to HaCaT cell and not suitable to develop as 5 $\alpha$ -R inhibitors. Further screening of 5 $\alpha$ -R inhibitory activities revealed that avicquinone C (WNK-5, **6.4**) and WNK-7 (**6.6**) exhibited 42.4% and 67.2% inhibition at a concentration of 5  $\mu$ M, respectively. Moreover, WNK-6 (**6.5**), 1,4-dihydroxyanthraquinone (**6.7**) and 2-hydroxy-1,4-naphthquinone (**6.9**) showed 60.0%, 47.7%, and 82.7% inhibition at a concentration of 40  $\mu$ M, respectively. The most potent candidate, 2-hydroxy-1,4-naphthquinone (**6.9**) was then analyzed for IC<sub>50</sub> value, which was 23.39  $\mu$ M. Interestingly, 2-hydroxy-1,4-naphthquinone (**6.9**) possessed better 5 $\alpha$ -R inhibitory activity than that of avicquinone C. Regarding the structure-activity relationship obtained from all avicquinone C and synthetic analogs, natural naphthoquinones and non-naphthoquinones, Naphthoquinone moiety was an important pharmacophore for 5 $\alpha$ -reductase inhibitory activity and naphthoquinone was potentially developed as a new series of 5 $\alpha$ -R inhibitors. According to our results, the new 5 $\alpha$ -R inhibitors having naphthoquinone core could be developed for the treatment of androgenic alopecia.

## Chapter VII

### Conclusions

Steroid 5 $\alpha$ -reductase (5 $\alpha$ -R) is a membrane bound enzyme in the oxidoreductase family. This enzyme plays important biological actions in steroid metabolism. At the present time, there are 3 types of 5 $\alpha$ -R; 5 $\alpha$ -reductase type 1 (5 $\alpha$ -R1), 5 $\alpha$ -reductase type 2 (5 $\alpha$ -R2) and 5 $\alpha$ -reductase type 3 (5 $\alpha$ -R3). Overexpression of 5 $\alpha$ -R, especially 5 $\alpha$ -R1 and 5 $\alpha$ -R2, has affected the balance between testosterone (T) and dihydrotestosterone (DHT), which implicate the androgenic disorders, including prostate cancer, hirsutism and androgenic alopecia. Lack of single crystal X-ray structures of 5 $\alpha$ -R has hindered mechanistic understanding and delayed the discovery and development of an effective inhibitor. In this study, we demonstrated the three-dimensional of 5 $\alpha$ -R1 and 5 $\alpha$ -R2 structures, which are known to be associated with human endocrine disorders caused by the overproduction of DHT. The *in silico* three-dimensional 5 $\alpha$ -R1 and 5 $\alpha$ -R2 structures were built by the homology modeling. The isoprenylcysteine carboxyl methyltransferase (ICMT, PDB code: 4A2N) was automatically selected by SWISS-MODEL as a homologous protein template for both 5 $\alpha$ -R1 and 5 $\alpha$ -R2. The pocket site of 5 $\alpha$ -R was confirmed by docking simulations of known inhibitors such as finasteride and dutasteride including several reported 5 $\alpha$ -R inhibitors.

According to a previous study, avicequinone C exhibited 5 $\alpha$ -R1 reductase inhibitory activities. Therefore, we hypothesized that furanonaphthoquinone potential involved the 5 $\alpha$ -R reductase inhibitory activities. Docking simulations of avicequinone C and analogs, natural naphthoquinones and non-naphthoquinones were performed by Autodock Vina using our predicted 5 $\alpha$ -R1 and 5 $\alpha$ -R2 structures as an *in silico* protein target. The results showed that avicequinone C performed the lowest binding energy ( $\Delta G$ ), among other naphthoquinones in both 5 $\alpha$ -R1 and 5 $\alpha$ -R2 docking studies. Based on  $\Delta G$  values, it indicated that furanonaphthoquinone and naphthoquinone

moieties were associated with 5 $\alpha$ -R1 and 5 $\alpha$ -R2 catalytic pocket and potentially important for biological activity of 5 $\alpha$ -R1 and 5 $\alpha$ -R2.

In addition, avicequinone C and analogs were designed and synthesized by chemical process. All synthetic furanonaphthoquinone and natural naphthoquinones were applied for examination of the 5 $\alpha$ -R inhibitory activity *via* HaCaT cell-based assay. The results suggested that 2-hydroxy-1,4-naphthoquinone remarkably inhibited 5 $\alpha$ -R expressed by HaCaT cell with IC<sub>50</sub> 23.93  $\mu$ M (82.7  $\pm$  14.4% inhibition at 40  $\mu$ M). Besides, we also found that WNK-6, which was dihydrofuran congener of avicequinone C showed similar 5 $\alpha$ -R inhibitory activity to avicequinone C with 60.0  $\pm$  9.4% inhibition at 40  $\mu$ M. However, WNK-6 showed less cytotoxicity toward HaCaT cell than that of avicequinone C. Thus, 2-hydroxy-1,4-naphthoquinone and WNK-6 are possible to develop as 5 $\alpha$ -R inhibitor possessing satisfy biological activity and low cellular toxicity.

Considering results between *in vitro* and *in silico* 5 $\alpha$ -reductase inhibitory activity *via* HaCaT cell-based assay and molecular docking with predicted 5 $\alpha$ -R1, we concluded that naphthoquinone moiety was important for 5 $\alpha$ -reductase inhibitory activity and it showed better inhibitory activity than furanonaphthoquinone based on interactions at catalytic region of predicted 5 $\alpha$ -R1.

Further studies in molecular dynamics along with *in vitro* experiment will provide insight information regarding biological mechanisms. Finally, a new series of naphthoquinone could be developed as potential 5 $\alpha$ -reductase inhibitors for the treatment of androgenic alopecia.



## REFERENCES

1. Azzouni, F., A. Godoy, Y. Li, and J. Mohler, The 5  $\alpha$  -reductase isozyme family: a review of basic biology and their role in human diseases. *Advances in Urology*, 2012: p. 1-18.
2. Godoy, A., E. Kawinski, Y. Li, D. Oka, B. Alexiev, F. Azzouni, M.A. Titus, and J.L. Mohler, 5  $\alpha$  -reductase type 3 expression in human benign and malignant tissues: A comparative analysis during prostate cancer progression. *The Prostate*, 2011. 71: p. 1033-1046.
3. Clark, R.V., D.J. Hermann, G.R. Cunningham, T.H. Wilson, B.B. Morrill, and S. Hobbs, Marked suppression of dihydrotestosterone in men with benign prostatic hyperplasia by dutasteride, a dual 5  $\alpha$  -reductase inhibitor. *The Journal of Clinical Endocrinology and Metabolism*, 2004. 89: p. 2179-2184.
4. Traish, A.M., A. Mulgaonkar, and N. Giordano, The dark side of 5  $\alpha$  -reductase inhibitors's therapy: sexual dysfunction, high gleason grade prostate cancer and depression. *Korean Journal of Urology*, 2014. 55: p. 367-379.
5. Jain, R., O. Monthakantirat, P. Tengamnuay, and W. De-Eknamkul, Avicquinone C isolated from *Avicennia Marina* exhibits 5  $\alpha$  -reductase type 1 inhibitory activity using an androgenic alopecia relevant cell-based assay system. *Molecules*, 2014. 19: p. 6809-6821.
6. Opella, S.J., Structure determination of membrane proteins by nuclear magnetic resonance spectroscopy. *Annual Review of Analytical Chemistry*, 2013. 6: p. 305-328.
7. Titus, M.A., C.W. Gregory, O.H.F. III, M.J. Schell, S.J. Maygarden, and J.L. Mohler, Steroid 5  $\alpha$  -reductase isozymes I and II in recurrent prostate cancer. *Clinical Cancer Research*, 2005. 11: p. 4365-4371.
8. Jain, R. and W. De-Eknamkul, Potential targets in the discovery of new hair growth promoters for androgenic alpecia. *Expert Opinion on Therapeutics Targets*, 2014. 18: p. 787-806.

9. Uemura, M., K. Tamura, S. Chung, S. Honma, A. Okuyama, and Y. Nakamura, Novel 5  $\alpha$ -steroid reductase (SRD5A3, type-3) is overexpressed in hormone-refractory prostate cancer. *Cancer Science*, 2008. 99: p. 81-86.
10. Langlois, V.S., D. Zhang, G.M. Cooke, and V.L. Trudeau, Evolution of steroid-5  $\alpha$ -reductases and comparison of their function with 5 $\beta$ -reductase. *General Comparative Endocrinology*, 2010. 166: p. 489-497.
11. Russell, D.W. and J.D. Wilson, Steroid 5  $\alpha$ -reductase: two genes/two enzymes. *Annual Review of Biochemistry*, 1994. 63: p. 25-61.
12. Randall, V.A., The endocrine control of hair follicle. *Hair growth and disorder*. 2008, Germany: Springer-Verlag Berlin Heidelberg.
13. Aggarwal, S., S. Thareja, A. Verma, T.R. Bhardwaj, and M. Kumar, An overview on 5  $\alpha$ -reductase inhibitors. *Steroids*, 2010. 75: p. 109-153.
14. Marks, L.S., 5  $\alpha$ -reductase: history and clinical importance. *Advances in Urology*, 2004. 6: p. S11-S21.
15. Narizhneva, N.V., N.D. Tararova, P. Ryabokon, I. Shyshynova, A. Prokvolit, P.G. Komarov, A.A. Purmai, A.V. Gudkov, and K.V. Gurova, Small molecule screening reveals a transcription-independent pro-survival function of androgen receptor in castration-resistant prostate cancer. *Cell Cycle*, 2009. 8: p. 4155-4167.
16. Hudak, S.J., J. Hernandaz, and I.M. Thompson, Role of 5  $\alpha$ -reductase inhibitors in the management of prostate cancer. *Clinical Interventions in Aging*, 2006. 1: p. 425-431.
17. Nicholson, T.M. and W.A. Ricke, Androgens and estrogens in benign prostatic hyperplasia: Past, present and future. *Differentiation*, 2011. 82: p. 184-199.
18. Thomas, L.N., R.C. Douglas, C.B. Lazier, C.K.L. Too, R.S. Rittmaster, and D.J. Tindall, Type 1 and Type 2 5  $\alpha$ -reductase expression in the development and progression of prostate cancer. *European Urology*, 2008. 53: p. 244-252.
19. Thiboutot, D., H.G. Knaggs, K. Gilliland, and G. Lin, Activity of 5  $\alpha$ -reductase and 17 $\beta$ -hydroxysteroid dehydrogenase in the infrainfundibulum of subjects with and without acne vulgaris. *Dermatology*, 1998. 196: p. 38-42.

20. Serafini, P. and R.A. Lobo, Increased 5  $\alpha$ -reductase activity in idiopathic hirsutism. *Fertility*, 1985. 43: p. 74-78.
21. Sachdeva, S., Hirsutism: Evaluation and treatment. *Indian Journal of Dermatology*, 2010. 55: p. 3-7.
22. Messenger, A., Male androgenetic alopecia. *Hair growth and disorder*. 2008, Germany: Springer-Verlag Berlin Heidelberg.
23. Harcha, W.G., J.B. Martinez, T.-F. Tsai, K. Katsouka, M. Kawashima, R. Tsuboi, A. Barnes, G. Ferron-Brady, and D. Chetty, A randomized, active- and placebo-controlled study of the efficacy and safety of different doses of dutasteride versus placebo and finasteride in the treatment of male subjects with androgenetic alopecia. *Journal of the American Academy of Dermatology*, 2014. 70: p. 489-498.
24. Bull, H.G., M. Garcia-Calvo, S. Andersson, W.F. Baginsky, H.K. Chan, D.E. Ellsworth, R.R. Miler, R.A. Stearns, R.K. Bakshi, G.H. Rasmusson, R.L. Tolman, R.W. Myers, J.W. Kozarich, and G.S. Harris, Mechanism-based inhibition of human steroid 5  $\alpha$ -reductase by finasteride: Enzyme-catalyzed formation of NADP-Dihydrofinasteride, a potent bisubstrate analog inhibitor. *Journal of American Chemical Society*, 1996. 118: p. 2359-2365.
25. Seo, E.-K., K.H. Kim, M.K. Kim, M.-H. Cho, E. Choi, K. Kim, and W. Mar, Inhibitors of 5 $\alpha$ -reductase type I in LNCaP cells from the roots of *Angelica koreana*. *Planta Medica*, 2002. 68: p. 162-163.
26. Shimizu, K., R. Kondo, K. Sakai, S. Buabarn, and U. Dilokkunanant, 5  $\alpha$ -reductase inhibitory components from leaves of *Artocarpus altilis*. *Journal of Wood Science*, 2000. 46: p. 385-389.
27. Hiipakka, R.A., H.-Z. Zhang, W. Dai, Q. Dai, and S. Liao, Structure-activity relationships for inhibition of human 5  $\alpha$ -reductase by polyphenols. *Biochemical Pharmacology*, 2002. 63: p. 1165-1176.
28. Kumar, N., W. Rungseevijitprapa, N.-A. Narkkhong, M. Suttajit, and C. Chaiyasut, 5  $\alpha$ -reductase inhibition and hair growth promotion of some Thai plants

- traditionally used for hair treatment. *Journal of Ethnopharmacology*, 2012. 139: p. 765-771.
29. Suphrom, N., G. Pumthong, N. Khorana, N. Waranuch, N. Limpeanchob, and K. Ingkaninan, Anti-androgenic effect of sesquiterpenes isolated from the rhizomes of *Curcuma aeruginosa* Roxb. *Fitoterapia*, 2012. 83: p. 864-871.
  30. Liu, J., K. Kurashiki, K. Shimizu, and R. Kondo, Structure-activity relationship for inhibition of 5  $\alpha$ -reductase by triterpenoids isolated from *Ganoderma lucidum*. *Bioorganic and Medicinal Chemistry*, 2006. 14: p. 8654-8660.
  31. Ruksiriwanich, W., J. Manosroi, M. Abe, W. Monosroi, and A. Manosroi, 5  $\alpha$ -reductase type 1 inhibition of *Oryza sativa* bran extract prepared by supercritical carbon dioxide fluid. *The Journal of Supercritical Fluids*, 2011. 59: p. 61-71.
  32. Hirata, N., M. Tokunaga, S. Naruto, M. Linuma, and H. Matsuda, Testosterone 5  $\alpha$ -reductase inhibitory active constituents of *Piper nigrum* leaf. *Biological and Pharmaceutical Bulletin*, 2007. 30: p. 2402-2405.
  33. Murata, K., K. Noguchi, M. Kondo, M. Onishi, N. Watanabe, K. Okamura, and H. Matsuda, Inhibitory activities of *Puerariae Flos* against testosterone 5  $\alpha$ -reductase and its hair growth promotion activities. *Journal of Natural Medicines*, 2012. 66: p. 158-165.
  34. Park, W.-s., C.-h. Lee, B.-g. Lee, and L.-s. Chang, The extract of *Thujae occidentalis* semen inhibited 5  $\alpha$ -reductase and androchronogenetic alopecia of B6CBAF1/j hybrid mouse. *Journal of Dermatological Science*, 2003. 31: p. 91-98.
  35. Park, W.S., E.D. Son, G.W. Nam, S.H. Kim, M.S. Noh, B.G. Lee, I.S. Jang, S.E. Kim, J.J. Lee, and C.H. Lee, Torilin from *Torilis japonica*, as a new inhibitor of testosterone 5 alpha-reductase. *Planta Medica*, 2003. 69: p. 459-461.
  36. Yao, Z., Y. Xu, M. Zhang, S. Jiang, M.C. Nicklaus, and C. Liao, Discovery of a novel hybrid from finasteride and epristeride as 5  $\alpha$ -reductase inhibitor. *Bioorganic and Medicinal Chemistry Letters*, 2011. 21: p. 475-478.

37. Min-Rui, O. and L. Jun-Qian, Modeling of steroid 5  $\alpha$ -reductase and characterizing its potential active sites. *Chinese Journal of Structure Chemistry*, 2012. 31: p. 1618-1626.
38. Schanzer, W., Metabolism of anabolic androgenic steroids. *Clinical Chemistry*, 1996. 42: p. 1001-1020.
39. Xiang, Z., Advances in homology protein structure modeling. *Current Protein and Peptide Science*, 2006. 7: p. 217-227.
40. Zhang, Z., An overview of protein structure prediction: from homology to Ab initio, in Final Project for Bioc218, Computational Molecular Biology. 2002. p. 1-10.
41. Dorn, M., M.B.e. Silva, L.S. Buriol, and L.C. Lamb, Three-dimensional protein structure prediction: Methods and computational strategies. *Computational Biology and Chemistry*, 2014. 52: p. 251-276.
42. Trott, O. and A.J. Olsen, Autodock Vina: improving the speed and accuracy of docking with a new scoring function, efficient optimization and multithreading. *Journal of Computational Chemistry*, 2010. 31: p. 455-461.
43. Spassov, V.Z., P.K. Flook, and L. Yan, Looper: a molecular mechanics-based algorithm for protein loop prediction. *Protein engineering design and selection*, 2007. 21: p. 91-100.
44. Niiyama, S., K. Kojima, T. Hamada, R. Happle, and R. Hoffmann, The novel drug CS-891 inhibits 5  $\alpha$ -reductase activity in freshly isolated dermal papilla of human hair follicles. *European Journal of Dermatology*, 2000. 10: p. 593-595.
45. Karnsomwan, W., T. Rungrotmongkol, W. De-Eknamkul, and S. Chamni, In silico structural prediction of human steroid 5  $\alpha$ -reductase type II. *Medicinal Chemistry Research*, 2016: p. 1049-1056.
46. Karnsomwan, W., S. Chamni, T. Rungrotmongkol, and W. De-Eknamkul. Homology modeling of 5  $\alpha$ -reductase type 1 and identification of steroid-binding active site. in *Pure and Applied Chemistry International Conference*. 2015.

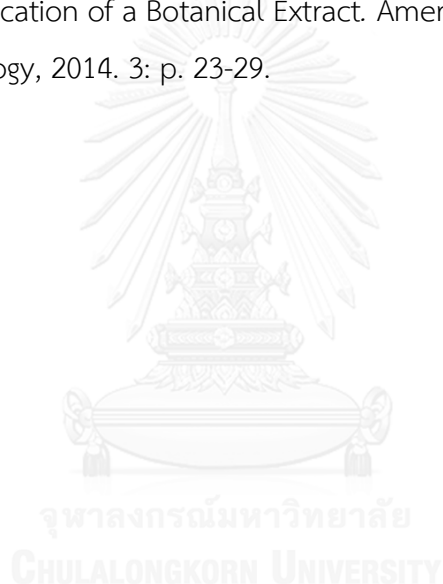
47. Kelley, L.A., S. Mezulis, C.M. Yates, M.N. Wass, and M.J.E. Sternberg, The phyte2 web portal for protein modeling, prediction and analysis. *Nature Protocols*, 2015. 10: p. 845-858.
48. Yang, J., R. Yan, A. Roy, D. Xu, J. Poisson, and Y. Zhang, The I-TASSER suite: protein structure and function prediction. *Nature Methods*, 2015. 12: p. 7-8.
49. Yang, J., K. Kulkarni, L. Manolaridis, Z. Zhang, R.B. Dodd, C. Mas-Droux, and D. Barford, Mechanism of isoprenylcysteine carboxyl methylation from the crystal structure of the integral membrane methyltransferase ICMT. *Molecular Cell*, 2011. 44: p. 997-1004.
50. Kumar, R., P. Malla, A. Verma, and M. Kumar, Design of potent human steroid 5  $\alpha$ -reductase inhibitors: 3D-QSAR CoMFA, CoMSIA and docking studies. *Medicinal Chemistry Research*, 2013. 22: p. 4568-4580.
51. Drury, J.E., L.D. Costanzo, T.M. Penning, and D.W. Christianson, Inhibition of human steroid 5 $\beta$ -reductase (AKR1D1) by finasteride and structure of the enzyme-inhibitor complex. *The Journal of Biological Chemistry*, 2009. 284: p. 19785-19790.
52. Ramachandran, G., C. Ramakrishnan, and V. Sasisekharan, Stereochemistry of polypeptide chain configurations. *Journal of Molecular Biology*, 1963. 7: p. 95-99.
53. Bjorkhem, I., Mechanism and stereochemistry of the enzymatic conversion of a  $\Delta^4$ -3-oxosteroid into a 3-oxo-5  $\alpha$ -steroid. *European Journal of Biochemistry*, 1969. 8: p. 345-351.
54. Li, X., C. Chen, S.M. Singh, and F. Labrie, The enzyme and inhibitors of 4-ene-3-oxosteroid 5  $\alpha$ -oxidoreductase. *Steroids*, 1995. 60: p. 430-441.
55. Drews, J., Drug discovery: A historical perspective. *Science*, 2000. 287: p. 1960-1964.
56. Sliwoski, G., S. Kothiwale, J. Meiler, and E.W. Lowe, Computational methods in drug discovery. *Pharmacological Reviews*, 2014. 66: p. 334-395.
57. Morris, G.M. and M. Lim-Wilby, Molecular docking. *Molecular Modeling of Proteins*, 2008: p. 365-382.

58. Sinha, C., A. Nischal, S. Bandaru, P. Kasera, A. Rajput, A. Nayariseri, and S. Khattri, An *In silico* Approach for Identification of Novel Inhibitors as a Potential Therapeutics Targeting HIV-1 Viral Infectivity Factor. *Current Topics in Medicinal Chemistry*, 2015. 15: p. 65-72.
59. Wang, S.-Q., Q.-S. Du, and K.-C. Chou, Study of drug resistance of chicken influenza A virus (H5N1) from homology-modeled 3D structures of neuraminidases. *Biochemical and biophysical research communications*, 2007. 354: p. 634-640.
60. Szklarz, G.D. and J.R. Halpent, Use of homology modeling in conjunction with site-directed mutagenesis for analysis of structure-function relationships of mammalian cytochromes P450. *Life sciences* 1997. 61: p. 2507-2520.
61. Ito, C., S. Katsuno, Y. Kondo, H.T.-W. Tan, and H. Furukawa, Chemical constituents of *Avicennia alba* isolation and structural elucidation of new naphthoquinones and their analogues. *Chemical and Pharmaceutical Bulletin*, 2000. 48: p. 339-343.
62. Han, L., X. Huang, H.-M. Dahse, U. Moellmann, H. Fu, S. Grabley, I. Sattler, and W. Lin, Unusual naphthoquinone derivatives from the Twigs of *Avicennia marina*. *Journal of Natural Products*, 2007. 70.
63. Ribeiro, C.M.R., P.P.d. Souza, L.D.M. Ferreira, S.L. Pereira, I.d.S. Martins, R.d.A. Epifanio, L.V. Costa-Lotufo, P.C. Jimenez, C. Pessoa, and M.O.d. Moraes, Natural furano naphthoquinones from lapachol: hydroxyiso- $\beta$ -lapachone, stenocarpoquinone-B and avicequinone C. *Letters in Organic Chemistry*, 2011. 8: p. 347-351.
64. Hagiwara, H., K. Sato, D. Nishino, T. Hoshi, T. Suzuki, and M. Ando, Domino Michael-O-alkylation: one pot synthesis of 2,4-diacylhydrofuran derivatives and its application to antitumor naphthofuran synthesis. *Journal of Chemical Society*, 2001: p. 2496-2957.
65. Aswathanarayanappa, C., E. Bheemappa, Y.D. Bodke, V.K. Bhovi, R. Ningegowda, M.C.Shivakumar, S.K. Peethambar, and S. Telkar, 5-phenyl-1-

- benzofuran-2-yl derivatives: synthesis, antimicrobial and antioxidant activity. *Medicinal Chemistry Research*, 2013. 22: p. 78-87.
66. Jiang, Z., A. Wang, H. Hu, J. Xu, Y. Hu, X. Li, Y. Ye, J. Wang, and Q. Li, 4,9-Dihydroxynaphtho[2,3-b]furan derivatives and their preparation and use for the treatment of cancer and other diseases, in *The International Patent System*. 2012.
67. Heltzel, C.E., A.A.L. Gunatilaka, T.E. Glass, and D.G.I. Kingston, Bioactive Furanonaphthoquinones from *Crescentia cujete*. *Journal of Natural Products*, 1993. 56: p. 1500-1505.
68. Eyong, K.O., P.S. Kumar, V. Kuete, G.N. Folefoc, E.A. Nkengfack, and S. Baskaran, Semisynthesis and antitumoral activity of 2-acetylfuranonaphthoquinone and other naphthoquinone derivatives from lapachol. *Bioorganic and Medicinal Chemistry Letters*, 2008. 18: p. 5387-5390.
69. Jonker, D.J., J. Stephenson, W.J. Edenfield, J.G. Supko, Y. Li, W. Li, M. Hitron, D. Leggett, D. Kerstein, and C. Li, A phase I extension study of BBI608, a first-in-class cancer stem cell (CSC) inhibitor, in patients with advanced solid tumors. *Journal of Clinical Oncology*, 2014. 32: p. 5s.
70. Wu, C., R.K. Johnson, M.R. Mattern, J.C. Wong, and D.G.I. Kingston, Synthesis of furanonaphthoquinones with hydroxyamino side chains. *Journal of Natural Products*, 1999. 62: p. 963-968.
71. Perez-Sacau, E., R.G. Diza-Penate, A. Estevez-Braun, A.G. Ravelo, J.M. Garcia-Castellano, L. Pardo, and M. Campillo, Synthesis and pharmacophore modeling of naphthoquinone derivatives with cytotoxic activity in human promyelocytic leukemia HL-60 cell line. *Journal of Medicinal Chemistry*, 2007. 50: p. 696-706.
72. Reichstein, A., S. Vortherms, S. Bannwitz, J. Tentrop, H. Prinz, and K. Muller, Synthesis and Structure–Activity Relationships of Lapacho Analogues. 1. Suppression of Human Keratinocyte Hyperproliferation by 2-Substituted Naphtho[2,3-b]furan-4,9-diones, Activation by Enzymatic One- and Two-Electron Reduction, and Intracellular Generation of Superoxide. *Journal of Medicinal Chemistry*, 2012. 55: p. 7273-7284.



73. Tseng, C.-H., Y.-L. Chen, S.-H. Yang, S.-l. Peng, C.-M. Cheng, C.-H. Han, S.-R. Lin, and C.-C. Tzeng, Synthesis and antiproliferative evaluation of certain iminonaphtho[2,3-b]furan derivatives. *Bioorganic and Medicinal Chemistry*, 2010. 18: p. 5172-5182.
74. Seiffert, K., H. Seltmann, M. Fritsch, and C.C. Zouboulis, Inhibition of 5  $\alpha$  - reductase activity in SZ95 sebocytes and HaCaT Keratinocytes *In vitro*. *Hormone and Metabolic Research*, 2007. 39: p. 141-148.
75. Izgi, A., M. Turglu, B. Akyildrum, S. Celen, and N. Celik, Investigation of the gene expression levels of 5  $\alpha$  -reductase, VEGF and IL-1  $\alpha$  in HaCaT cells after the application of a Botanical Extract. *American Journal of Dermatology and Venereology*, 2014. 3: p. 23-29.





APPENDIX

จุฬาลงกรณ์มหาวิทยาลัย  
CHULALONGKORN UNIVERSITY

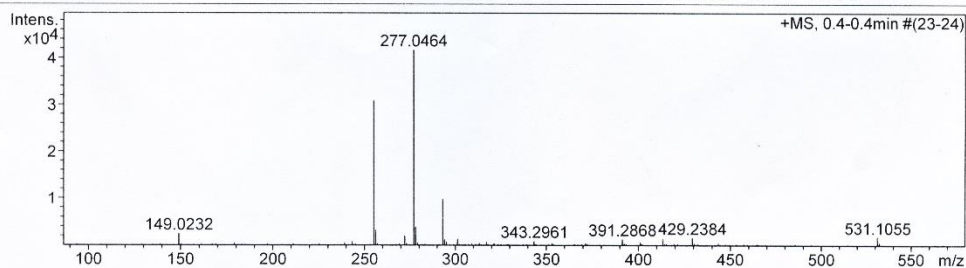
## Mass Spectrum List Report

### Analysis Info

Analysis Name	OSCUWNK580318001.d	Acquisition Date	3/19/2015 12:15:15 PM
Method	MKE_tune_low_positive_20130204.m	Operator	Administrator
Sample Name	WNK-1	Instrument	micrOTOF 72
	WNK-1		

### Acquisition Parameter

Source Type	ESI	Ion Polarity	Positive	Set Corrector Fill	79 V
Scan Range	n/a	Capillary Exit	100.0 V	Set Pulsar Pull	406 V
Scan Begin	50 m/z	Hexapole RF	90.0 V	Set Pulsar Push	388 V
Scan End	3000 m/z	Skimmer 1	45.5 V	Set Reflector	1300 V
		Hexapole 1	25.0 V	Set Flight Tube	9000 V
				Set Detector TOF	1910 V



#	m/z	I	I%	S/N	FWHM	Res.
1	149.0232	2441	5.9	313.3	0.0252	5922
2	179.0698	417	1.0	48.4	0.0301	5944
3	239.1511	472	1.1	46.2	0.0433	5518
4	243.1141	770	1.9	74.6	0.0410	5933
5	255.0638	30873	74.2	2917.0	0.0397	6417
6	256.0679	3186	7.7	299.9	0.0406	6312
7	257.0714	389	0.9	36.2	0.0436	5899
8	272.0902	1967	4.7	177.8	0.0425	6402
9	273.0917	395	0.9	35.3	0.0423	6461
10	277.0464	41587	100.0	3722.4	0.0411	6737
11	278.0503	3925	9.4	350.2	0.0426	6529
12	279.0547	373	0.9	32.8	0.0494	5650
13	279.1596	406	1.0	35.8	0.0485	5759
14	293.0200	9730	23.4	838.6	0.0443	6617
15	294.0252	1144	2.8	98.0	0.0454	6482
16	295.0243	632	1.5	53.9	0.0507	5821
17	301.1410	1313	3.2	110.8	0.0459	6563
18	313.1741	425	1.0	34.6	0.0519	6039
19	317.1148	618	1.5	50.1	0.0526	6032
20	321.2384	390	0.9	31.2	0.0576	5575
21	343.2961	858	2.1	65.9	0.0510	6732
22	353.1573	413	1.0	30.9	0.0751	4702
23	371.3174	443	1.1	33.5	0.0516	7201
24	391.2868	1259	3.0	98.1	0.0672	5818
25	401.0666	622	1.5	48.8	0.0565	7100
26	413.2638	1236	3.0	98.7	0.0553	7479
27	429.2384	1554	3.7	126.6	0.0666	6443
28	443.2680	479	1.2	39.3	0.0763	5810
29	531.1055	1715	4.1	158.5	0.0944	5628
30	532.1075	546	1.3	50.1	0.0799	6658

Figure 38 Mass spectrum of WNK-1

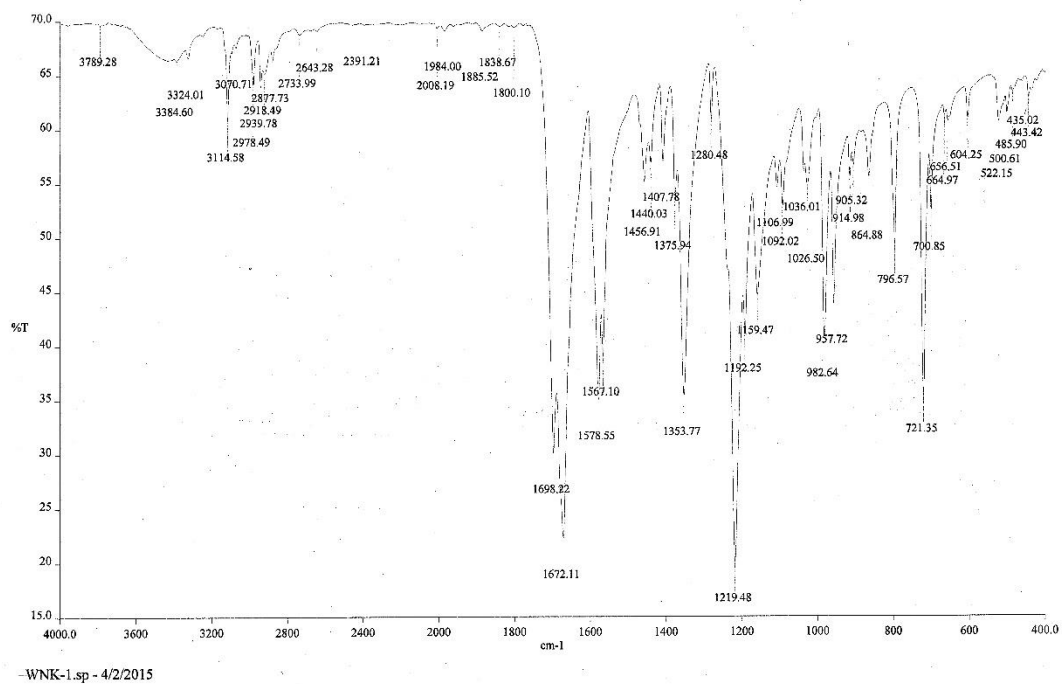
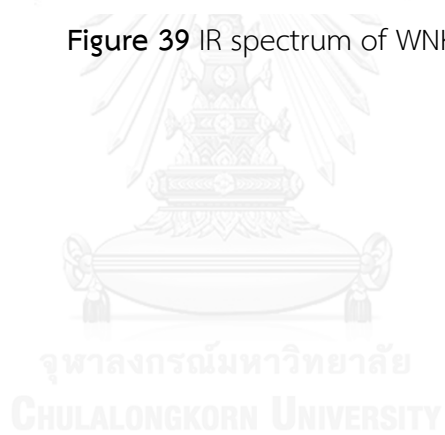


Figure 39 IR spectrum of WNK-1



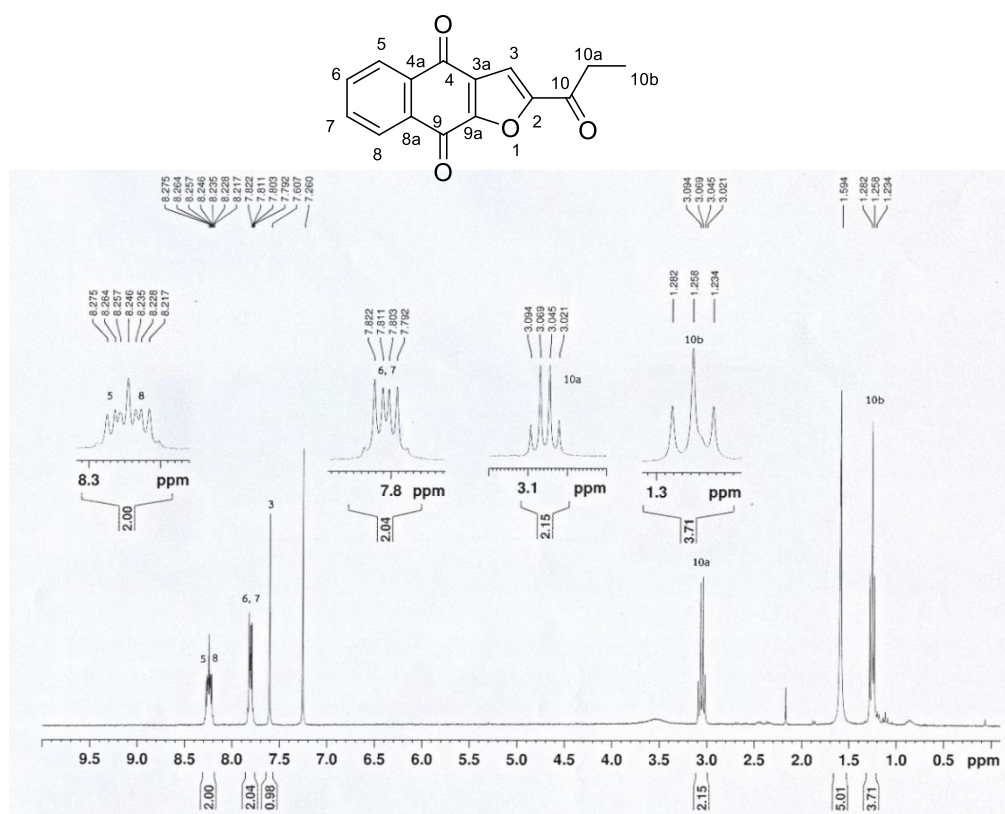


Figure 40  $^1\text{H}$  NMR (300 MHz) spectrum of WNK-1

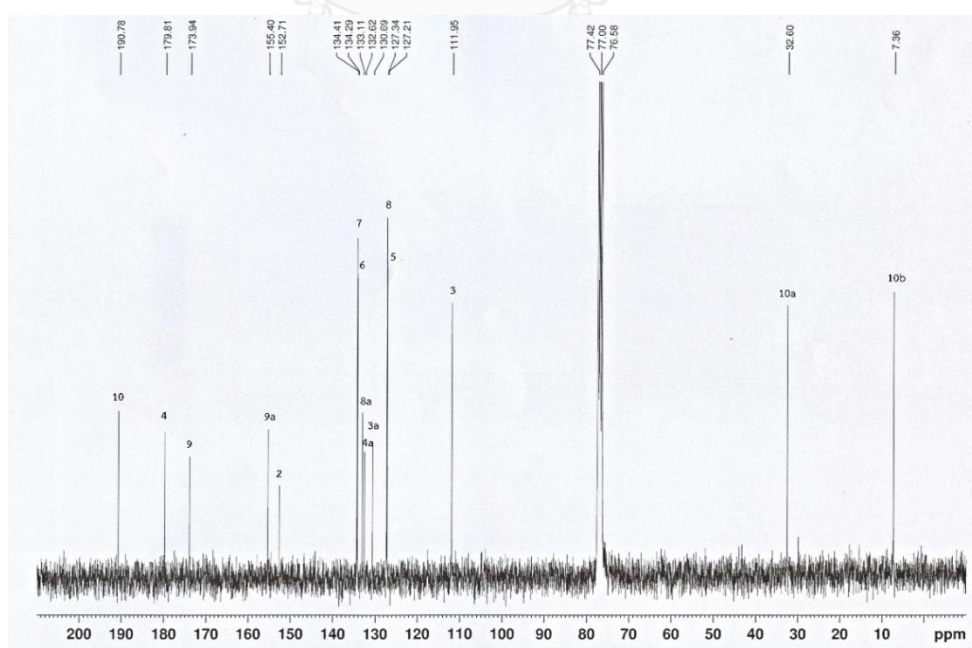


Figure 41  $^{13}\text{C}$  NMR (300 MHz) spectrum of WNK-1

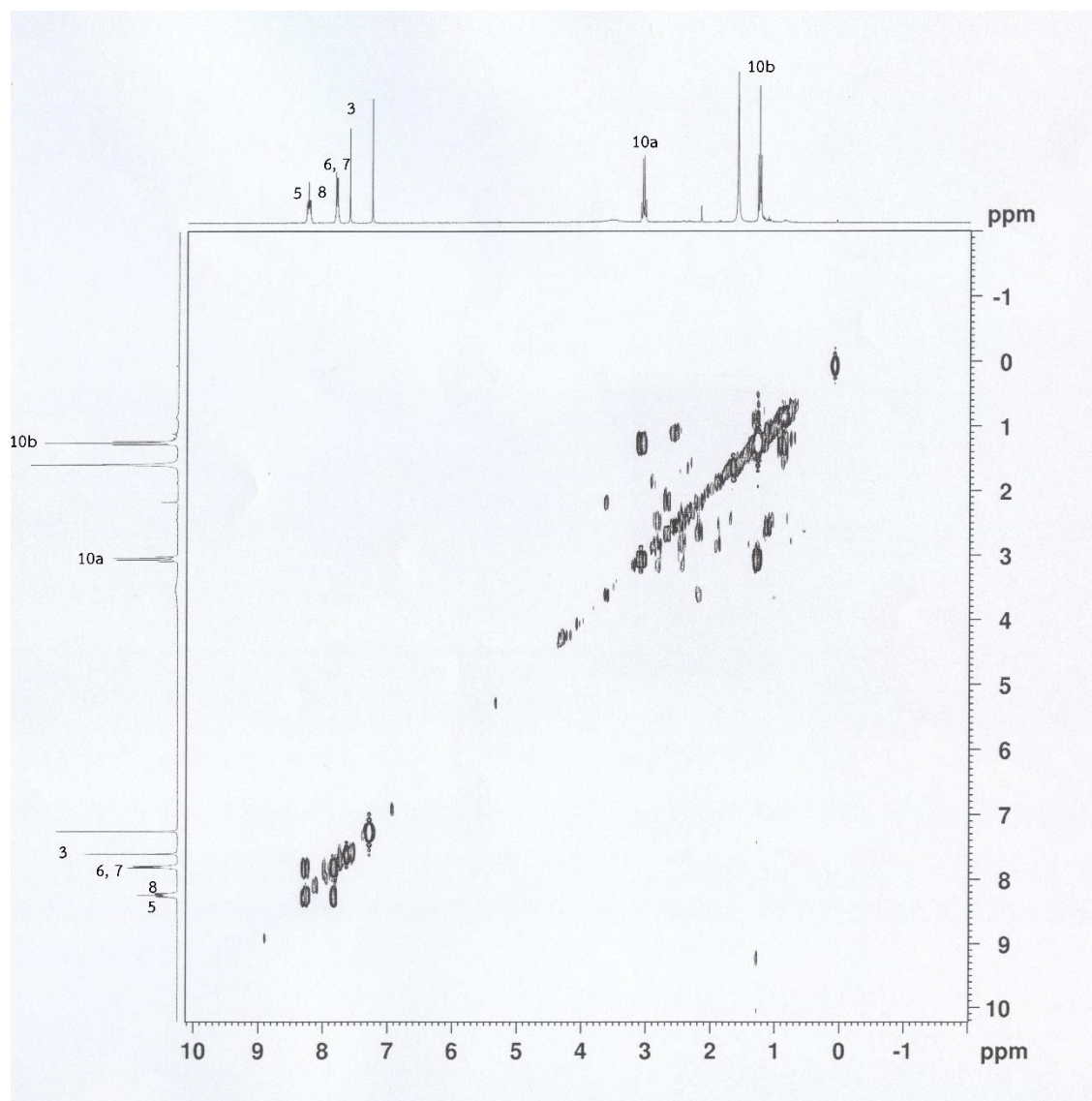
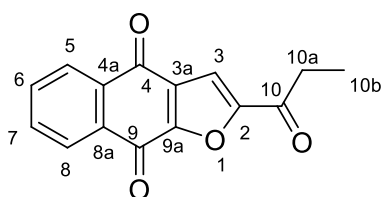


Figure 42 COSY spectrum of WNK-1



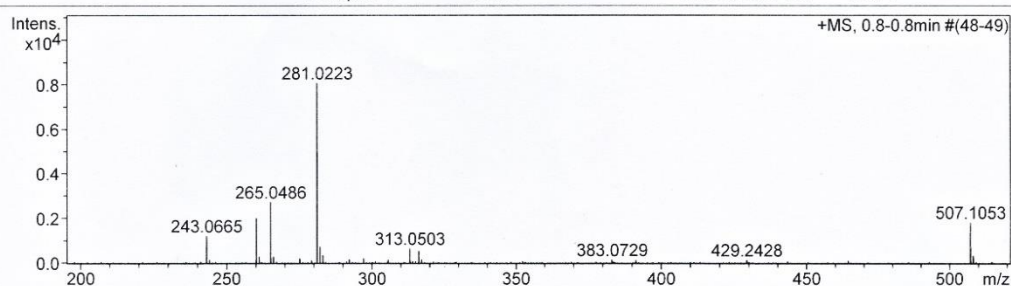
## Mass Spectrum List Report

### Analysis Info

Analysis Name	OSCUWNK580318003.d	Acquisition Date	3/19/2015 12:21:20 PM
Method	MKE_tune_low_positive_20130204.m	Operator	Administrator
Sample Name	WNK-3	Instrument	micrOTOF 72
	WNK-3		

### Acquisition Parameter

Source Type	ESI	Ion Polarity	Positive	Set Corrector Fill	79 V
Scan Range	n/a	Capillary Exit	60.0 V	Set Pulsar Pull	406 V
Scan Begin	50 m/z	Hexapole RF	90.0 V	Set Pulsar Push	388 V
Scan End	3000 m/z	Skimmer 1	45.5 V	Set Reflector	1300 V
		Hexapole 1	25.0 V	Set Flight Tube	9000 V
				Set Detector TOF	1910 V



#	m/z	I	I %	S/N	FWHM	Res.
1	57.0690	113	1.4	18.1	0.0052	10915
2	81.3133	121	1.5	19.5	0.0062	13198
3	243.0665	1205	14.9	196.7	0.0418	5814
4	244.0703	146	1.8	23.4	0.0457	5342
5	260.0924	2007	24.9	327.8	0.0450	5776
6	261.0966	279	3.5	45.1	0.0400	6534
7	265.0486	2716	33.7	444.0	0.0436	6084
8	266.0537	298	3.7	48.3	0.0452	5881
9	275.0928	215	2.7	34.6	0.0427	6441
10	279.1623	116	1.4	18.5	0.0477	5858
11	281.0223	8063	100.0	1318.8	0.0452	6222
12	282.0270	724	9.0	118.1	0.0455	6198
13	283.0241	350	4.3	56.7	0.0535	5290
14	292.1206	164	2.0	26.4	0.0569	5137
15	297.0777	206	2.5	33.1	0.0596	4982
16	305.5649	145	1.8	23.3	0.0118	25890
17	313.0503	646	8.0	105.2	0.0508	6162
18	316.1568	537	6.7	87.4	0.0496	6374
19	317.1347	146	1.8	23.4	0.0879	3606
20	383.0729	139	1.7	22.8	0.0611	6266
21	391.2934	134	1.7	22.1	0.0863	4534
22	429.2428	113	1.4	19.3	0.1026	4182
23	464.3758	109	1.3	19.1	0.0391	11889
24	507.1053	1780	22.1	335.7	0.1046	4847
25	508.1073	334	4.1	62.7	0.1056	4810
26	523.0878	211	2.6	40.0	0.1114	4698
27	539.1342	143	1.8	27.5	0.1230	4384
28	2374.1527	110	1.4	25.4	0.0318	74673

Figure 43 Mass spectrum of WNK-3

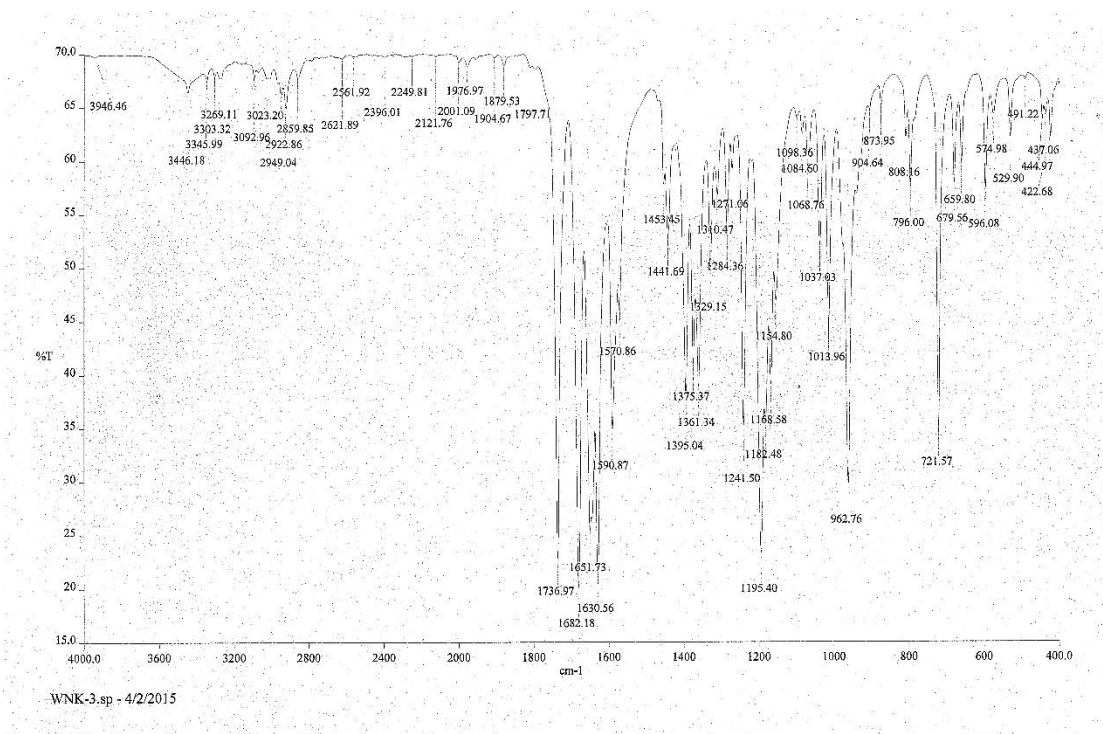


Figure 44 IR spectrum of WNK-3



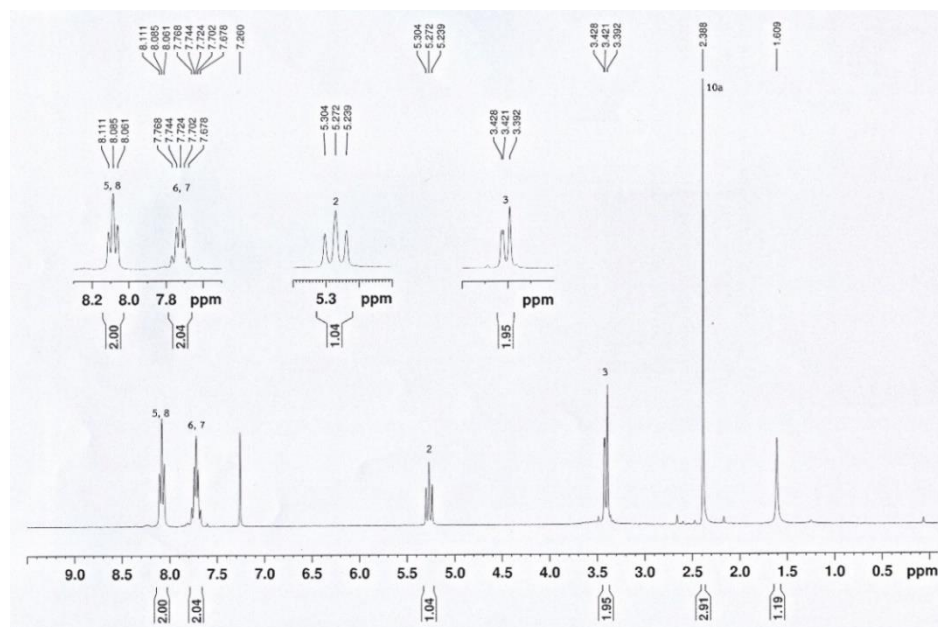
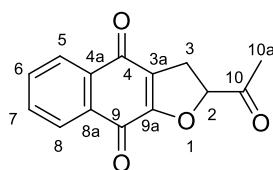


Figure 45  $^1\text{H}$  NMR (300 MHz) spectrum of WNK-3

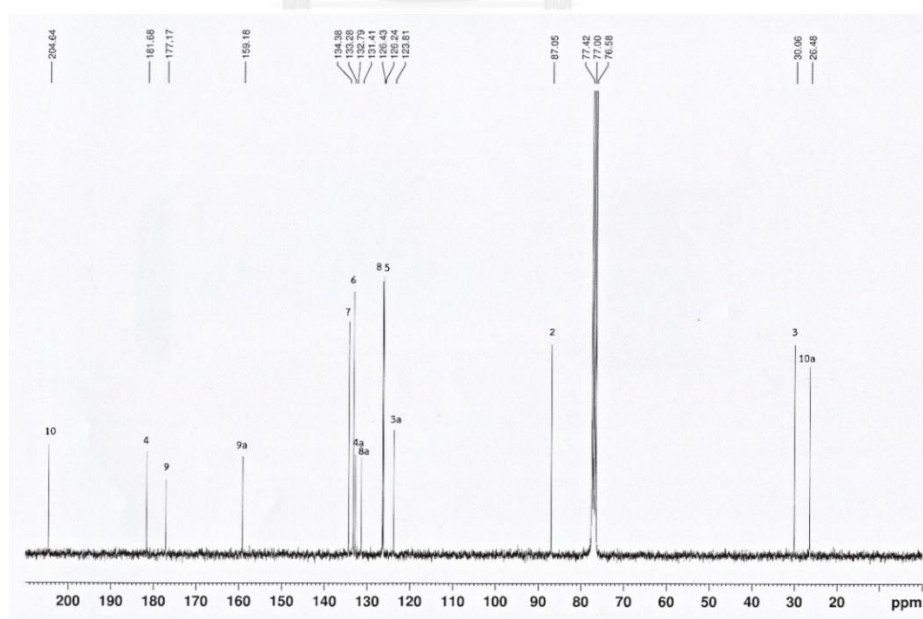


Figure 46  $^{13}\text{C}$  NMR (300 MHz) spectrum of WNK-3

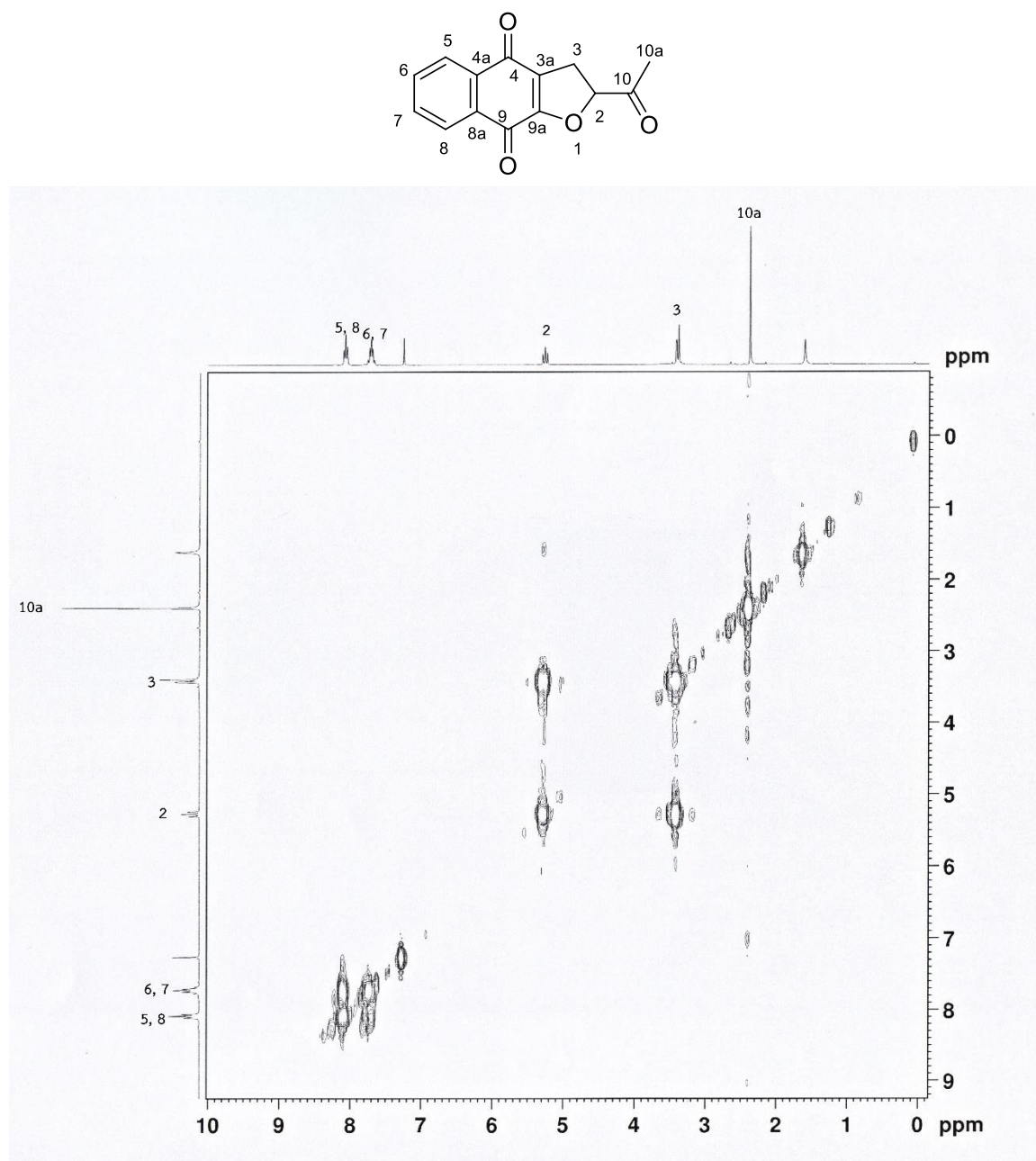


Figure 47 COSY spectrum of WNK-3

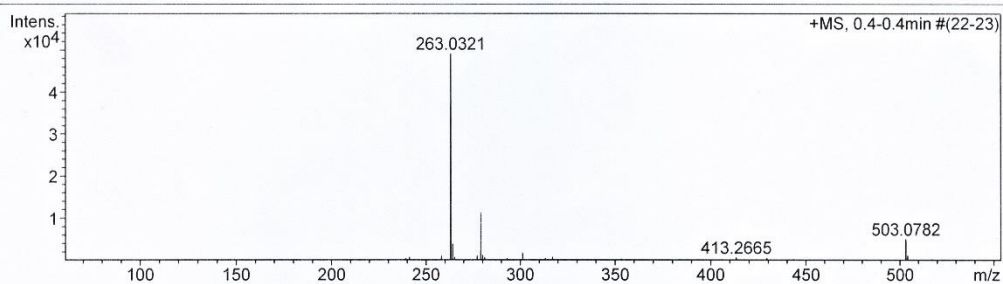
## Mass Spectrum List Report

### Analysis Info

Analysis Name	OSCUWNK580318004.d	Acquisition Date	3/19/2015 1:51:38 PM
Method	MKE_tune_low_positive_20130204.m	Operator	Administrator
Sample Name	WNK-4	Instrument	micrOTOF 72
	WNK-4		

### Acquisition Parameter

Source Type	ESI	Ion Polarity	Positive	Set Corrector Fill	79 V
Scan Range	n/a	Capillary Exit	90.0 V	Set Pulsar Pull	406 V
Scan Begin	50 m/z	Hexapole RF	90.0 V	Set Pulsar Push	388 V
Scan End	3000 m/z	Skimmer 1	45.5 V	Set Reflector	1300 V
		Hexapole 1	25.0 V	Set Flight Tube	9000 V
				Set Detector TOF	1910 V



#	m/z	I	I %	S/N	FWHM	Res.
1	211.0973	297	0.6	37.9	0.0412	5126
2	239.1570	519	1.1	62.5	0.0395	6053
3	241.0531	843	1.7	101.4	0.0423	5698
4	245.0787	279	0.6	33.0	0.0463	5297
5	258.0765	1035	2.1	120.2	0.0384	6715
6	263.0321	49078	100.0	5661.3	0.0404	6519
7	264.0352	3962	8.1	455.7	0.0444	5947
8	265.0434	791	1.6	90.6	0.0423	6265
9	277.0474	1151	2.3	128.7	0.0442	6273
10	278.0518	195	0.4	21.5	0.0388	7173
11	279.0060	11297	23.0	1262.0	0.0429	6498
12	279.1622	239	0.5	26.3	0.0567	4921
13	280.0111	1219	2.5	135.6	0.0429	6532
14	281.0113	732	1.5	81.1	0.0529	5311
15	281.1713	215	0.4	23.6	0.0665	4230
16	293.0236	524	1.1	56.6	0.0504	5810
17	295.0587	212	0.4	22.6	0.0569	5186
18	301.1429	1859	3.8	198.7	0.0481	6260
19	302.1461	281	0.6	29.7	0.0489	6178
20	313.1762	527	1.1	54.9	0.0468	6686
21	317.1184	844	1.7	87.4	0.0521	6086
22	329.1526	247	0.5	24.8	0.0482	6827
23	353.1608	393	0.8	37.9	0.0602	5869
24	380.0485	294	0.6	29.4	0.0514	7390
25	413.2665	760	1.5	81.4	0.0607	6808
26	429.2476	614	1.3	67.8	0.0887	4839
27	443.2750	329	0.7	37.1	0.0953	4650
28	503.0782	5104	10.4	662.3	0.0956	5264
29	504.0821	1161	2.4	150.7	0.0985	5115
30	517.0999	248	0.5	32.8	0.1065	4854

Figure 48 Mass spectrum of WNK-4

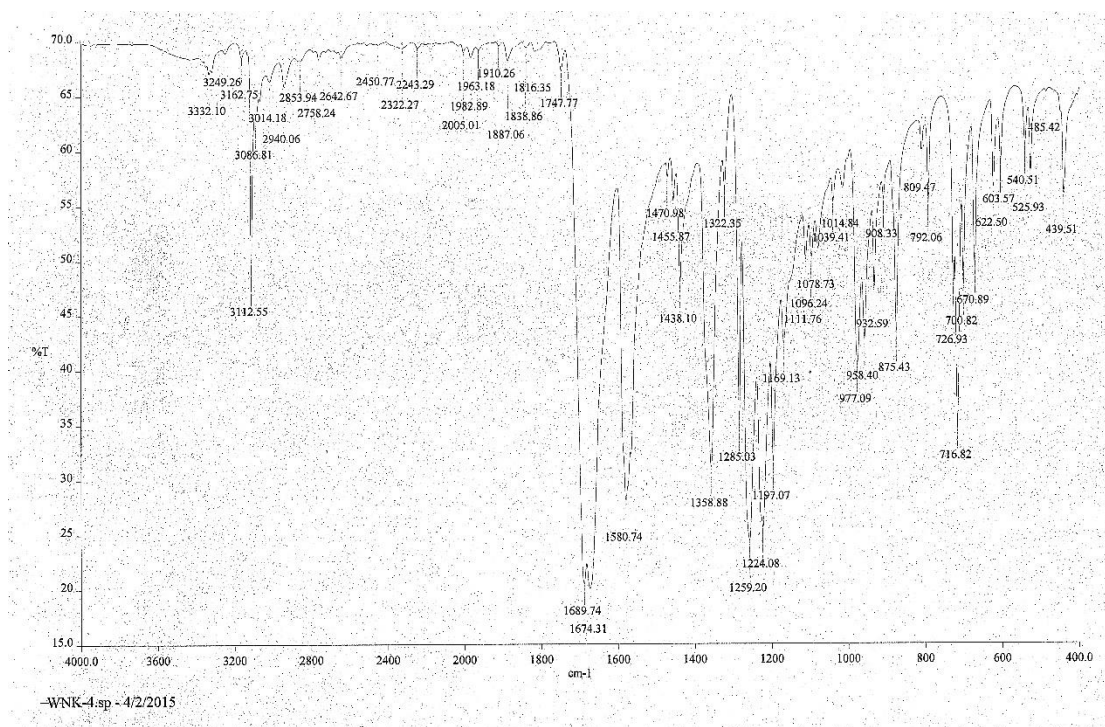
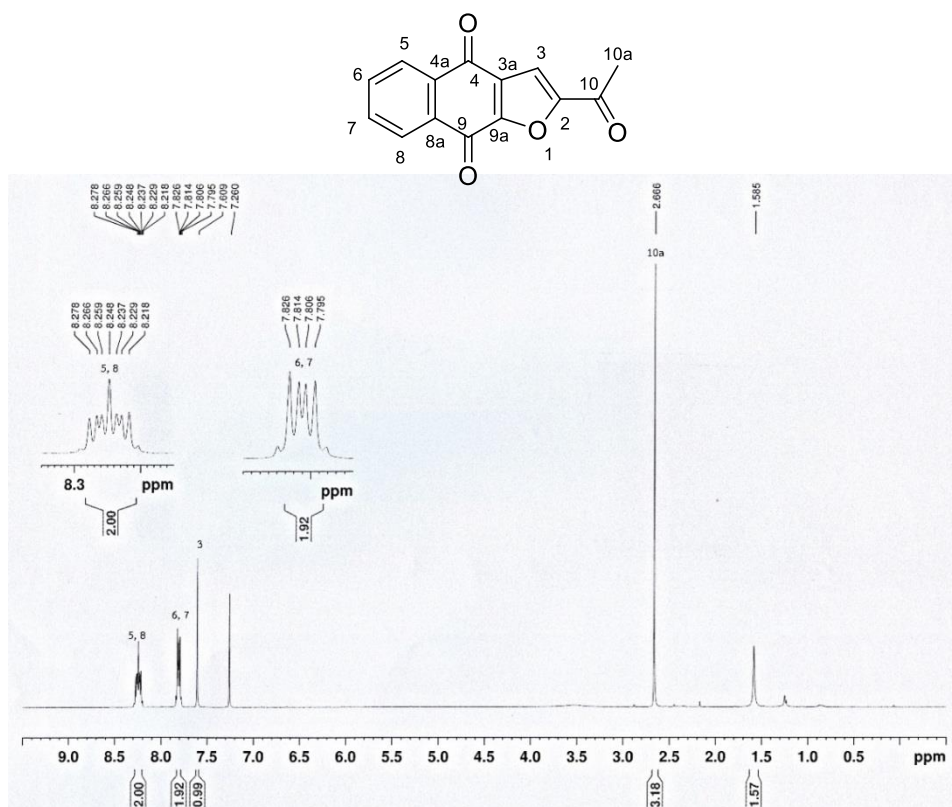
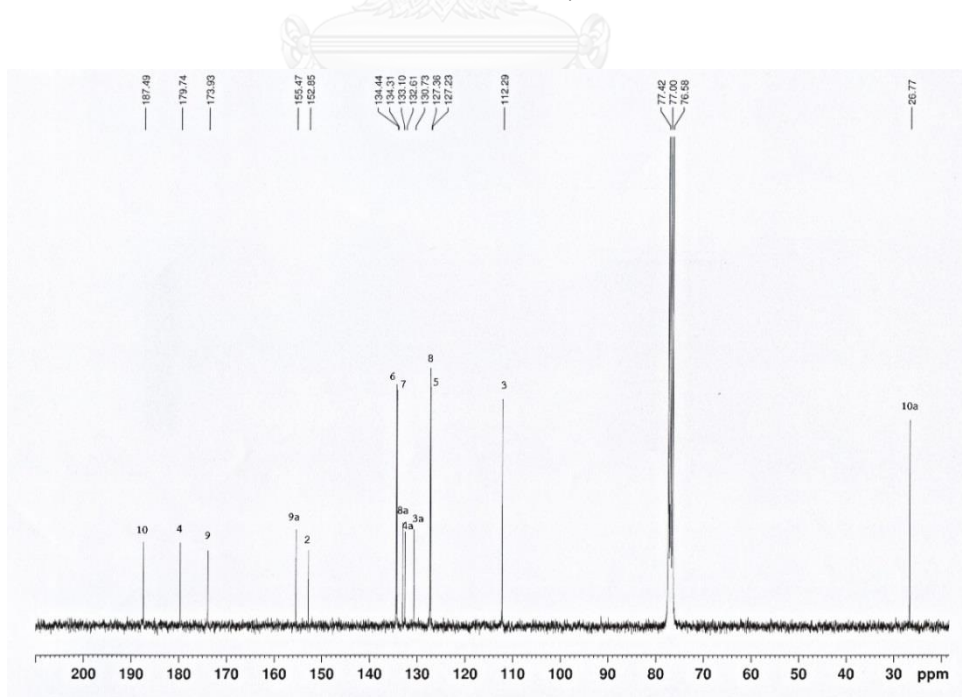


Figure 49 IR spectrum of WNK-4

Figure 50  $^1\text{H}$  NMR (300 MHz) spectrum of WNK-4Figure 51  $^{13}\text{C}$  NMR (300 MHz) spectrum of WNK-4



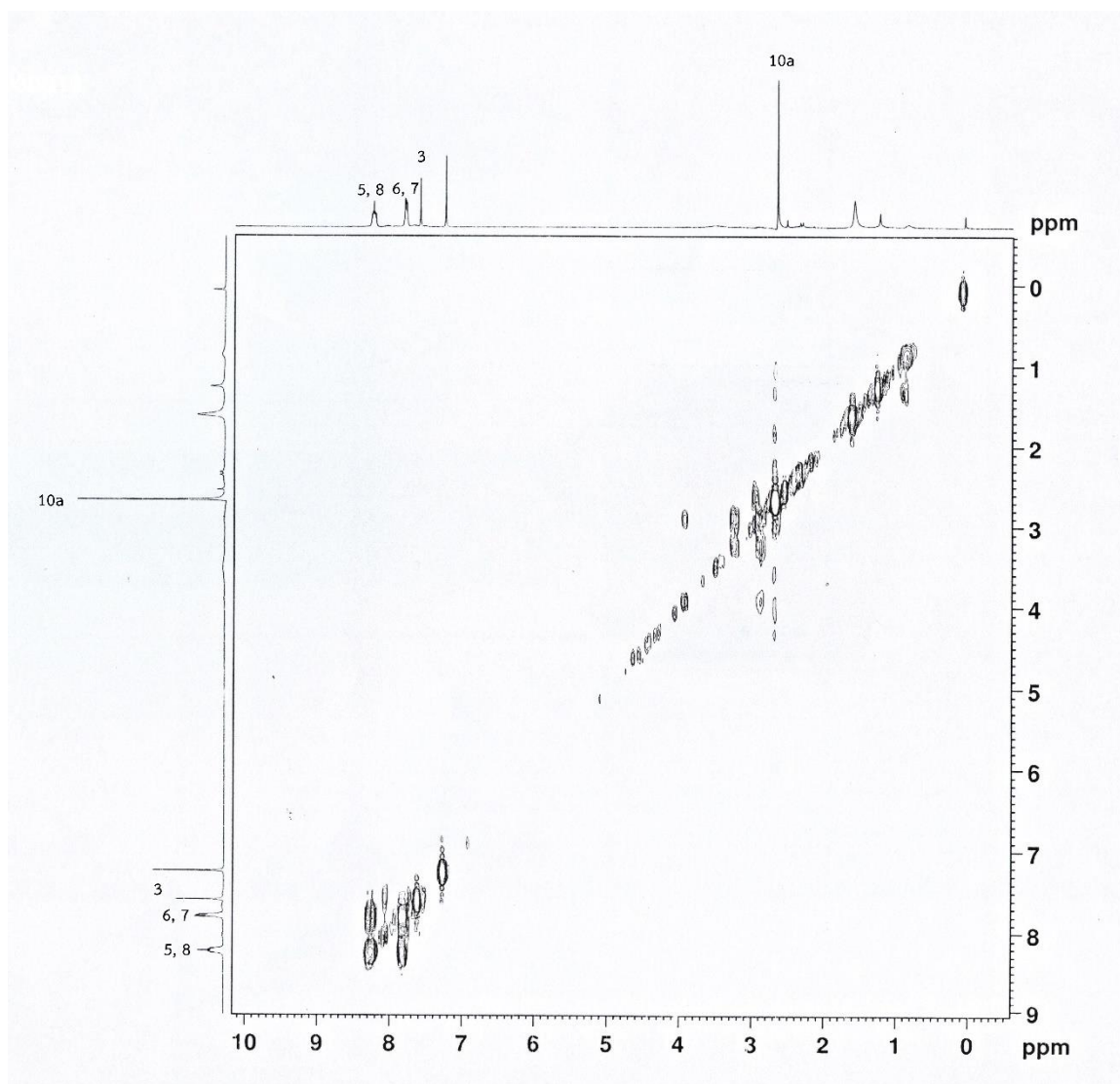
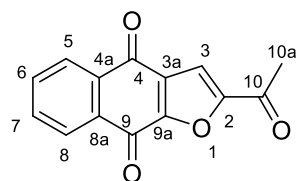


Figure 52 COSY spectrum of WNK-4

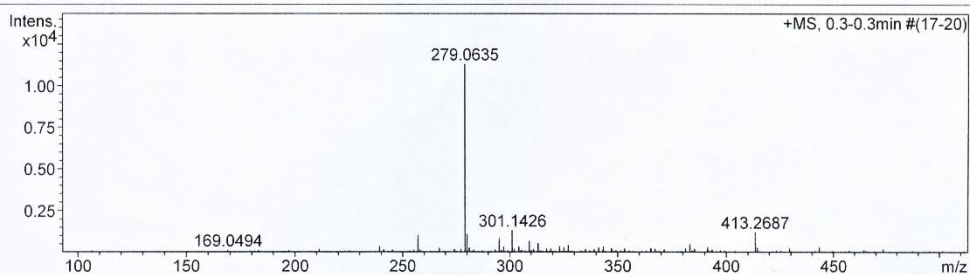
## Mass Spectrum List Report

### Analysis Info

Analysis Name	OSCUWNK580318005.d	Acquisition Date	3/19/2015 1:59:40 PM
Method	MKE_tune_low_positive_20130204.m	Operator	Administrator
Sample Name	WNK-5	Instrument	micrOTOF 72
	WNK-5		

### Acquisition Parameter

Source Type	ESI	Ion Polarity	Positive	Set Corrector Fill	79 V
Scan Range	n/a	Capillary Exit	90.0 V	Set Pulsar Pull	406 V
Scan Begin	50 m/z	Hexapole RF	90.0 V	Set Pulsar Push	388 V
Scan End	3000 m/z	Skimmer 1	45.5 V	Set Reflector	1300 V
		Hexapole 1	25.0 V	Set Flight Tube	9000 V
				Set Detector TOF	1910 V



#	m/z	I	I%	S/N	FWHM	Res.
1	239.0734	371	3.3	47.8	0.0465	5138
2	239.1496	241	2.1	30.9	0.0416	5747
3	257.0831	1038	9.2	128.4	0.0414	6215
4	279.0635	11304	100.0	1328.6	0.0384	7267
5	280.0679	1103	9.8	129.0	0.0471	5941
6	281.0784	291	2.6	33.7	0.0546	5150
7	295.0452	797	7.1	89.9	0.0626	4714
8	297.1061	346	3.1	38.7	0.0530	5606
9	301.1426	1327	11.7	147.8	0.0494	6096
10	304.2621	378	3.3	41.6	0.0528	5764
11	309.1316	698	6.2	76.3	0.0765	4040
12	313.1746	567	5.0	61.2	0.0471	6642
13	323.1025	369	3.3	38.8	0.0689	4687
14	325.1217	298	2.6	31.1	0.0925	3515
15	327.1273	431	3.8	45.1	0.0693	4718
16	341.1363	301	2.7	30.4	0.0680	5015
17	343.2973	356	3.2	35.9	0.0506	6791
18	347.1283	256	2.3	25.5	0.0646	5370
19	365.1408	247	2.2	24.2	0.0840	4349
20	365.2717	265	2.3	26.0	0.0634	5763
21	381.1453	241	2.1	23.6	0.0866	4404
22	383.1464	498	4.4	49.4	0.0741	5173
23	391.2963	330	2.9	32.6	0.0896	4368
24	413.2687	1221	10.8	123.0	0.0655	6309
25	414.2729	312	2.8	31.0	0.0618	6699
26	429.2865	265	2.3	26.3	0.1144	3751
27	443.2798	366	3.2	36.7	0.0983	4511
28	535.1418	4336	38.4	454.4	0.0850	6295
29	536.1417	946	8.4	98.5	0.1051	5102
30	537.1541	271	2.4	27.6	0.0855	6282

Figure 53 Mass spectrum of WNK-5

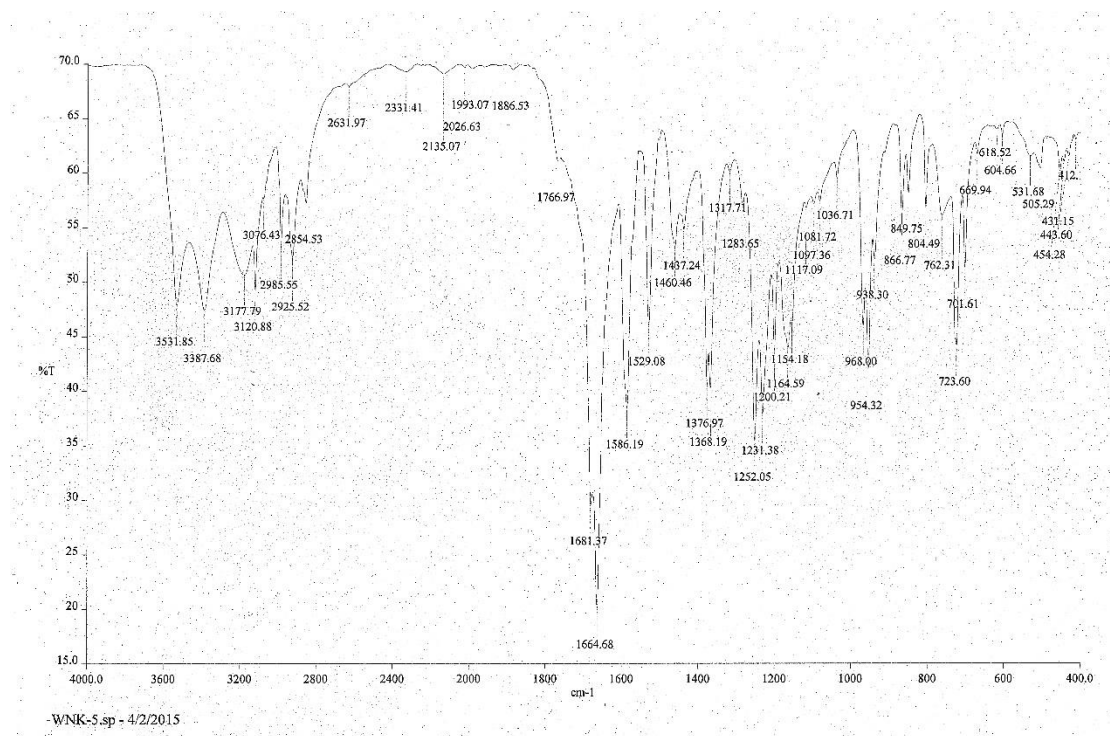
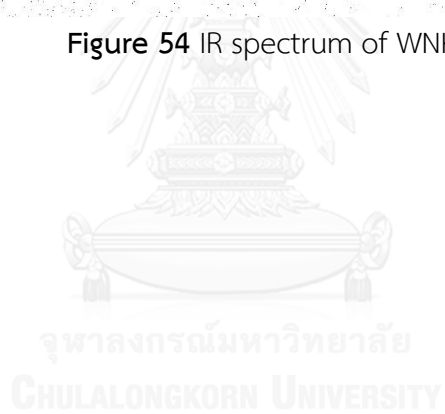


Figure 54 IR spectrum of WNK-5





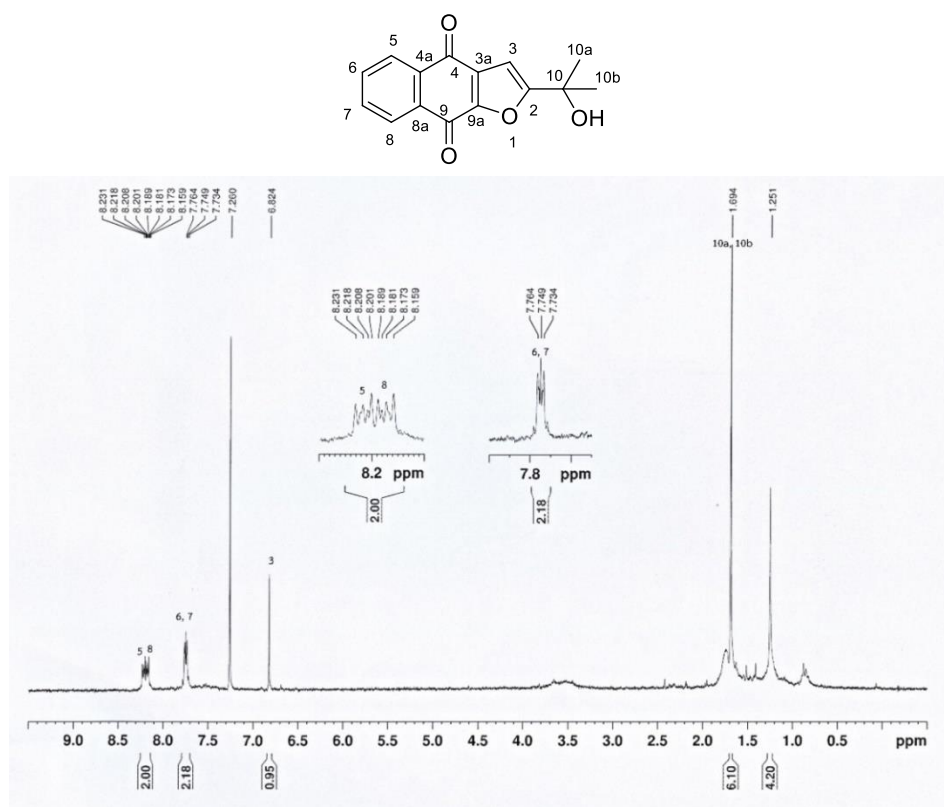


Figure 55  $^1\text{H}$  NMR (300 MHz) spectrum of WNK-5

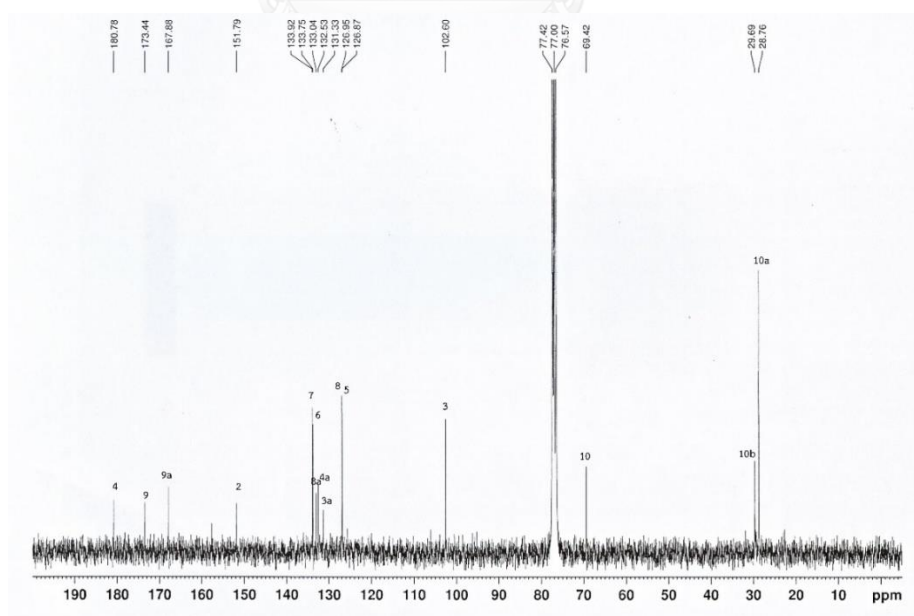


Figure 56  $^{13}\text{C}$  NMR (300 MHz) spectrum of WNK-5

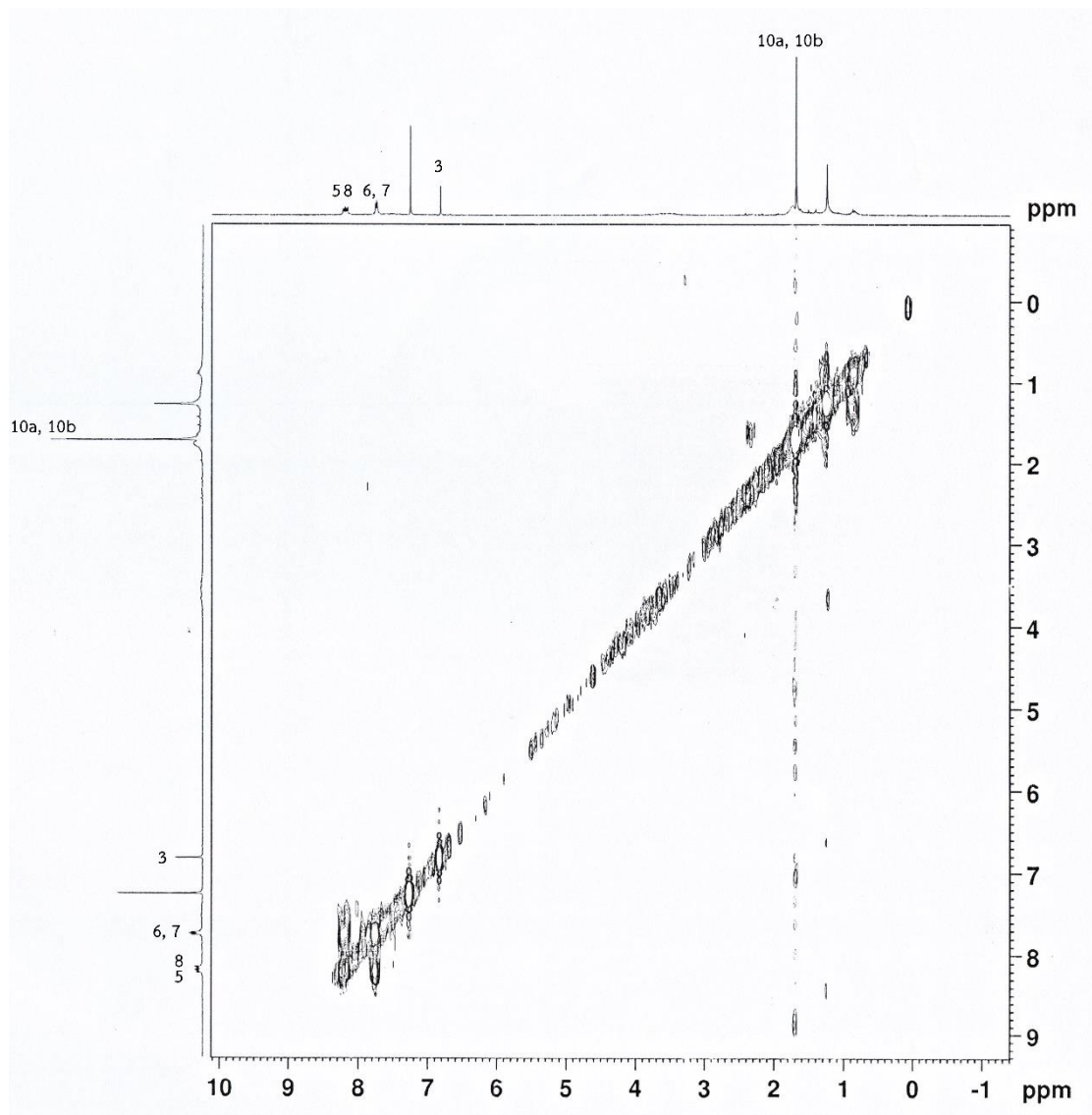
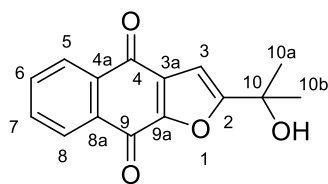


Figure 57 COSY spectrum of WNK-5

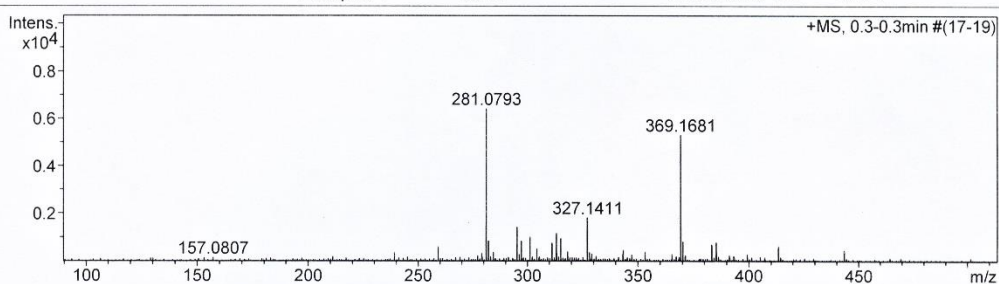
## Mass Spectrum List Report

### Analysis Info

Analysis Name	OSCUWNK580318006.d	Acquisition Date	3/19/2015 2:04:41 PM
Method	MKE_tune_low_positive_20130204.m	Operator	Administrator
Sample Name	WNK-6	Instrument	micrOTOF 72
	WNK-6		

### Acquisition Parameter

Source Type	ESI	Ion Polarity	Positive	Set Corrector Fill	79 V
Scan Range	n/a	Capillary Exit	90.0 V	Set Pulsar Pull	406 V
Scan Begin	50 m/z	Hexapole RF	90.0 V	Set Pulsar Push	388 V
Scan End	3000 m/z	Skimmer 1	45.5 V	Set Reflector	1300 V
		Hexapole 1	25.0 V	Set Flight Tube	9000 V
				Set Detector TOF	1910 V



#	m/z	I	I %	S/N	FWHM	Res.
1	239.1560	345	5.4	38.9	0.0391	6119
2	259.0986	594	9.3	63.7	0.0485	5339
3	279.0661	328	5.1	33.2	0.0370	7549
4	281.0793	6407	100.0	652.5	0.0452	6212
5	282.0826	852	13.3	86.1	0.0423	6667
6	284.3307	381	5.9	38.0	0.0431	6604
7	295.1293	1440	22.5	141.2	0.0469	6290
8	296.1329	295	4.6	28.4	0.0413	7170
9	297.0828	836	13.1	81.4	0.0874	3397
10	301.1419	1019	15.9	98.3	0.0487	6190
11	304.2634	482	7.5	45.9	0.0578	5264
12	311.1144	763	11.9	71.7	0.0759	4099
13	313.1067	1174	18.3	110.1	0.0491	6377
14	315.0875	955	14.9	89.1	0.0514	6136
15	318.2398	397	6.2	36.4	0.0427	7457
16	327.1411	1826	28.5	166.0	0.0690	4741
17	328.1445	365	5.7	32.7	0.0709	4626
18	329.1543	306	4.8	27.3	0.1096	3004
19	343.1331	285	4.4	24.6	0.0892	3845
20	343.2974	464	7.2	40.3	0.0529	6495
21	353.1516	387	6.0	32.8	0.0718	4917
22	365.2748	296	4.6	25.3	0.0603	6061
23	369.1681	5307	82.8	465.8	0.0606	6090
24	370.1743	825	12.9	72.1	0.0624	5929
25	383.1535	704	11.0	63.1	0.0681	5626
26	385.1616	791	12.3	71.2	0.0776	4964
27	385.2881	346	5.4	30.9	0.0591	6523
28	399.1555	276	4.3	25.2	0.0855	4668
29	413.2698	630	9.8	60.1	0.0769	5375
30	443.2922	458	7.2	46.6	0.1143	3879

Figure 58 Mass spectrum of WNK-6

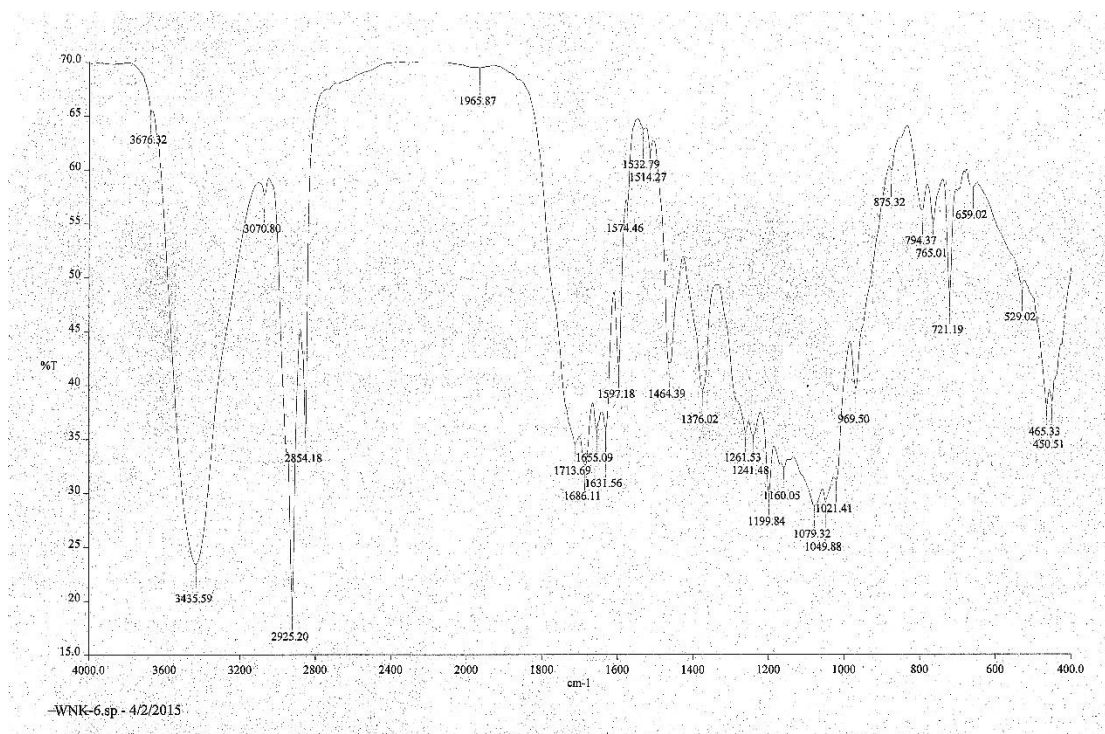
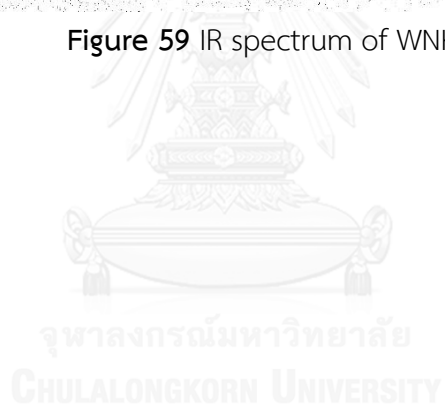


Figure 59 IR spectrum of WNK-4



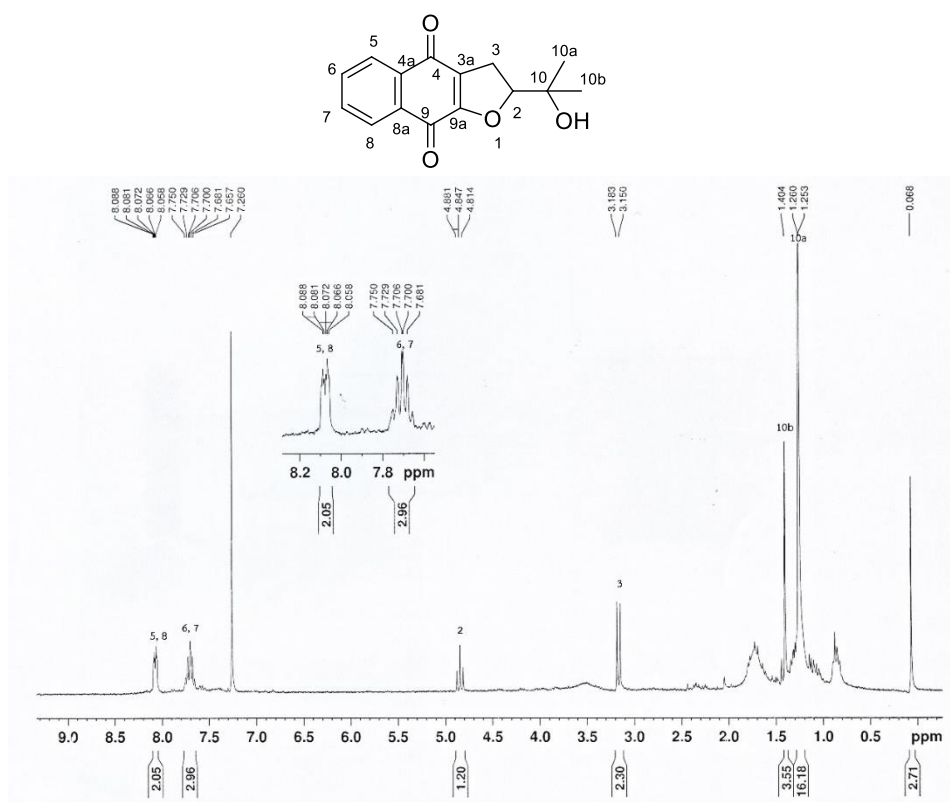


Figure 60  $^1\text{H}$  NMR (300 MHz) spectrum of WNK-6

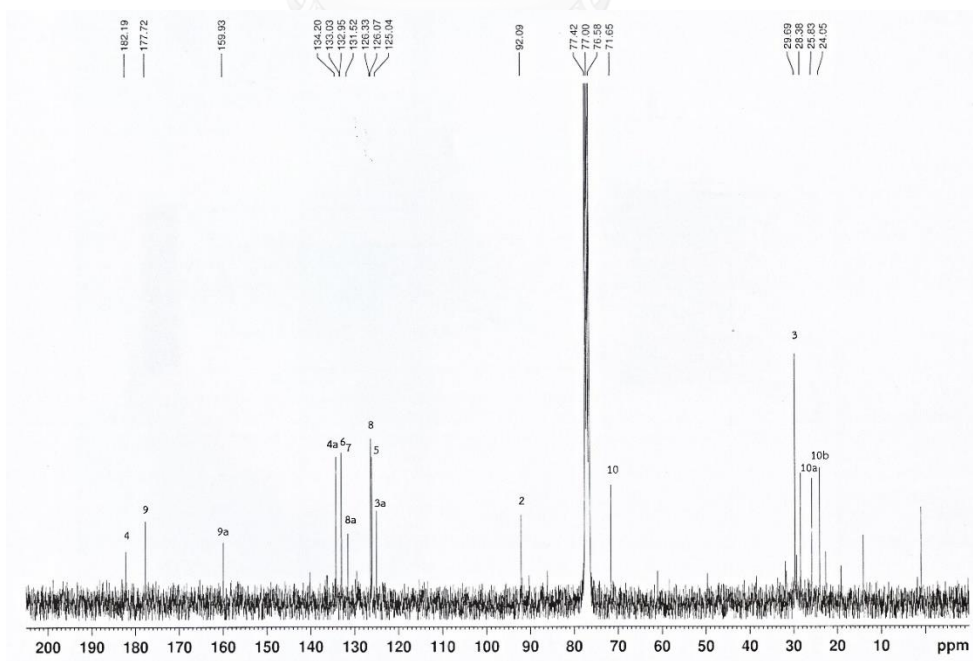


Figure 61  $^{13}\text{C}$  NMR (300 MHz) spectrum of WNK-6

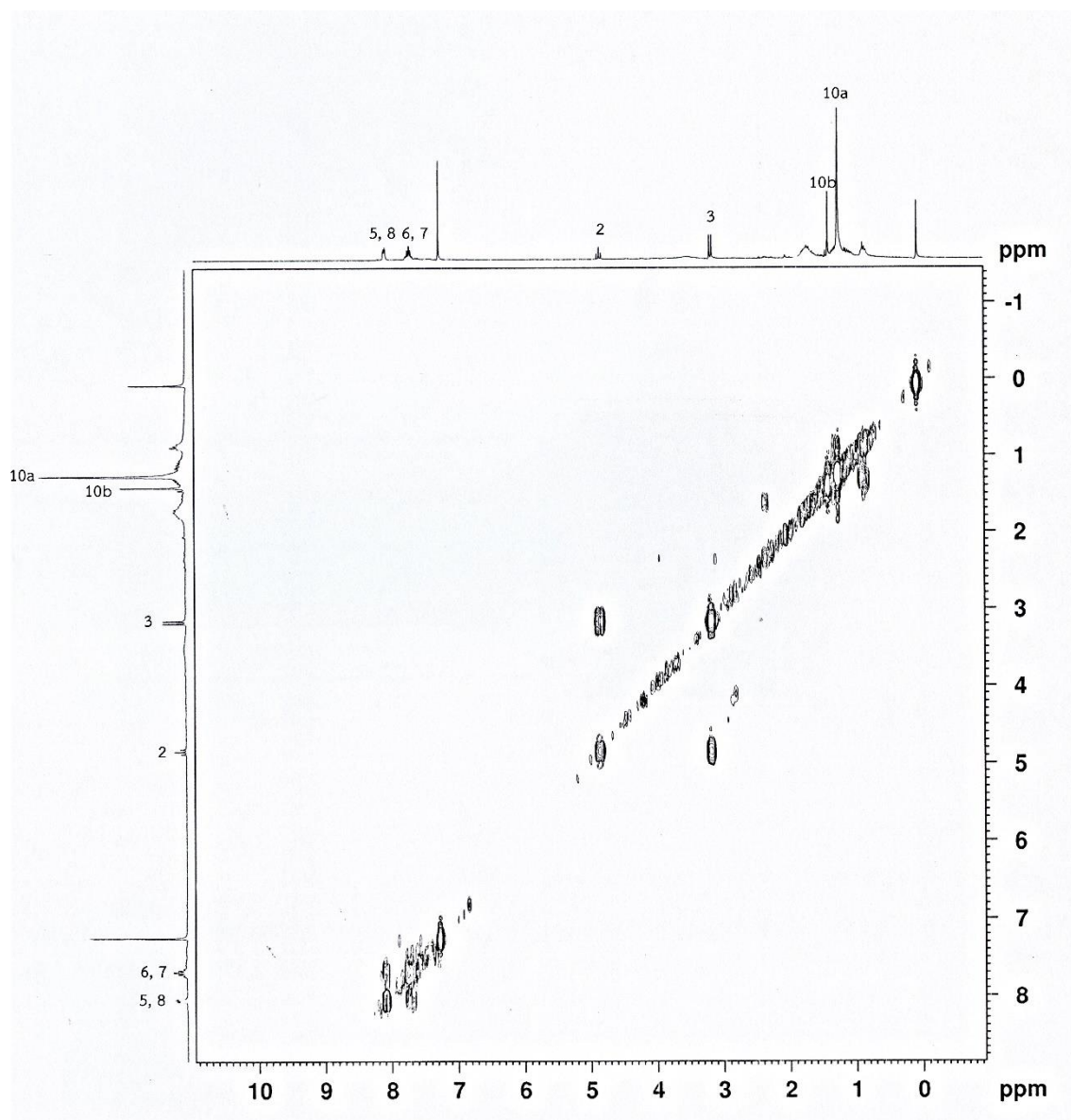
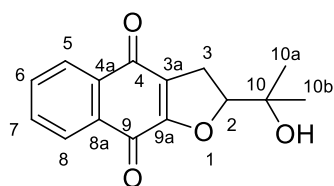


Figure 62 COSY spectrum of WNK-6



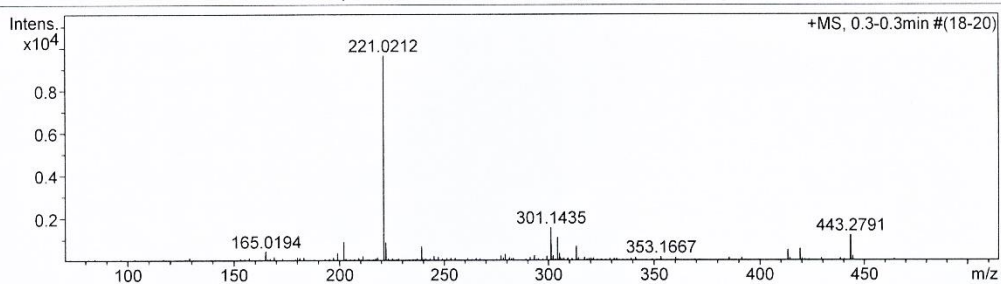
## Mass Spectrum List Report

### Analysis Info

Analysis Name	OSCUWNK580318007.d	Acquisition Date	3/19/2015 2:07:54 PM
Method	MKE_tune_low_positive_20130204.m	Operator	Administrator
Sample Name	WNK-7	Instrument	micrOTOF 72
	WNK-7		

### Acquisition Parameter

Source Type	ESI	Ion Polarity	Positive	Set Corrector Fill	79 V
Scan Range	n/a	Capillary Exit	60.0 V	Set Pulsar Pull	406 V
Scan Begin	50 m/z	Hexapole RF	90.0 V	Set Pulsar Push	388 V
Scan End	3000 m/z	Skimmer 1	45.5 V	Set Reflector	1300 V
		Hexapole 1	25.0 V	Set Flight Tube	9000 V
				Set Detector TOF	1910 V



#	m/z	I	I %	S/N	FWHM	Res.
1	165.0194	449	4.7	66.9	0.0337	4901
2	169.0516	216	2.2	31.8	0.0257	6586
3	180.0517	163	1.7	23.6	0.0333	5410
4	199.0418	382	4.0	54.6	0.0341	5839
5	202.0292	912	9.5	130.4	0.0319	6332
6	211.0973	219	2.3	30.7	0.0416	5074
7	218.0207	179	1.9	24.8	0.0323	6744
8	221.0212	9637	100.0	1352.2	0.0338	6536
9	222.0245	875	9.1	122.2	0.0366	6065
10	239.1580	685	7.1	93.7	0.0408	5857
11	245.0817	230	2.4	31.0	0.0507	4835
12	247.0898	184	1.9	24.7	0.0432	5725
13	277.1700	261	2.7	33.9	0.0817	3391
14	279.1771	284	3.0	37.0	0.0674	4144
15	281.1734	161	1.7	20.6	0.0674	4174
16	293.2431	271	2.8	34.6	0.0506	5795
17	299.1609	240	2.5	30.4	0.0622	4811
18	301.1435	1574	16.3	202.0	0.0475	6339
19	302.1470	259	2.7	32.7	0.0490	6170
20	304.2637	1100	11.4	140.6	0.0551	5525
21	305.2587	351	3.6	44.4	0.0609	5015
22	313.1785	696	7.2	88.0	0.0513	6104
23	341.2666	166	1.7	20.0	0.0562	6072
24	353.1667	201	2.1	24.0	0.0681	5187
25	360.1309	166	1.7	19.9	0.0817	4409
26	385.2915	163	1.7	20.5	0.0599	6436
27	413.2719	499	5.2	67.8	0.0917	4506
28	419.0583	579	6.0	79.9	0.0722	5805
29	443.2791	1228	12.7	179.6	0.0991	4472
30	444.2874	197	2.0	28.4	0.1208	3678

Figure 63 Mass spectrum of WNK-7

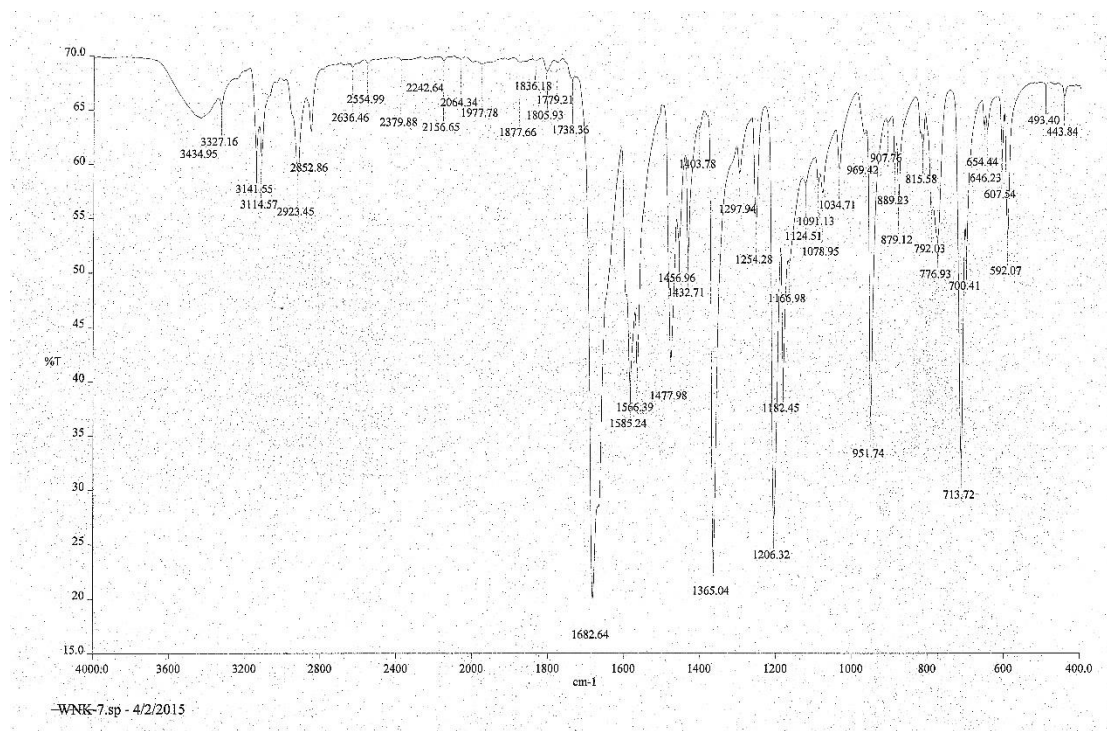
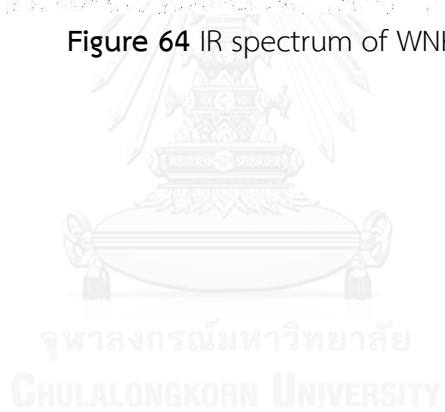


Figure 64 IR spectrum of WNK-7





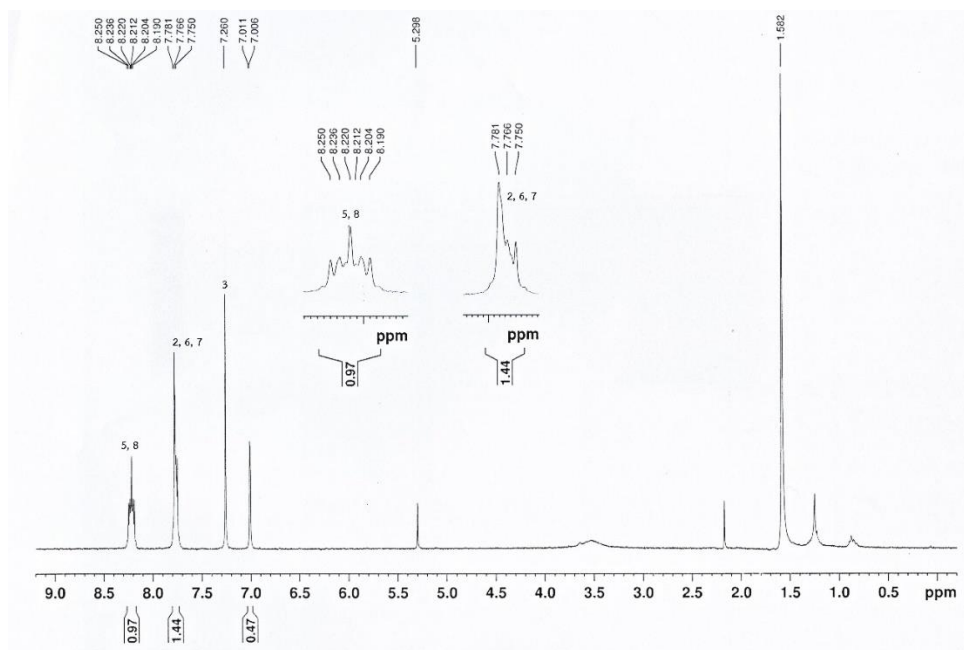
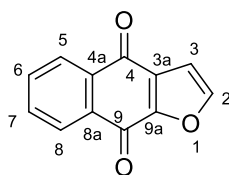


Figure 65  $^1\text{H}$  NMR (300 MHz) spectrum of WNK-7

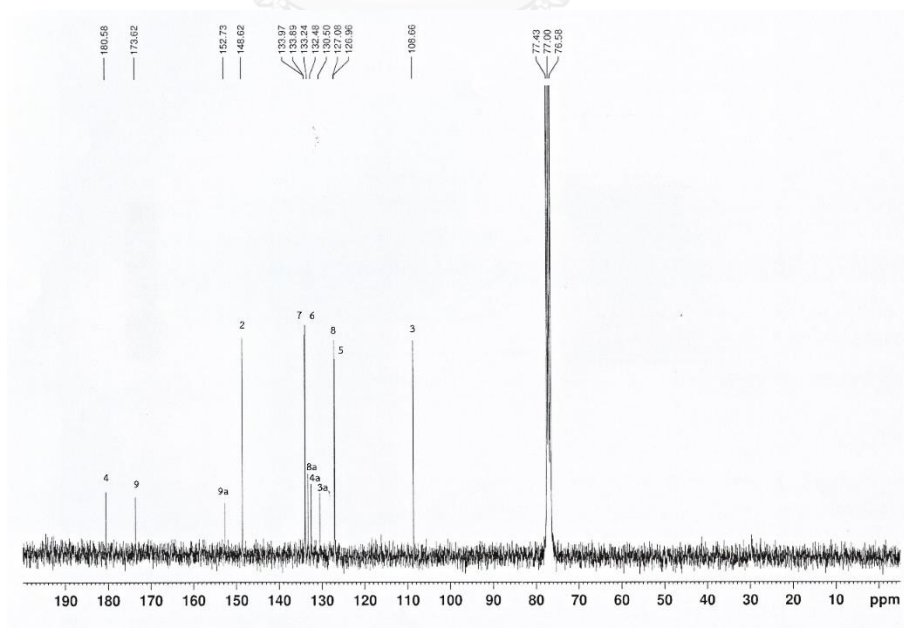


Figure 66  $^{13}\text{C}$  NMR (300 MHz) spectrum of WNK-7

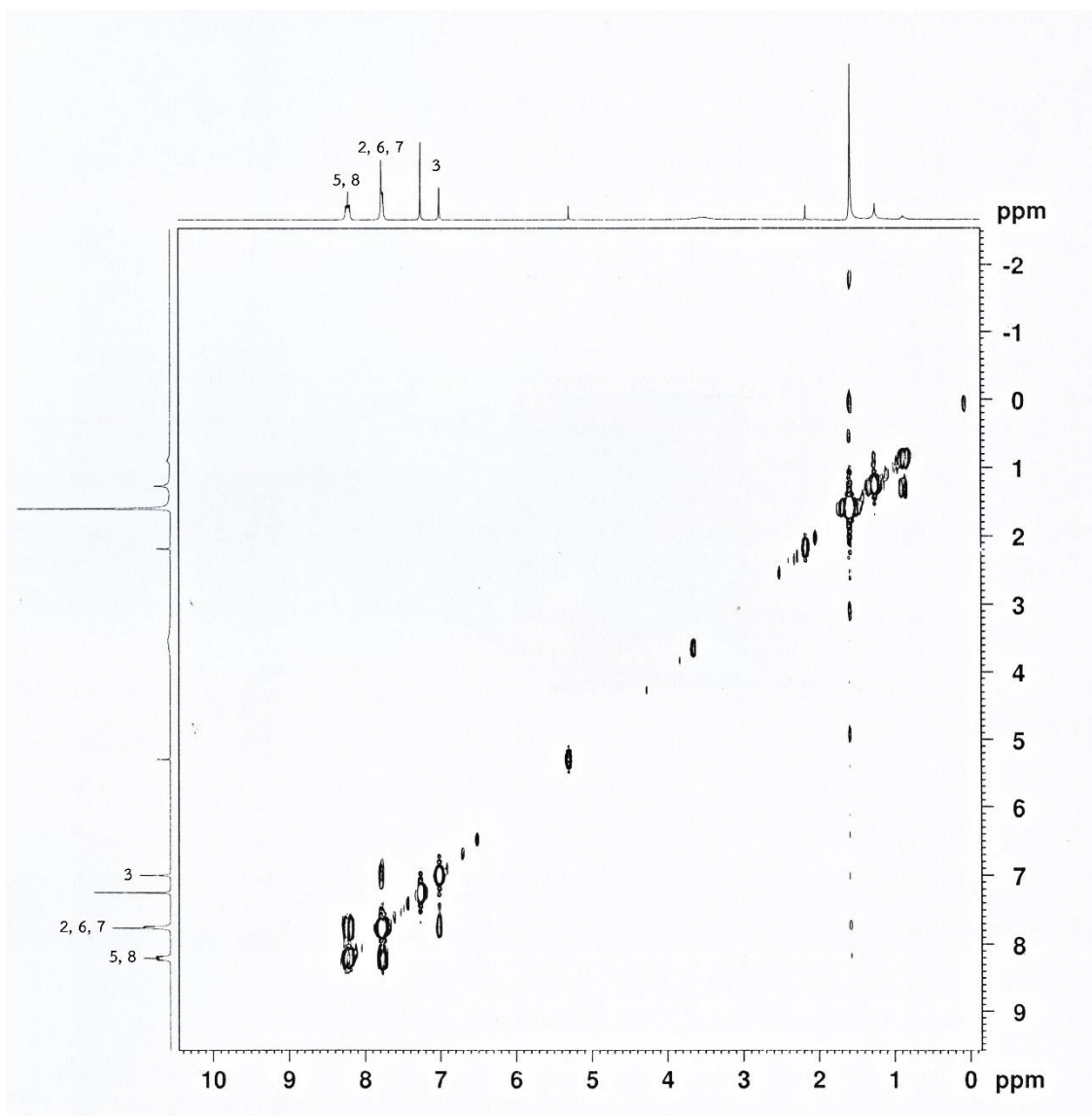
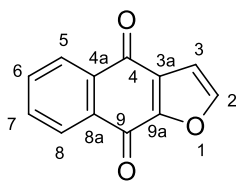


Figure 67 COSY spectrum of WNK-7

## VITA

Miss Wiranpat Karnsomwan was born on 12th November, 1988 in Ranong, Thailand. She graduated with Bachelor of Pharmacy from Faculty of Pharmaceutical Sciences, Khon Kaen University in 2013. She pursued her Master of Science in Pharmacy at the Department of Pharmacognosy and Pharmaceutical Botany, Faculty of Pharmaceutical Sciences, Chulalongkorn University during 2013-2016.

### Publications

1. Karnsomwan, W., S. Chamni, T. Rungrotmongkol, and W. De-Eknamkul. Homology modeling of 5  $\alpha$  -reductase type 1 and identification of steroid-binding active site. Pure and Applied Chemistry International Conference. 2015.
2. Karnsomwan, W., T. Rungrotmongkol, W. De-Eknamkul, and S. Chamni, In silico structural prediction of human steroid 5  $\alpha$  -reductase type II. Medicinal Chemistry Research, 2016: p. 1049-1056.